VALIDATING AN EX VIVO 3D KIDNEY PROXIMAL TUBULE MODEL FOR DRUG-INDUCED NEPHROTOXICITY SCREENING

by

Dorina Eva Lisa Diekjürgen

A dissertation submitted to the faculty of
The University of Utah
in partial fulfillment of the requirements for the degree of

Doctor of Philosophy

Department of Pharmaceutics and Pharmaceutical Chemistry

The University of Utah

August 2017

The University of Utah Graduate School

STATEMENT OF DISSERTATION APPROVAL

The dissertation of **Dorina Eva Lisa Diekjürgen**

has been approved by the following supervisory committee members:

David W. Grainger	, Chair	**5/26/2017** Date Approved
James N. Herron	, Member	**5/26/2017** Date Approved
Shawn C. Owen	, Member	**5/22/2017** Date Approved
Tara Lynn Deans	, Member	**5/25/2017** Date Approved
Brenda K. Mann	, Member	**5/26/2017** Date Approved

and by **Carol Lim** , Chair/Dean of

the Department/College/School of **Pharmaceutics and Pharmaceutical Chemistry**

and by David B. Kieda, Dean of The Graduate School.

ABSTRACT

Kidney toxicity is the second highest cause of new drug candidate failure, after liver toxicity, leading to drug withdrawals from the market and failed clinical trials. Therefore, development of more reliable and accurate in vitro screening systems for assessing drug nephrotoxicity is of high importance. Ideally, future new drug toxicity testing models will be highly sensitive, minimize animal use, and allow for high-throughput screening modalities. Recent technologies emphasize a shift away from monolayer-cultured and immortalized cells on plastic plates to novel three-dimensional (3D) matrix-based culture systems more similar to actual tissue constructs (i.e., organoids, micro-tissues, spheroids and cell/gels).

This dissertation focuses on characterization of a recently developed ex vivo 3D murine proximal tubule model and comparison to currently used two-dimensional (2D) kidney cell monocultures which are used for nephrotoxicity drug screening. The overall goal of this dissertation is to establish a scientific basis for justifying this ex vivo 3D model as a more reliable and predictive toxicity testing system for high-throughput drug screening in early drug development stages than currently available.

Therefore, expression levels and profiles for key kidney proximal tubule markers and important proximal tubule transporters with known roles in drug transport were obtained from the ex vivo 3D proximal tubule model. These data demonstrate more abundant and enduring apical and basolateral transporter expression than transporters in 2D cell lines, suggesting that they will provide a more reliable response to pharmaceutical compounds in 3D cultures.

To test the transporter functional ability and predictive toxicity, the model was further analyzed for its capability to detect nephrotoxicity in early stages using clinically relevant known nephrotoxic and nonnephrotoxic drugs. The obtained assay responses were compared to patient drug toxicity data from the clinic to assess the model's translational capacity. Data collected during

the concentration-response study demonstrate that the model is capable of accurately predicting nephrotoxicity for all tested compounds, producing toxicity responses highly correlated to known human clinical experience with the tested drugs. The 3D murine proximal tubule model's predictive values were found to be highly improved compared with predictive values from the current industrial "gold standard" for 2D kidney cell cultures still widely used for similar toxicity assessments. Furthermore, this model could be used to gain insight into specific drug structural mechanisms that drive toxicity and facilitate rapid assay of different chemical moieties during structure activity relationship screening.

The knowledge gained through this study provides greater understanding of how drug toxicity testing results compare between standard 2D cell assays, 3D assays, and human clinical data. The data underscore the 3D proximal tubule model's promising future as an improved, more reliable toxicity testing system for high-throughput screening during early phases of drug development.

TABLE OF CONTENTS

LIST OF TABLES

Tables

LIST OF FIGURES

Figures

ACKNOWLEDGEMENTS

I would have not been able to get my Ph.D. without some amazing people who have helped and supported me along this journey. First, I would like to thank my advisor Dr. David Grainger for the opportunity to work in his lab and being supportive and understanding when my research did not work the way we wanted it to. Thank you for always believing in me and challenging me to become a better scientist by helping me to develop my critical thinking and writing skills. I would also like to thank my committee members – Dr. Shawn Owen, Dr. James Herron, Dr. Brenda Mann, and Dr. Tara Deans – your feedback and scientific critique have helped shape these research endeavors.

I also thank past and present members of the Grainger group for their encouragement, daily interactions, and for being a source of fun in the lab. I would especially like to thank Dr. Anna Astashkina, who laid the foundation for my final project and provided tremendous help and support during my research work, for being such a great friend and mentor.

I am very grateful for all my friends here as well as back in Germany and many other places in the world who have shared the joys and frustrations along the way and have always been supportive by serving as a reminder of the world outside the lab.

Lastly, and most importantly, I am extremely grateful for all the support, love and encouragement from my parents Ingrid and Hanspeter Diekjürgen, my sister Diana Diekjürgen, and my boyfriend Joe Aamodt. You all have been an indispensable source of inspiration and support throughout my graduate career and you have always believed in me and kept reminding me that science is not all there is in life.

CHAPTER 1

INTRODUCTION TO THIS DISSERTATION

Kidney toxicity is the second highest cause of new drug failure after liver toxicity and causes many new pharmaceutical drug performance issues in clinical trials [91]. Lack of reliable drug candidate identification and reliable toxicity screening methods result in costly consequences when drugs fail [92]. Currently, only 8% of new pharmaceutical compounds tested in clinical trials actually reach the market. This low success rate does not sufficiently balance the input of time (typical timeframes averaging 9 years) and expenses (around one to two billion dollars) [93]. Hence, the demand for improved, more reliable and more predictive testing models to screen drug toxicity in early research stages and eliminate toxic drug candidates before clinical trials is high [91]. Besides the liver, kidneys are the main drug metabolism and elimination site, making kidney cell cultures the predominant preliminary drug nephrotoxicity model. However, the currently used screening models for nephrotoxicity eliminate only about 7% of pharmaceutical compounds in preclinical tests, a low amount considering that drug-induced acute renal failure cases are estimated between 30-50% [93-95]. This suggests that there is a significant gap between the screening data and real human in vivo response [93, 96, 97]. This discrepancy is mainly based on interspecies differences in drug response when animal in vivo models are used to predict human responses [97]. In addition to interspecies response differences, currently available two-dimensional (2D) drug toxicity screening models do not reliably screen physiologically relevant toxicity markers: 2D-cultured kidney cells lose native cellular phenotypes and in vivo-like properties, leading to the loss of in vivo-relevant pharmacological indicators, like kidney cell gene expression up- or down-regulation based on drug exposure and toxicity [98].

Ideally, future new drug testing models will be highly sensitive to drug dose, minimize

animal use, and allow for high-throughput screening modalities. It is important to validate new drug toxicity models that respond accurately to pharmaceutical compounds and use clinically relevant toxicity and/or disease biomarkers [99].

This dissertation aims to characterize and compare our recently developed ex vivo three-dimensional (3D) murine proximal tubule (PT) model against the current industrial standard of 2D monoculture kidney cell lines; to gain a greater understanding of the proximal tubule model's advantages and limitations and assess how the 3D proximal tubule model bridges the current toxicity screening gap to translate predictions to human clinical data in a correlative matter. The overarching hypothesis for this dissertation is that *3D proximal tubule organoid culture will better maintain in vivo-like properties and create a more reliable model for toxicity screening than currently used 2D cell culture.* Our 3D kidney PT culture model preserves native proximal tubule structure sufficiently to retain essential functions that are important in the nephron for drug-induced nephrotoxicity, and therefore has the potential for improved high-throughput toxicity screening.

Proximal tubules are the primary site of drug-induced nephrotoxicity. This is due to the fact that proximal tubules have specialized transporters for the uptake of organic compounds (e.g., OAT1, OAT3, OCT2). This active transport then results in high levels of drug, drug metabolite or toxin inside the proximal tubule cell, leading to cell damage and death. Additional drug toxicity can be achieved by drug biotransformation. In proximal tubule cells, biotransformation can occur enzymatically (e.g., brush border enzyme γ-glutamyl-transferase, lysosomal enzyme N-acetyl-β-D-glucosamine, cytosolic enzyme glutathione-S-transferase), or through metabolism through several cytochrome P450 enzymes. Cytochrome P450 is predominantly localized in the proximal tubule and not in other parts of the nephron. Therefore, nephrotoxic effects from compounds which require cytochrome P450 metabolism are ideally studied in the proximal tubules as well [100, 101]. These components play a major role in why proximal tubules are an ideal target for a drug toxicity screening models. Chapter 2 gives further insight into drug-induced nephrotoxicity.

Previously, 3D cell culture has demonstrated many benefits compared to conventional 2D cell culture, which is the current toxicity testing standard in the pharmaceutical industry in combination with animal studies [14]. In 2D cell culture, primary proximal tubule cells lose their

polarization sometimes within min [102], while secondary cells are often missing important transporters critical for drug toxicity [98]. Therefore, recent technologies emphasize a shift away from monolayer-cultured cells on plastic plates to novel 3D matrix-based culture systems more similar to actual tissue constructs (i.e., organoids, micro-tissues, spheroids and cells in gels) [103, 104].

Our recently developed 3D kidney organoid toxicity model [60] fulfills many of these requirements and improves on current 2D kidney cell monocultures on plastic by using viable mouse kidney-derived proximal tubules [105]. This allows proximal tubule epithelial cells to remain in their native tertiary tissue-like structure, keep their cell-matrix and natural cell-cell communication intact, and maintain differentiated states and cell functionalities. Proximal tubule cells therefore reside and interact in a more natural environment and reflect toxicity states with more fidelity when interacting with drug compounds. In previous studies, we were able to show that our 3D organoid model shows more sensitive responses to drugs compared to secondary 2D kidney cell cultures. This was shown by enzyme release (γ-glutamyl-transferase, N-acetyl-β-D-glucosamine) and gene expression (KIM-1, VIM, CLU, HO-1) [47].

Currently used drug kidney toxicity markers in clinical trials are blood urea nitrogen (BUN) and serum creatinine. The drawback for these markers is that they are rather insensitive as a 50-70% decrease in glomerular filtration rate (GFR) must first occur to see increases in BUN and serum creatinine amounts [100]. This slow response and the lack of better available markers lead the FDA's Critical Path Initiative call for development of better tools and more predictive, early nephrotoxicity screening [84, 91]. More reliable models to detect drug toxicity early in development should be able to measure responses to compounds in a reliable and clinically relevant way with high predictive values, specificity and sensitivity. To exploit the advantages of the newly developed nephrotoxicity screening model, this dissertation seeks to provide greater insight to reliability, predictability, and interspecies comparability by assessing the 3D model drug responses against currently used 2D kidney cell culture lines and human clinical data, and analyze overall advantages and limitations. This will provide more detailed information to overcome the currently available toxicity assays' challenges and better bridge the gap to human data and nephrotoxicity incidence

by creating a better, early-phase drug toxicity screening model.

Validation of the ex vivo 3D proximal tubule organoid model as a reliable drug screening tool used gene expression analyses relevant to asserting proximal tubule cell phenotypes, molecular and biochemical renal biomarkers via quantitative real-time PCR (qPCR) (Chapter 4) and verification of proximal tubule cell membrane protein and pump genotypes necessary to produce the toxicity responses reported in Chapter 5. The necessity of using a commercial Utah-developed hyaluronic acid-based hydrogel (HA-gel) matrix for encapsulating harvested viable proximal tubule organoid fragments was assessed against media-only cultured fragments.

Encapsulation in 3D gel matrices is often proposed to mimic extracellular matrix and allow proximal tubule epithelial cells to remain in their native tertiary tissue-like structure with added support (Chapter 3). Therefore, transporter and metabolism enzyme expression levels were compared not only to published 2D kidney cell culture lines but also between 3D HA-gel embedded proximal tubules versus proximal tubule fragment suspension cultures (Chapter 4). Even though most toxicity screening tests are performed after 24h of compound exposure, expression levels for proximal tubule markers in cultures was assayed for out to seven days (Chapter 4).

To validate the drug toxicity screening capability of the ex vivo 3D proximal tubule model, clinically relevant, known nephrotoxic (cidofovir, cisplatin, doxorubicin, polymyxin B, polymyxin B nonapeptide, and vancomycin) and nonnephrotoxic (cimetidine and probenecid) drugs were used in validation assays described in Chapter 5. Model sensitivity and specificity at different therapeutic index (TI) cutoff values were analyzed by using compound concentration-PT response curves and the molar concentration of each test compound producing 50% inhibition (IC_{50}), lowest effective concentration (LEC) and area under the concentration-response curve (AUC) values were calculated as standard clinically relevant drug therapy parameters. Additionally, the model's predictive values were analyzed and receiver operating characteristic (ROC) analysis was performed and data compared to currently used 2D kidney cell culture lines (Chapter 5). Significantly, the toxicity data from the ex vivo 3D model was compared to known reported human clinical toxicity incidence data for each compound, and the correlation/translation was analyzed (Chapter 5).

Clinical therapy strategies seek to minimize drug nephrotoxicity by using co-administered specific proximal tubule transporter competitive inhibitors. Hence, the 3D assay model's ability to reveal kidney tubule epithelial cell substrate-inhibitor competitive interactions was assayed by comparing response with the toxic drug alone versus the same drug in combination with a potent, receptor-specific inhibitor/competitor selected from the 9 compounds was tested. This analysis was performed to substantiate if the model could eventually provide more specific information on drug structure-activity relationships that drive toxicity, and facilitate rapid assay of different new chemical entities (NCEs) during drug candidate screening (Chapter 5).

Overall, this kidney proximal tubule fragment culture approach provides a unique opportunity to gain greater insight in the much-needed correlations between known nephrotoxic and nonnephrotoxic compound toxicity results found in animals and humans versus in vitro kidney cell culture assays. Results of this study address some long-standing challenges of reliably sorting through libraries of therapeutically relevant molecules, and provide a better, more reliable toxicity testing model for high-throughput screening and ultimately reducing costly clinical trial failures and late-stage drug product withdrawals. The data described in this dissertation clearly support the study hypothesis that this ex vivo 3D proximal tubule model is more reliable and allows for better predictive toxicity values than the simplified 2D kidney cell culture lines, and that the data obtained are more relevant and impacting to modern drug screening assays.

Furthermore, this model validation opens up future capabilities for exploiting specifically designed proximal tubule mutations in transgenic knock-in mice, as well as new, analogous investigations in other organ toxicity studies (e.g., hepatotoxicity and cardiotoxicity studies). Approaches to these studies are outlined in Chapter 6. Also, while this current kidney toxicity model relies on harvest of proximal tubules from mice, requiring murine sacrifices, this approach could avoid animal use by exploiting new vitro functional kidney organoids derived from stem cells [106-109]. Additional validation of the model using human proximal tubules from discarded kidney harvests would provide even closer correlations, genomically profiled or specific screens, or even disease-specific approaches to drug toxicity assays (Chapter 6).

CHAPTER 2

DRUG-INDUCED NEPHROTOXICITY

Introduction

The kidney is a major target for drug-induced toxicity. Nephrotoxic drug use is often unavoidable in the clinic, and therefore, drug-induced nephrotoxicity is a recognized major problem [95, 110]. For pharmaceutical companies, development of ideal nonnephrotoxic drugs or at least those with a reduced toxicity potential is of high priority [94, 99]. To do so, predictive nephrotoxicity screening assays are needed to overcome the current challenges of late-stage human nephrotoxicity incidence. Current in vitro models are not successfully validated, standardized nor accepted, and animal testing is still used with some uncertainty to predict drug toxicity risks [111].

Nephrotoxic drug administration often leads to acute kidney injury (AKI) and is linked with increased patient morbidity and mortality. The late detection of nephrotoxic effects and the currently often underestimated nephrotoxic potential of newly developed drug candidates lead to increased development costs for pharmaceutical industries. Therefore, more reliable nephrotoxicity screening models are needed to predict adverse events early in development and avoid costly drug failures from toxicity late in clinical testing or even post-market approval.

Pathological mechanisms of drug-induced nephrotoxicity

Changes in intraglomerular hemodynamics

The glomerular filtration rate (GFR) is defined as the total volume of filtered fluid by the glomeruli of both kidneys together per unit time. For healthy humans with normal blood pressure the GFR is approximately 120 ml per minute. Through the regulation of the blood flow in afferent and efferent arteries, the kidneys can maintain or adjust the intraglomerular pressure. This allows

them to maintain the filtration rate constant and preserve urine output. The expansion of afferent arteries relies on circulating prostaglandin. Therefore antiprostaglandin drugs (e.g., nonsteroidal anti-inflammatory drugs (NSAIDs)) show nephrotoxic effects in the glomeruli [112]. A second group of drugs that have been shown to induce nephrotoxicity are the angiotensin converting enzyme (ACE) inhibitors as well as angiotensin receptor blockers (ARBs) [113, 114]. Their toxicity mechanism is based on interfering with the angiotensin-II-mediated vasoconstriction of the efferent arteries which is an important pathway to maintain intraglomerular pressure [81, 115, 116].

Tubular cell toxicity

Renal tubule cells, especially proximal tubule cells, have an increased surface area created by microvilli and highly in-folded plasma membranes, which makes them susceptible to toxic drug exposure and effects. Additionally, proximal tubules are exposed to high levels of circulating toxicants due to their role in concentrating and reabsorbing the glomerular filtrate [81, 115, 116]. Furthermore, active transport of toxicants by specialized cellular transporters for uptake of organic compounds leads to high levels of toxicants inside proximal tubule cells, leading to cell damage and death [117, 118]. Drug cytotoxic effects arise from impairment of mitochondrial function, interference with tubular transport, increase in oxidative stress as well as formation of free radicals [115, 117, 118]. Another factor influencing proximal tubule toxicity is that cytochrome P450 is predominantly localized in the proximal tubule and not in other parts of the nephron. Therefore, nephrotoxic effects from drugs that utilize cytochrome P450 metabolic pathways mainly affect proximal tubules as well [87]. Drug classes known to induce tubular cell toxicity are aminoglycosides, antifungal compounds, antiretroviral, and chemotherapeutic drugs.

Inflammation

Inflammation in different parts of the nephron (glomerulus, proximal tubules as well as the surrounding matrix) is often caused by nephrotoxicants. This inflammation can lead to fibrosis and scarring of the affected kidney tissue and then changes normal kidney functions by inducing toxicity. Glomerulonephritis is primarily caused by immune responses and often associated with proteinuria

[119]. Drugs such as interferon-alfa, lithium, NSAIDs, hydralazine, and gold salts are known to cause this type of nephrotoxic response [117, 119]. Another type of inflammation-induced nephrotoxicity is acute interstitial nephritis, an allergic response triggered by NSAIDs and antibiotic drugs. This immune reaction is proposed to be caused by toxic compounds binding to antigens in the kidney, or drugs acting as antigens, which are then deposited into the interstitium [115, 120]. Even while it is less likely to be drug-induced, the development of chronic interstitial nephritis can be triggered by certain chemotherapeutic agents, calcineurin inhibitors, and lithium, but also by NSAIDs chronically used in high doses [112, 121]. Early detection and prevention of chronic interstitial nephritis is important as otherwise this can lead to end-stage renal diseases [122].

Crystal nephropathy

Renal function can be altered by drugs that produce insoluble crystals in human urine. The formation of these crystals is dependent on urine acidity and drug concentration. Drug or metabolite crystals usually develop in the distal tubule, obstruct urine flow, and then induce an interstitial reaction [117]. Antiviral and antibiotic drugs can cause crystal nephropathy [81]. If patients have volume depletion and/or underlying renal insufficiency, the risk of crystal nephropathy is increased [115].

Rhabdomyolysis

Rhabdomyolysis is the rapid break down of damaged skeletal muscle. When skeletal muscle is destroyed, muscle fiber contents, myoglobin, and serum creatine kinases are released into the blood stream. The myoglobin degrades and causes tubular obstruction and alterations in glomerular filtration rate, leading to acute tubular necrosis or renal failure [81, 115]. Drugs known to cause rhabdomyolysis are statins and methadone [81].

Thrombotic microangiopathy

Circulating platelet thrombi cause organ damage through inflammation or direct renal epithelial cytotoxicity, which leads to thrombic microangiopathy (thrombosis in capillaries and

arterioles). Drugs causing thrombotic microangiopathy are antiplatelet agents and quinine [81, 115].

Risk factors for nephrotoxicity

Specific clinical situations and patient groups are more prone to develop drug-induced nephrotoxicity. Therefore, knowledge of patient-related risk factors, drug-related risk-factors and recognition, and early intervention are important to successfully prevent or limit drug-induced nephrotoxicity [116, 123].

Patient-related risk factors

Patient-related risk factors generally associated with nephrotoxins are advanced age (over 60 years), GFR of less than 60 ml per minute (indicator for underlying renal insufficiency), diabetes, heart failure, metabolic disorders that alter the pH of the urine, sepsis, intravascular volume depletion, and exposure to multiple nephrotoxins simultaneously [115, 116, 124, 125]. Other risk factors like race, genetic variation, and gender are controversial, and could also depend and vary based on the toxicant [124]. Overall, the risk of drug-induced nephrotoxicity and acute renal failure generally increases with additional risk factors. Therefore, patients with any of these risk factors, especially with combinations of risk factors, should be closely monitored under drug exposure.

Drug-related risk factors

Several administrated agents are known to be intrinsically nephrotoxic, like aminoglycosides, cisplatin, imaging contrast dyes, cyclosporine, and amphotericin B [116, 124], while others exhibit dose-dependent or duration-dependent nephrotoxic effects [116, 124]. Drugs that affect tubular cells directly or induce crystal deposition are especially known to produce dose-dependent nephrotoxicity [117, 126]. A therapy with multiple nephrotoxic drugs can result in potentiating nephrotoxic effects and increased risks of renal injury [115, 116].

Preventing drug-induced renal impairment

Prevention

To prevent the onset of drug-induced nephrotoxicity, the obvious first clinical intervention is to exploit nonnephrotoxic drugs (i.e., those lacking nephrotoxic effects, or those exhibiting a high therapeutic index) whenever possible. Additionally, it is important to address risk factors as well as determine baseline renal function values before therapy start, which allows for drug dose adjustments [115, 116]. It is highly recommended to avoid combinations of multiple nephrotoxic drugs because of the previously mentioned potentiating effect [115]. Some nephrotoxic effects can be avoided by adequate hydration (e.g., doxorubicin, ACE inhibitors, and NSAIDs) [113, 114].

Recognition and early intervention

As most drug-induced renal impairments are reversible, early recognition and intervention is important. Reductions in renal function noted clinically by decreased GFR or increased serum creatinine levels after drug administration are common signs of drug-induced nephrotoxicity. Drugs that compete with creatinine for tubular secretion (e.g., cimetidine) can lead to false positive results and are not associated with kidney damage [115, 127]. If changes in GFR or serum creatinine levels are observed, the drug dose should be adjusted or if necessary, drug administration needs to be stopped. Additionally, blood pressure should be monitored, hydration levels should be adequate, other possible nephrotoxins should be discontinued, and a staggered drug administration approach should be adopted [115, 128].

Assessing nephrotoxicity

Clinical nephrotoxicity markers

Clinical nephrotoxicity detection commonly uses laboratory measurements of increased serum creatinine and plasma urea in patient blood samples [129-131]. Also, measurement of urine output is used clinically in AKI diagnostics [129-131]. All of these measurements, especially urine output, are insensitive markers of decreased GFR, the clinical indicator of toxicity. Actually, 50-70% reduction in GFR must first occur to observe increases in blood urea nitrogen (BUN, normal range:

7-20mg/dl) and serum creatinine (SCr, normal range: 0.6-1.3 mg/dl). Additionally, the levels of BUN and SCr can be influenced by unrelated factors like food and fluid intake, muscle mass and injury, gender, age, and drugs like steroids [111].

This slow and insensitive clinical response, and the lack of better available kidney toxicity markers, both limit the clinical detection and possible therapeutic options to prevent AKI. This scenario has prompted the FDA's Critical Path Initiative call for the development of better tools and more predictive early nephrotoxicity markers [84, 91]. Based on this initiative, the following novel predictive markers for drug-induced nephrotoxicity were proposed and remain under investigation [54, 84]: KIM-1 [68], NGAL [75], GST [69], and cytokines IL-6 and IL-8 [86, 132]. All of these markers demonstrate increased sensitivity to nephrotoxicity and present earlier than BUN and serum creatinine. Correlation of their clinical presentation with AKI with validated preclinical assays showing predictive use in drug-induced nephrotoxicity are required.

Preclinical in vitro testing approaches for predicting drug-induced nephrotoxicity

The problem with most current in vitro testing approaches for predicting drug-induced nephrotoxicity is the lack of validation with clinical pathology, and that the number of tested nephrotoxic compounds is too small in most studies to produce clinical reliability and relevance [111, 133]. Additionally, few studies include major analytical performance metrics like sensitivity, specificity, positive predictive value (PPV), and negative predictive value (NPV). In vitro assays allow for ready manipulation of variables and measurements, and therefore, mechanistic aspects of toxicity can also be investigated. It must be kept in mind though, that results from cell-based assays must be interpreted carefully: no model to date represents the fully functional status or complex homeostatic or pathological mechanisms of kidney cells in vivo. Therefore, drug processing in vitro and subsequent toxicity results must be analyzed, verified, and compared to in vivo results to validate proper translation.

Newer, advanced in vitro 3D cell culture systems, multicell type co-culture systems, organoid cultures, and microfluidic models are more complex than conventional cell cultures [133] but remain largely early phase nonvalidated experimental innovations. Limitations of these

approaches lie in their slow, often low-throughput performance. They are more expensive and complicated to set up, resulting in intrinsic variability and lack of reliability, and incompatibilities with current cell culture assay read-outs and quantitative endpoints. These issues limit the number of compounds screened and also require special optimization of assays to assure performance and reliability [111, 133]. Assay standardization and validation to clinical endpoints in nephrotoxicity are currently lacking. For a detailed overview on currently used in vitro approaches for drug-induced nephrotoxicity see the review by Tiong et al. [111].

Kidney proximal tubule cells remain the preferred cell type for drug-induced nephrotoxicity screening assays because they are the major target for toxic drug effects clinically. Traditional cell-based assays are monocultured secondary kidney cell lines on plastic plates (i.e., 2D). Cell line functional validations are often lacking and many kidney cells do not represent the proper or stable phenotype to yield reliable kidney-drug toxicity predictions [111]. Recent shifts to primary kidney cell 3D cultures improve phenotypic fidelity and assay responses to drugs [19, 47, 60].

Transitioning to three-dimensional (3D) kidney cell cultures is a recent innovation [19]. Different approaches to 3D cell culture exploit various matrices to suspend and embed cells, which promotes cell-cell interactions more typical of an in vivo microenvironment [19, 133]. Additionally, microfluidic devices provide, versatile interfaced fluidics and electronic controls, multiple co-culture chambers and capabilities to alter assay inputs and output as well as exploit miniaturization benefits (so-called organ-on-a-chip). These approaches generally seek to investigate cell-drug behaviors in more complex culture environments to compare to in vivo drug responses. For a detailed overview on current kidney-on-a-chip approaches for drug-induced nephrotoxicity screening, see review from Wilmer et al. [133].

2D cell culture systems are routine, simple, and inexpensive to maintain, and have the benefit that most drug response performance assays are developed and validated for 2D cell culture systems. The downside is that 2D cell culture system responses are often very different than in vivo response due cell phenotypic behavior on rigid 2D plastic culture dishes. This culture condition influences cellular responses to drugs as well as cell transporter expression known to be critical to drug-induced nephrotoxicity [12, 47]. The typical 2D assay endpoint is a cell viability

assessment under arbitrary drug dosing conditions in monoculture with cells that often lack proper in vivo phenotypes [103]. This naturally leads to predictions that are not clinically correlated. More complex 3D or microfluidic systems incorporate more biomimetic features seeking to achieve more normal in vivo-like cell behavior but are also more complex to perform, more variable, and more expensive. Organ-on-a-chip systems use varying combinations of cell layers in 2D cultures or exploit 3D gel matrices and applied shear forces through microfluidic systems [61, 133-136] but remain unverified, early-stage experimental systems. The use of stem cell-derived organoid cultures for kidney physiological recapitulation is now increasing [106, 108, 109, 137-139]. While organoids are in general understood to be functional parts of an organ (i.e., independently functioning if harvested or self-grown), stem cell-derived organoids derive from a few stem cells and are achieved by either self-organization in 3D structures or by using gel or scaffold templates to enforce specific culture organization and morphologies that yield specific limited organ-like functions. While many different approaches and designs are reported, no fully biomimetic models exhibiting drug responses similar to human in vivo drug-induced toxicities are known. The main performance criteria for all such approaches is to establish reliable in vitro-in vivo correlations (IVIVC) for diverse drug classes, as well as validate the models thoroughly using diverse human-derived cells (e.g., iPS cells, human explants, primary cell lines). Assay metrics (e.g., figures of merit) should be produced to assert such validation. These important assay criteria include assay sensitivity, specificity, limits of detection, dynamic range, coefficient of variation, positive predictive validation, and negative predictive value (NPV). If that validation is done successfully in new in vitro models of drug-induced nephrotoxicity, then in vitro toxicity results can be interpreted properly and confidently, to allow more reliable and predictive responses in early drug candidate screens to predict anticipated human toxicity responses. This unmet challenge provides the primary motivation for the drug-induced nephrotoxicity studies described in this dissertation.

CHAPTER 3

POLYSACCHARIDE MATRICES USED IN 3D IN VITRO CELL CULTURE SYSTEMS[1]

Abstract

Polysaccharides comprise a diverse class of polymeric materials with a history of proven biocompatibility and continual use as biomaterials. Recent focus on new matrices appropriate for three-dimensional (3D) cell culture offers new opportunities to apply polysaccharides as extracellular matrix mimics. However, chemical and structural bases for specific cell-polysaccharide interactions essential for their utility as 3-D cell matrices are not well defined. This review describes how these naturally sourced biomaterials satisfy several key properties for current 3D cell culture needs and can also be synthetically modified or blended with additional components to tailor their cell engagement properties. Beyond their benign interactions with many cell types in cultures, their economical and high quality sourcing, optical clarity for ex situ analytical interrogation and in situ gelation represent important properties of these polymers for 3D cell culture applications. Continued diversification of their versatile glycan chemistry, new biosynthetic sourcing strategies and elucidation of new cell-specific properties are attractive to expand the polysaccharide polymer utility for cell culture needs. Many 3D cell culture priorities are addressed with the portfolio of polysaccharide materials available and under development. This review provides a critical analysis of their properties, capabilities and challenges in 3D cell culture applications.

[1] Reprinted with permission from Biomaterials: Diekjürgen, Dorina and Grainger, David. Polysaccharide matrices used in 3D in vitro cell culture systems, 2017

Introduction

Three-dimensional (3D) cell culture has many known research benefits compared to normal conventional two-dimensional (2D) cell culture [14, 15, 19, 21]. One commonly observed difference is the change in cell morphology witnessed across diverse cell types: cells seeded in 2D grow flat and widely spread, eliciting a forced, apical-basal polarity; this lacks requisite support to grow in a vertical dimension [21]. While this is normal behavior for some cell types (e.g., epithelial cells), other cells (e.g., mesenchymal cells) grow in a stellate manner in 3D matrices, polarizing simply for migration purposes [21, 140]. Cells forced unnaturally into artificial morphologies can exhibit altered functions and phenotypes [21, 141]. Major differences can be seen in gene and protein expression, viability, enzymatic and biological activities, differentiation and proliferation, motility, and general response to stimuli and metabolism.

The majority of cells functioning in the native in vivo environment are integrated within a 3D, hydrated, flexible, porous gel, surrounded by other cells, called the extracellular matrix (ECM) (Figure 3.1). Both technological and scientific objectives attempt to recapitulate native cellular microenvironments to most reliably reproduce cell phenotypes in cultures that best duplicate in vivo behaviors. This has stimulated recent approaches that emphasize a shift away from monocultured cells on rigid plastic plates to novel 3D matrix-based culture systems more similar to actual tissue constructs (i.e., organoids, micro-tissue, spheroids and cell/gels) [103]. These strategies seek to produce and sustain certain cell behaviors and technical performance advantages, compiled in Table 3.1. An overview of commonly used 3D cell culture methods and some examples of commercially available products are provided in Table 3.2.

Scaffold-free culture platforms like spheroids provide no ECM or matrix in culture [27, 28, 30-33]. Therefore, cells must produce and organize their own matrix in these systems. Spheroid cultures have no physical support structure nor porosity, and the overall multicellular spheroid size has a limit of approximately 0.5-0.6 mm [32], whereby size can be adjusted by cell seeding amounts and drop volume. Spheroids are shown to mimic developmental aspects of tissues, tumors, and embryoid bodies, therefore showing physiologic relevance in studies of cancer and stem cells [142]. Given their size and lack of diffusive obstruction, spheroids exhibit metabolic (e.g., via gases,

nutrients, wastes) and proliferative gradients that duplicate some in vivo contexts.

The second 3D culture method comprises physical 3D matrices or scaffolds fabricated from many different types of materials exhibiting different chemistries, porosities, permeabilities, architectures, and mechanical characteristics intended to mimic aspects of native ECM [25, 67]. Scaffolds can be cast or polymerized in the absence or presence of living cells and media, or fabricated from these materials in 3D by techniques like electrospinning, particulate leaching, soft lithography, or bioprinting [25, 43]. Within these matrices that mimic features of native ECM, cells, tissues and organoids are encapsulated in tissue-like microporous, soft 3D structures. This approach seeks to maintain matrix and natural cell-cell communications and differentiated states and cell functionalities. ECM-like architectural, mechanical, and chemical properties (see Figure 3.1) are critical for duplicating natural ECM environmental properties, and often reflect these native scenarios much more than 2D cell cultures [143]. While not all matrices are equivalent in properties or performance, cells are often shown to reflect this 3D ECM context in producing more in vivo-like behaviors; for example more reliable phenotypes to tissues and diseases, and toxicity responses to exogenous compounds [13, 14, 103, 144].

In vitro matrix requirements for 3D cultures

Three-dimensional cell culture models that effectively and reliably produce the cellular advantages of native ECM in vitro require biomimetic scaffold materials and architectures to support cells in appropriate in vivo context. Many different naturally derived and synthetic materials are currently available to mimic select properties of extracellular matrix (ECM) [16, 42, 43, 145, 146]. Despite the plethora of cell culture materials published and their claims to ECM-like fidelity for improved 3D cell culture, few claims are validated beyond isolated examples or select short-term, arbitrary culture conditions, and requirements. Cell culture matrix materials commonly need to be: 1) nontoxic, with high mass fractions of water to produce “soft” mechanical properties, 2) allow free diffusion of nutrients, oxygen, and cell waste products, 3) promote normal cell growth, proliferation, natural cell cycle control, and migration, and 4) preserve cell-matrix physical and chemical engagements to promote specific phenotypic states [67, 147]. As a class of well-studied

biomaterials, hydrogels are attractive for 3D matrix applications, They swell spontaneously in water to high levels without being water soluble, and provide readily chemically modified, cross-linked, hydrated, elastic networks [148, 149]. Historically, 3D culture matrices are physically characterized for gel-like properties and architectures. More relevant 3D culture assessments include specific matrix interactions with cultured cells, drug responses, time-dependent matrix changes (i.e., degradation or cell-induced modifications), and cell phenotypic stability [19]. Furthermore, optical transparency for in situ microscopy and noninvasive optical assays of cell behaviors are also increasingly sought for matrix utility and reporting needs: many cell-based viability, phenotyping and cytotoxicity assays use luminescence or fluorescence signals propagating through optically transparent media. Table 3.3 collates previously formulated requirements for 3D cell culture systems, assembled from diverse literature sources.

One prominent example of a commercially available ECM product for 3D cell culture applications is Matrigel™ (Corning Life Sciences and Becton Dickinson, USA), derived from Engelbreth-Holm-Swarm mouse sarcoma. This natural ECM extract includes growth factors, proteins, and glycoproteins similar to those found in connective tissues [37]. Matrigel™ cultures successfully reproduce useful 3D aspects of many cell types for cell cultures of various applications [77, 79, 109, 150], including developmental biology, epithelial polarization, and tumor invasion and colonization, even moving from 3D tumor culture into immune-deficient rodents xenografts. Its legacy and performance has provided an important benchmark that defines 3D cell culture matrix success as a prototype for synthetic ECM duplication. Nonetheless, Matrigel is a highly heterogenous blend of millions of molecular components of diverse biochemistry. Moreover, significant concerns about Matrigel's batch-batch variability, immunogenicity, pathogen transmission, animal tumor origin, and limited availability at significant cost limit its general use [2, 16]. Other commercial cell culture matrices extracted from natural, living materials are PureCol™, Purematrix™, alginate and Extracel™ [2, 151]. These simpler hydrogel matrices achieve gelation, hydration, and 3D architectures amenable to cell culture by changing aqueous solution temperature or pH, peptide self-assembly or ionic or covalent crosslinking [2]. None, however, intrinsically reproduce all aspects of native ECM, nor of Matrigel, including their molecular complexity. This

then defines the current “designer challenges” for fabricating biologically derived, synthetic, or biohybrid materials for 3D cell culture. *Significantly, what is required compositionally for a minimally competent ECM mimic for cell culture currently lacks a detailed recipe.*

Advantages and disadvantages of currently used natural polymer matrices in 3D cell culture systems are summarized in Table 3.4. Known deficiencies of most 3D culture systems to date are recognized to include suboptimal 3D matrix compositions for recapitulating precise ECM structure-function relationships in 3D, suboptimal support of specific cell type(s), lack of rigorously determined or defined matrix compositions or requirements, complex materials origins with lot-to-lot variability or residual animal-derived components and cytotoxic degradation products. Therefore, while many naturally derived complete ECMs apparently recapitulate essential features for 3D cell cultures, reproduction of precise molecular and microstructural features essential to reproducing these features in simpler materials systems are not well described. For example, ECM is well-known to universally comprise networks of many matricellular proteins, diverse growth factors (morphogens and mitogens), and several glycosamino- and proteo- glycans. Compositional roadmaps for 3D culture matrices are proposed based on this analysis. Yet what from ECM is essential and minimally defining for 3D cell culture remains confusing: many isolated components (e.g., hyaluronan, collagen I, laminin, heparin sulfate, among many others) can each support aspects of 3D cell culture. Analogously, the micro-architectural and mechanical properties for native ECM are known in many regards. However, how to control this in vitro, and how finely it must duplicate ECM in a synthetic 3D matrix to be effective for culture are not possible currently. These criteria collectively represent critical benchmark design criteria for fabricating effective 3D cell culture materials.

Precise mimicry of the exact native ECM structure and biochemistry may not in fact be necessary for many aspects desired for faithful 3D cell culture. Hence, a more pragmatic, cell line-dependent and outcome-related, biomimetic approach may lie in satisfying only selective cell culture needs to guarantee cell qualities sufficient for certain research needs [2]. For example, type I collagen has a substantial history in 3D cell culture and tissue engineering efforts [152], despite the observation that it represents only one of many matricellular components of native ECM [43,

153-155]. Other materials such as alginates [156-159] and self-assembling synthetic peptides [160-162] bear little resemblance chemically to native human polymers or ECM, yet produce hydrogel materials with substantial practical 3D culture value. It is essential to distinguish what is necessary versus what is sufficient in ECM structure and function to adapt for 3D culture use. For example, native ECM proteoglycans present their glycosaminoglycans (e.g., dermatans, heparans, chondroitins) in a bottle-brush morphology, covalently attached and extended from a protein core. Classical use of glycosaminoglycans in 3D cultures to date, does not exploit ECM proteoglycan chemistry or morphology. Instead purified, homogeneous glycan polymers lacking protein cores are used as matrices.

Defining minimally acceptable performance requirements for these cell culture materials requires assays and assertions for equivalence and validation in the context of a specific 3D culture application. As long as this technical vetting is thoroughly performed using prescriptive requirements and technical criteria, and with logical connections between desired in vivo cell behavior and their in vitro equivalence in culture, many biomaterials may qualify as valuable 3D culture materials. Future studies must assert these qualities and seek to converge on common, accepted consensus 3D matrix standards for matrix qualifications and necessary validation.

Cell-specific polysaccharide binding

ECM, with its many (>300) matricellular proteins, is well-recognized for cell-specific recognition and cell receptor-specific binding of selected protein chemistries and peptide motifs, typically involving primarily integrins, but also membrane glycoproteins, proteoglycans and glycolipids,[163-166]. Cell receptor engagement with specific ECM ligands is well recognized to modulate and control cell signaling, phenotypic fate, differentiation potential and functional fidelity [167, 168]. By contrast, glycosaminoglycan network engagement with many ECM proteins (e.g., laminins, collagens, and fibronectins) is ubiquitous and essential to normal chemical and physical ECM involvement with cells. Nonetheless, despite specific matricellular protein-glycan interactions, specific receptor-ligand motifs and signaling functions from cell receptor-glycan ligand binding is less described compared to ECM protein analogs. Many polysaccharides are not known to have

specific receptor engagements with mammalian cells (e.g., alginates [169]; and agarose [67, 170]. Reasons for their empirical acceptance as 3D materials are largely physical, not biochemical. Beyond more generic hydrogel properties, molecular design features in the chemistry of many polysaccharides that convey useful 3D cell culture engagement is not that obvious. Hence, custom synthesis efforts require improved structure-activity relationships to rationally pursue ECM 3D material mimics.

Polysaccharides used in 3D culture systems

Due to the extensive use of diverse polysaccharide and glycan-based materials in 3D cell culture, both historically and presently, full review of their documented vetting in 3D cell culture applications and their recognized matrix properties in vitro is provided here.

Generally, polysaccharides are biopolymers comprising multiple saccharide units in covalently linked chains. Each polysaccharide has between 10 to 10 million monosaccharide units connected by O-glycosidic bonds [171, 172]. Based on their diversity, polysaccharides can be divided into 1) homopolysaccharides containing only one kind of monosaccharide repeat unit, and 2) heteropolysaccharides, having 2 or more different monosaccharide repeats linked in the polymer. Polysaccharides form either linear or branched structures; branched structures can vary from multiple short side chains to just a few, long side chains or also bush-like highly branched structures [173, 174]. Overall, more branched polysaccharides are known than linear polysaccharides but on a mass basis, linear polysaccharides dominate natural sources as they are important structural components for higher plants and marine algae.

Polysaccharides are also called “glycans” and their systematic nomenclature is based on that term. Nevertheless, multiple polysaccharides were named before systematic nomenclature was invoked and therefore do not follow these rules in recognized, common naming conventions. Examples include celluloses, hyaluronic acids, heparins, and alginic acids.

Many mammalian polysaccharides are also only found chemically attached to core proteins. These complexes are called protein-polysaccharides or glycoproteins [175]. A subgroup of the glycoproteins of animal origin and high glycan mass fraction are the proteoglycans [176]. For

polysaccharides produced by bacteria, two more classifications are used as they are either derived from their cell walls (in capsules, hence capsular polysaccharides) or excreted into extracellular medium (exopolysaccharides) [172].

In general, natural polysaccharides are polydisperse, meaning that their molecular weight from a single source varies. Additionally, their finer molecular structure and monomer sequences varies from molecule to molecule, making them polymolecular. Polysaccharides with regularly repeating single saccharide units (i.e., homoglycans lacking polymolecularity) are typically bacterial in origin, with the exception of cellulose, and a few other plant polysaccharides. Overall, the structure of polysaccharides is highly influenced by the growth conditions and taxa, and can vary even between tissues of the same plant [172]. All polysaccharides are solvated by water and can be depolymerized by acids and heat, high pH followed by oxidation and specific enzymes [172].

At least 90% of all carbohydrates found in nature reside in polysaccharides. Polysaccharides serve various diverse biological functions, but with many still unknown: they are structural components in primary and secondary cell walls and middle lamella, and serve as reserve food material in leaves, stems, roots, seeds, and other plants tissues. In bacteria they can be extracellular constituents [172]. Polysaccharides used for food or nonfood industrial applications and commercially available are also called hydrocolloids or gums [177]. As no ideal system exists for classification of polysaccharides, those industrially used are classified by source [172, 173]. Some polysaccharides can form gels alone, while others require additional substrates or co-additives to gel. This review focuses on polysaccharides that form gel matrices useful for 3D cell culture.

Polysaccharides used currently in 3D cell culture systems

Alginate (algal/seaweed-derived polysaccharide). Alginate refers to alginic acid and its derivatives/salts, a natural polysaccharide extracted from the cell walls of brown algae (*Phaeophyceae*). Commercial harvests of alginate, commonly exploit *Laminaria, Macrocystis, Lessonia, Ascophylum, Durvillea, and Ecklonia* algae. Alginate comprise two saccharides monomers: β-(1-4)-D-mannuronic acid and α-(1,4)-L-guluronic acid, connected as linear chains in

blocks of D-mannuronic acid repeats and blocks of L-guluronic acid repeats (Figure 3.2). These blocks form a folded structure that plays an important role in alginate gelling processes. Gels formed from alginate with high D-mannuronic acid contents have high flexibility but poor rigidity, while gels from high L-guluronic acid contents are much more rigid. By adjusting the polysaccharide ratio of these blocks, gel properties can be adjusted as well. Alginate gels can be somewhat modified and controlled by different molecular weights, concentration and composition [178]. Alginic acid and salt derivates from polyvalent metal cations (e.g., calcium ions) are insoluble in water, with the exception of magnesium salts. Sodium, potassium, and ammonium salts are water-soluble, while sodium alginate is the most used derivate. Alginates degrade through heat, oxygen, and metallic ions, with their stability decreasing from sodium alginate to ammonium alginate to alginic acid. Bouhadir et al. developed a biodegradable alginate by partial oxidation. Modified alginate macromers provided controlled gel degradation by their degree of oxidation [179]. Alginate has many different uses in food and pharma industry, but the controlled drug release field takes much advantage of this material as well as numerous cell culture studies [157-159, 169, 180, 181].

Alginate will gel spontaneously in situ if divalent cations are present [19, 178, 182]. The cations bridge and electrostatically shield the electrostatic repulsion of repeated monomer carboxylate groups [183-190]. Divalent cations facilitate gelation more than monovalent cations [182, 188, 190]. These alginate hydrogels can be redissolved in the absence of cations, leading to unpredictable and uncontrolled network dynamics in cell media conditions, but chemical degradation is generally not observed in physiological conditions [148].

Alginate hydrogels intrinsically lack cell adhesion capability, and have low serum protein absorption so that cells can be encapsulated within gels but do not spread, move, or undergo haptotactic responses typical of cells in ECM [157-159, 169, 178, 191]. Multiple different approaches are employed to overcome these cell culture limitations. To improve alginate-cell engagement, Mooney's group incorporated the well-known cell adhesion peptide, RGD, into the alginate network [169, 192] and Balakrishnan et al. incorporated gelatin [193]. Gelatin-incorporated alginate hydrogels degraded after 5 weeks in phosphate buffered saline (PBS) solution and were used to encapsulate hepatocytes. Increased albumin secretion in culture confirmed hydrogel

support for cultured hepatocytes [193]. The RGD peptide-incorporated alginate was further studied as a potential scaffold for skeletal muscle engineering [194]. Another study used light-sensitive liposomes that release calcium chloride to trigger gelation of the alginate hydrogel with optical triggers [195]. Light-activated gelation was then used to encapsulate bone marrow cells from rats [196]. Alginate has been exploited as an injectable cell delivery vehicle [197, 198] and alginate gel beads were used to transplant chondrocytes [199, 200], hepatocytes [201] and islets of Langerhans [156]. In several studies alginate hydrogels have been mixed with chondrocytes and then been injected or formed into an implantable scaffold for cartilage treatment [197, 200, 202, 203]. Pangas et al. showed that reproductive follicles encapsulated in an alginate in vitro in culture were able to develop normally and could be fertilized [204]. A recent study used sulfated alginate hydrogels as well as sulfated alginate microspheres to culture human chondrocytes, showing suppressed inflammatory cytokine (e.g., IL-1β, TNF, IL-6, IL-8, MIP-1α) production from this protective microenvironment for encapsulated chondrocytes [205, 206]. Gel anti-inflammatory properties were noted in addition to increased gel stability and gel network swelling [205].

Alginate hydrogel is also commercially available under the brand name AlgiMatrix™ by Life Technologies [207] and NovaMatrix ®-3D (www.novamatrix.biz) [208], as well as alginate-coated core magnetic beads under the name GEM™ (Global Cell Solutions). Godugu et al. used previously lyophilized, sterile AlgiMatrix™ scaffold plates to develop a 3D lung cancer model and tested different chemotherapeutics on different types of stem cells seeded into the AlgiMatrix™ scaffold [209]. Their results showed that the 3D cultured cells were more resistant to the drugs tested, and therefore, this system exhibited a high potential for further drug screening and evaluation of chemotherapeutic drug activity [209]. Global Cell Solutions developed beads that exploit the highly anionic alginate core but combined with a gelatin coating to enhance cell adhesion. The beads also consist of a magnetic core, which is beneficial for downstream applications (e.g., separations and collection for media changes) [39]. Mellor et al. used these beads to successfully culture primary chondrocytes in a rotating wall vessel bioreactor and found that cells better maintained their phenotypic morphology as well as gene expression patterns [210].

Overall, alginate hydrogels have a substantial record in cell culture gels as a transparent,

nontoxic, relatively biologically inert substrates. It can be further modified with specific cell reactivity based on culture needs. Its optical transparency is well-suited to ex situ interrogation by microscopy and other optical reporting assays on cell phenotyping and metabolism. Gelation under mild conditions in the presence of culture media, assay reagents, and living cells is a primary attraction. Additionally, gel stiffness is important to control, and cells must be recovered from within the gel when required. Endotoxin and residual protein contaminant removal is also required for all polysaccharides obtained from natural sources and fermentation cultures. Alginate purity has high batch-to-batch variation that makes it necessary to test and characterize every batch [157]. Otterlei et al. show that alginates high in D-mannuronic acids are immunogenic and have an increased ability to induce cytokine production compared to alginates with high L-guluronic contents [211]. Zimmermann et al. reported in contrast that they found no immuno-response to alginates [212]. Different study conclusions reflect differences in cellular response to alginates, depending on the purity, and underscore the necessity of more standardized approaches for impurity removal and characterization to verify batch materials cell culture requirements [157, 213-215].

Carrageenan (algal/seaweed-derived polysaccharide). Carrageenan is the collective term for a group of linear, anionic hydrocolloids extracted from *Rhodophyta* marine plants, namely *Gigartina, Eucheuma, Chondrus, Iridaea, and Hypnea*. As an algae cell wall extract and intercellular matrix, depending on the sourcing species, different carrageenan types are produced. Chemical structures of the different carrageenans (shown in Figure 3.2) differ as do the resulting properties. All carrageenans are formed by alternating repeats of D-galactose and 3,6-anhydro-galactose connected by α-1,3 and β-1,4-glycosidic linkers. Primary carrageenan differences are both the position and number of ester sulfate groups and amounts of 3,6-anhydro-galactose. Increased ester sulfate groups reduce the solubility temperature and gel strength. The three main types of carrageenan are κ-carrageenan (25-30% ester sulfate and 28-35% 3,6-anhydro-galactose), ι-carrageenan (28-30% ester sulfate and 25-30% 3,6-anhydro-galactose) and λ-carrageenan (32-39% ester sulfate and no 3,6-anhydro-galactose). Thermo-reversible gels are formed in the presence of potassium ions (κ-carrageenan) and calcium ions (ι-carrageenan), respectively, by forming double helix cationic-bridged structures. κ-carrageenan produces rigid and brittle gels with

a high gel strength and syneresis, while ι-carrageenan gels are elastic and thixotropic, showing no syneresis.

Carrageenans differ from other hydrocolloids in their substantial interactions with milk proteins. This is based on strong electrostatic interactions between the positively charged casein protein in milk and carrageenan negatively charged ester sulfate groups. Additionally, carrageenan ester sulfate groups form links with protein acidic amino acid carboxylate groups. This interaction is a function of temperature, pH, type of protein, and carrageenan concentration [216].

Carrageenan's mild gelation properties make them interesting candidates for 3D cell culture. The thixotropic behavior of κ-carrageenan makes it relevant for injectable matrices for cell delivery [217-219] and inclusion of other macromolecules [220, 221]. Challenges with high gel swelling ratios and stability issues in physiological conditions are overcome by different approaches, like mixing with other biopolymers [217, 222-224], adding photo-cross linkers [225] and polyelectrolyte complexation [226]. Combinations of κ-carrageenan and chitosan influence cell viability and behavior [227-230]. Mihaila et al. tried using κ-carrageenan fibers produced by ionotropic gelation followed by chitosan polyelectrolyte complexation to increase fiber stability, incorporating these enforced fibers into a hydrogel and applying these constructs for micro-vascularized bone tissue engineering applications [230]. A similar approach was used for encapsulating chondrocytes in alginate-carrageenan beads and fibers [217]. Rocha et al. used carrageenan-based hydrogels to successfully encapsulate human adipose-derived stem cells in combination with transforming growth factor-β1, observing cultured cell differentiation to cartilage phenotypes [231].

Agar (algal/seaweed-derived polysaccharide). Agar, also called agar-agar, is a galactose polymer derived from the cell walls of agarophytes algae, more precisely *Rhodophyta*. Commercially relevant species are primarily *Gracilaria, Pterocladia, Gelidiopsis. and Gelidium*. Agar comprises mixtures of different polysaccharides, with agarose and agaropectin as primary components (Figure 3.2). Agarose serves as agar's gelling fraction, forming aggregates of double helices to form 3D structures. Agaropectin is the nongelling fraction and consists of agarose with different percentages of ester sulfate, D-glucuronic acid, and pyruvic acids. The ratio of agarose

and agaropectin varies depending on algae species but most are at least two-thirds are agarose.

Agar-agar's gelling strength is high even at very low concentrations, holding about 20 times its own weight in water, forming gels that are thermos-reversible. It is insoluble in cold water while soluble in water and other solvents at 95-100°C. The gel point is around 32-34°C and the melting point from a formed gel is approximately 85-95°C. Agar's thermal reversible hydrogels formed with agarose can be controlled by using different agarose concentrations. This then leads to different gel pore (mesh) sizes.

Dillon et al. found that large gel pore sizes combined gel softness enhances neurite cell growth, migration, and proliferation [232]. Another effort incorporated chitosan to agar to show that this modification significantly improved neurite growth [233]. A different approach increased gel cell interaction by adding a common cell adhesion peptide [234]. Agar is also applied as an cell adhesion-preventing surface coating used in spheroid in vitro culture models [19]. Agar is commonly used as a media in microbiology bacterial cultures, as well as in the food industry and used intensively in pharmaceutical products as laxatives, drug carrier and suspension or stabilizing substrate in solutions [216].

Dextran (microbial-derived polysaccharide). Dextrans are exopolysaccharides with a high molecular weight from ≥1000 Da and consisting only of glucose repeat units (Figure 3.3) [172]. These homoglycans are extracted from extracellular matrices of bacterial strains including *Leuconostoc mesenteroides, Lactobacillus brevis, and Streptococcus mutans*. Dextran secretion is used by bacteria to form biofilms or also protective microbial coatings [235, 236].

Dextrans are divided into three classes depending on their structure. Class 1 dextrans like the oligosaccharide, isomaltose, have a α-1,6-linked-d-glucopyranosyl backbone modified with small α-1,2-, α-1,3-, or α-1,4-linked side chains of D-glucose branches. This dextran varies in molecular weight, degree and type of branching, length of branch, and spatial arrangement with their microbial producing strain and culture conditions [237-241]. Class 2 dextrans are also called alternans and have an alternating α-1,3- and α-1,6- linked d-glucopyranosyl structure with α-1,3-linked branches. Class 3 dextrans are called mutans and their backbone consists of consecutive α-1,3-linked d-glucopyranosyl elements with α-1,6- linked branches. The dextran pyranose ring is

the key structural unit for controlling chain elasticity based on a force-induced elongation and a conformation transition from chair to boat-like repeat unit structure. Dextrans can thereby withstand mechanical stress and play an important role in ligand binding modulation in biological systems [242]. All dextrans are highly soluble in water and behave like Newtonian fluids [243].

Van Tomme at el. developed and analyzed a dextran hydrogel comprising dextran microspheres modified with either dimethylaminoethyl methacrylate or poly(sodium methacrylate). Negatively and positively charged particles form gels that useful for encapsulation of proteins and/or cells [244]. A methacrylate and lysine-functionalized dextran combined with gelatin forms a hydrogel for smooth muscle cell culture, with a mechanical stiffness and amount of swelling dependent on the amount of functionalized groups added to the dextran and the dextran/ gelatin ratio. Softer gels of this dextran derivative promoted rapid cell spreading and formation of cellular networks [245]. Commercially available dextran-based beads are sold as Cytodex (GE Heathcare).

Xanthan gum (microbial-derived polysaccharide). Xanthan gum is a natural extracellular, high molecular weight polysaccharide (300-8000 kDa) produced by *Xanthomonas campestris* bacteria. Xantum gum has a β-1,4-d-glucose backbone with a β-D-mannopyranosyl-(1,4)-β-D-glucuronopyranosyl-(1,2)-6-O-acetyl-α-D-mannopranosyl trisaccharide branch on every other glucose unit (α-1,3-linked) (Figure 3.3). Additionally, ~50% of the terminal mannose units form a ketal with the 4,6-hydroxyl groups and pyruvic acid. Xanthan gum is polyanionic from acetic and pyruvic acid groups [246-250]. The amount of pyruvic acid influences the viscosity of xanthan gum solutions and varies by *Xanthomonas campestris* strain. High concentration xanthan gum solutions exhibit weak gel-like properties [251, 252].

Mendes et al. used a novel micro-droplet generator to form microcapsules (average diameter 500 μm) of xanthan gum-encapsulated chondrocytes. Cells remained viable and proliferated for 21 days with enhanced metabolic activity [252]. This group was also able to create a matrix consisting of xanthan gum and cationic multidomain peptides, using this 3D environment to encapsulate chondrocytes and showing their viability and proliferation over 21 days [162].

Gellan gum (microbial-derived polysaccharide). Gellan gum is a linear anionic extracellular polysaccharide produced by microbial fermentation of *Sphingomonas paucimobilis*.

The polymer is a tetra-saccharide repeating unit of β-1,3-D-glucose, β-1,4-D-glucuronic acid, β-1,4-D-glucose, and α-1,4-L-rhamnose, also including one carboxyatel side group (Figure 3.3) [253, 254]. Two different forms of gellan gum are used: the acetylated gellan gum that forms soft and elastic thermoreversible gels, and the deacetylated form forming hard and brittle thermoreversible gels [183, 255]. While gellan gum exists in coil form at high solution temperatures, it transitions into a double-helix form when temperature decreases. At that transition point, so-called junction zones form by creating oriented bundles of antiparallel aligned double helices. Finally, links between these junction zones and extended helicial chains of coiled polysaccharide chains form and facilitate gel formation [184]. These gel junctions provide heat resistance, withstanding up to 120°C before unfolding [188]. Consistent with previously mentioned alginate gelation and in general with all glucuronic-containing polysaccharides, stable gellan gum gels require cations in solution, as the cations bridge and electrostatically shield anionic carboxylate groups [157, 169, 182-190].

Gellan gum crosslinked with cations created self-supporting hydrogels by simply mixing gellan gum and alpha-modified minimum essential cell culture medium. This allowed direct encapsulation of rat bone marrow cells within the gel, showing viability for 21 days [256]. Oliveira et al. used gellan gum to create hydrogel disks with encapsulated human nasal chondrocytes in the context of cartilage regeneration, showing that cells remained viable in culture for 14 days [257].

Pullulan (microbial-derived polysaccharide). Pullulan is an exopolysaccharide produced by fermentation by the fungus *Aureobasidium pullulans* [258]. These intracellular homoglycans are linear, neutral, nontoxic, noncarcinogenic, and ostensibly hemocompatible, consisting of α-1,6- and α-1,4-glucosidic-bonded glucose repeat units (Figure 3.3) [259-261]. This unique α-1,6 to α-1,4 interchanging maltotriose pattern endows pullulan with useful physical properties: biodegradability, high adhesion, fiber formation, solubility, and structural flexibility [259, 260, 262]. Even though it is considered primarily as a maltotriose polymer, pullulan can also consist of panose or isopanose subunits [260]. Dry pullulan powder can easily be dissolved in cold and hot water [260]. Depending on fermentation conditions, pullulan molecular weight varies between 10-2000 kDa [177, 263].

Autissier et al. created a transparent pullulan gel by crosslinking aqueous pullulan solutions

with sodium trimetaphosphate. Resulting gels exhibited higher than 90% water content [264]. Seeded with rabbit vascular smooth muscle cells, gels were monitored for growth and proliferation for 7 days [264]. Bae et al. developed a pullulan methacrylate hydrogel controlled by the degree of methacrylation and polymer concentration. They then encapsulated NIH 3T3 fibroblasts and HepG2 cells and reported cell proliferation and organization into cell clusters, but no cell elongation. By incorporating gelatin methacrylate into these gels, they reported enhanced cell morphological behaviors and elongation [263]. Fricain et al. developed a hydrogel consisting of nano-hydroxypatite pullulan/dextran and encapsulated human bone marrow stromal cells in cultures for up to 21 days [265]. Bulman et al. reported that the retention of MSCs on the fibrillated surface of osteoarthritic articular cartilage is highly improved by using pullulan and that the transmembrane Dectin-2 C-type lectin complex expression is upregulated [266].

Cellulose (plant-derived polysaccharide). Cellulose is the main component of higher plant cell walls and most abundant organic compound on the planet [172, 267-270]. Cellulose is also found in algae (brown, red, green) and some fungi, and excreted extracellulary by some bacteria. Cellulose polymer consists only of (1,4)-β-D-glucopyranosyl repeat units representing a homoglycan with just one type of linkage (Figure 3.4). It is partially crystalline with high molecular weight. Additionally, so-called hemicelluloses comprise all other polysaccharides in which cellulose is mixed as found in primary and secondary cell walls. Hemicellulose is like the name implies: similar to cellulose. However, this is true only for its physical properties and not structural properties. While cellulose is a homo-glycan, hemicellulose polysaccharides are mostly hetero-polysaccharides, with the exception of β-glucans and some polysaccharides consisting of D-xylose. Hemicellulose can be linear or brush-like with many branches [172, 271-276].

Cellulose can be made thermoresponsive by transforming it into cellulose ethers, namely methyl cellulose, hydroxypropyl cellulose, and hydroxymethyl propyl cellulose [277, 278]. The induced hydrophobic zones from alkoxy ether modifications are needed to create hydrogels by thermal dehydration [278]. These materials have substantial biomaterials use, including gelation and cell culture. Bhattacharya et al. used nanofibrillar cellulose hydrogels to culture human hepatic progenitor HepaRG and HepG2 cells with added bioactive components. While they observed no

cytotoxicity, nonexponential growth of the cells was described, contrasting normal standard cell culture exponential growth in 2D plasticware cultures [279]. This was supported by mRNA expression showing changes in hepatocyte markers and improvements in their 3D model over normal 2D hepatocyte cell culture [280]. Recently, nanofibrillar cellulose hydrogels were used for culturing human pluripotent stem cells. Cell cultures over 26 days with expression of important cell markers were reported [281]. A different approach to use cellulose material in cell culture was pursued by Derda et al. who seeded cells on cellulose paper sheets and stacked these as seeded layers in cultures. Cellulose stacks created a cell-seeded gradient for HS-5 cell motility monitoring [282]. Modulevsky et al. found that three different mammalian cell types (mouse NIH3T3 fibroblasts, human HeLa epithelial cells and mouse C2C12 myoblasts) proliferated normally, produced distrinct actin stress fibers (a morphological characteristic of substrate-adherent cells) and remained viable in 3D cellulose scaffolds derived from decellularized apple hypanthium tissue for up to 12 weeks [283]. Overall, the natural porosity and ability to modify cellulose mechanical properties as well as the ease of production of these materials as scaffolds makes cellulose a promising biomaterial for 3D cell culture systems. A commercially available cellulose-based hydrogel is GrowDex® (UPM Biochemicals).

Pectin (plant-derived polysaccharide). Pectins can be found in the middle lamellae and in primary cell walls of plants. They are especially abundant in fruits and vegetables [177]. Pectins can exhibit more complex structures with different types of polysaccharide chains in a single molecule [272]. The primary structure of pectins, also called rhamnogalacturonans, comprises α-D-galacturonopyranosyluronic acid sequences, but other monosaccharides have also been found (Figure 3.4) [172]. Pectins are mostly water soluble and exist as anionic random coil confirmations in solution with some rigidity [177]. The anionic chemical structure of pectin is similar to alginate, and therefore the viscosity of pectin solutions can be also increased by adding polyvalent cations to the solution, producing ionic bridging across accessible pectin carboxylate groups, and therefore chelated pectin hydrogels [284].

Munarin et al. used pectin either with or without added RGD oligopeptides to encapsulate MC3T3-E1 preosteoblast cells. In both cases, cells maintained constant viability and differentiation

for 29 days. In RGD-containing pectin cell adhesion and proliferation was improved [285]. Promising results were also seen for preosteoblasts growing out from the gel microspheres, expressing their own extracellular matrix [285]. Embedded human mesenchymal stem cells in both pectin variations are comparable to results from the first study: the cells in pure pectin stayed in round-shaped and isolated, while cells in the RGD-modified pectin hydrogel spread, established cell-to-cell contacts and migrated out while producing their own extracellular matrix [286].

As pectin is similar to alginate in many properties, it is also nontoxic and biocompatible after removal of impurities. Additionally, pectin gel networks can degrade under physiological conditions based their hydrophilic nature, yielding a benefit (e.g, short-term cell delivery) or downside (e.g., long-term 3D cell culture matrix stability issues). Currently, no ultrapure pectins are commercially available and therefore purification steps to remove impurities (e.g., proteins, endotoxins) are needed.

Starch (plant-derived polysaccharide). Starch is the main energy-storage carbohydrate form in higher plants, and second most abundant carbohydrate after cellulose [287-289]. In addition to being the energy-storage form for plants, starch also serves as an energy source for animals when consumed (i.e., supplying about 70% of human caloric intake) [172]. The unique aspect of starch is that it is naturally produced as dense and insoluble granules that include two polysaccharides: amylose, a linear polysaccharide composed of α-1,4-linked D-glucopyranose, and amylopectin, a highly branched polysaccharide of α-1,4-linked glucose segments with α-1,6-linked branch points (Figure 3.4). The ratio of these two varies by plant source but commonly starch comprises 20-25% amylose and 75-80% amylopectin [290]. Amylose is the gel-forming part of starch. To form hydrogels aqueous starch solutions must first be boiled and gelation occurs spontaneously through reassociation of solubilized starch polymer chains upon cooling. In contrast to cellulose gels, starch gels have a high nutritional energy and can be easier degraded [283].

Gomes et al. compared two starch-containing scaffolds under static and flow conditions: 1) an extruded hybrid of starch with ethylene vinyl alcohol copolymer, and 2) a combination of starch and polycaprolactone obtained by a fiber bonding process. After seeding rat bone marrow stromal cells in both matrices under both conditions, they showed that static conditions led to cell

monolayers while flow conditions distributed cells throughout the scaffold that differentiated better. The cell distribution was increased in the starch-polycaprolactone scaffolds over the starch-ethylene vinyl alcohol scaffolds, likely due to limited pore interconnectivity in the latter scaffolds [291]. These starch polycaprolactone scaffolds were then used to grow human umbilical vein endothelial cells after argon plasma treatment. Cells adhered, proliferated, maintained morphology and remained viable for the 7-day study period, behaving much the same as cells on adhesive protein precoated scaffolds [292]. Liau's group crosslinked poly(vinyl alcohol) and starch to form a scaffold polymer for fibroblast 3D culture. Scaffolds of different composition supported differing fibroblast growth and different extents of degradation over 3 days of culture [293].

Chitin and Chitosan (fungal, insect and crustacean derived). The only naturally occurring cationic polysaccharides are chitin and chitosan. Chitin is found in primary cell walls of certain fungi and a major structural component of insect and crustacean exoskeletons [294]. Both are structurally closely related to cellulose, consisting of 1,4-linked-2-acetamido-2-deoxy-β-D-glucopyranosyl (N-acetyl-β-D-glucosaminyl) units (Figure 3.4). Both are therefore poly-β-1,4-glucosamines that only differ in their respective degrees of acetylation at the sugar C2 position. Chitin forms fibrils and is water-insoluble despite its cationic nature. Most often chitin is bound to protein, existing as a proteoglycan [172].

N-acetyl groups are removed (deacetylated) after treating chitin with strong alkali, and converted to amino groups. This process yields chitosan, the more cationic deacetylated derivative of chitosan, and water-soluble under diluted acid conditions (< pH 6) [148]. As deacetylation is rarely complete, chitosan is often a copolymer of (deacetylated) glucosamine and natural intact N-acetylglucosamine units. Given its amine pKa ~ 6.5, chitosan is partially cationically charged under physiological pH conditions. Chitosan however can form physically cross-linked hydrogels with added polyvalent anions (e.g., citrate, phosphate) and transition metal cations, and also through careful treatments with base that convert some charged groups to neutral more hydrophobic, self-associating strands. Additionally, chitosan can form thermo-irreversible gels via chemical and enzymatic reactions, or by additions of large organic counterions, and can be used for cell encapsulation in their natural environment [177, 295]. After chitin deacetylation, the resulting

chitosan has a high homology to mammalian polysaccharides, with good biocompatibility and low toxicity, making it an interesting matrix for cell encapsulation [296, 297]. Changing the degree of chitosan deacetylation alters the chitosan matrix properties at physiological pH, changing degradation times from lysozyme-mediated hydrolysis [298], and altering cell adhesion properties [148, 299].

The lack of endogenous chitin or chitosan production in mammalian cells makes these polymers potential targets for innate immune system recognition. Both chitin and chitosan particles are readily phagocytosed [300, 301], supporting their possible recognition via specific cell receptors mediating phagocytosis, but putative receptors that induce these phagocytic responses are not yet identified. Certain cell proteins are known to exhibit affinities for chitin or chitin oligosaccharides, including intestinal FIBCD1 [302]; NK cell-specific NKR-P1 [303]; and RegIIIγ, a secreted C-type lectin [304]; and galectin-3, a lectin with affinity for β-galactosides [301, 305]. Their roles as a chitin-specific receptor as opposed to a protein that binds chitin have not been delineated.

Due to both polymer amino and hydroxyl groups, chitosan offers many approaches for potential modifications to increase or optimize cell culture usage. Yeo et al. modified chitosan with photo-reactive azido benzoic acid groups to create a photopolymerizable macromer that formed azo crosslink after UV exposure [306, 307]. This was exploited to encapsulate cardiomyocytes and myoblast cells after additional incorporation of RGD to the photopolymerizable chitosan [307]. A different study added polylysine to the chitosan backbone and was better able to grow neural cells within it and show neurite extension growth [308]. Other approaches to increase its cell-specific acceptance include adding sugar residues like fructose and galactose to successfully culture hepatocytes [309, 310] or blended composite proteins like collagen, albumin and gelatin for neural cells [311]. The creation of methylpyrrolidinone-derivatized chitosan facilitated bone formation studies in vivo [312]. Chitosan fibers and 3D fiber meshes were produced by wet spinning [313] and electrospinning [314] and tested for tissue engineering applications. Fukuda et al. used a photocrosslinkable chitosan hydrogel to co-culture different cell types to better mimic the natural environment of cells by allowing both 3D environment and multiple different cell types [315]. Also cytotoxicity studies have been reported using chitosan 3D scaffolds [315, 316]. To increase

chitosan scaffold properties and cell acceptance even more, two efforts have combined chitosan with chondroitin sulfate, gelatin and/or dermatan sulfate [317, 318]. A similar approach used a blend of chitosan and collagen to create a lyophilized scaffold capable of culturing 4T1 cancer cells. Comparisons of cells between 3D and 2D plate cultures showed slower proliferation rates and enhanced cell resistance to chemotherapeutic drugs and x-ray irradiation in 3D scaffolds [319]. Cho et al. developed a thermo-reversible glycol chitosan hydrogel which allowed them to form consistent cell-containing gel spheroids that maintained their shape and cellular functions as well allowing cell retrieval without enzymatic digestion, a benefit to cell quality as the method avoids cell surface protein degradation by trypsinization that produces phenotypic problems [320].

Glycosaminoglycans used in 3D cell culture systems

Glycosaminoglycans (GAGs) are specific polysaccharides comprising only 2-amino-2-deoxy sugar units. With the exception of hyaluronic acid, glycosaminoglycans are covalently bound to proteins to form proteoglycans [321-324]. GAGs are prominently featured side chains in extracellular matrix proteoglycans and connective tissue in mammalian tissue, and are integral in forming the extracellular macromolecular framework [172, 325]. Based on their strong negative charge density arising both from their carboxylate and sulfate groups, and glycosidic linkages, GAGs form extended anionic helices with the ability to extend and occupy large, hydrated polymer domains [326]. Additionally, they can bind and hold cations [325]. Proteoglycans play important roles in homeostatic and physiological processes like inflammation and immune response [172]. Actually many diseases (e.g., some kinds of cancers and Alzheimer's disease) are related to changes in biosynthesis and processing of proteoglycans [327, 328].

Chondroitin sulfate (animal-derived polysaccharide). Chondroitin sulfates have repeating units of disaccharide units: D-glucuronic acid and 2-acetamido-2-deoxy-D-galactose, also called N-acetylgalactosamine (Figure 3.5). Chondroitin sulfate is glycosidically linked by a D-xylopranosylserine to the core protein to form the proteoglycan. These proteoglycans are mainly present in cartilage and intervertebral disc tissue but also in other varieties of mammalian tissues. Mammalian chondroitin sulfate is stored in mast cell granules [172, 325]. Chondroitin sulfate

classification is based on the sulfate group location and content, and this composition depends on the chondroitin sulfate source organism [329].

Chondroitin sulfate was synthetically modified with methacrylate groups to make it photocrosslinkable and to control resulting hydrogel properties through methacrylate group density and polymer concentrations. Independent of this modification, chondroitinase enzyme can still degrade the hydrogel [330, 331]. These chondroitin sulfate hydrogels were used both for direct chondrocyte encapsulation [332], and also as an adhesive to attach encapsulated chondrocyte scaffolds to host tissue surfaces [333]. As with chitosan, multiple approaches exist to improve cell-matrix interactions by combining chondroitin sulfate with chitosan, gelatin and/or dermatan sulfate [317, 318]. Varghese et al. grew and differentiated mesenchymal stem cells in chondroitin sulfate-PEG hydrogels [334]. Lee et al. reported that PVA hydrogels with chondroitin sulfate increased cell culture efficiency over pure PVA hydrogels [335]. In a different study, Conovaloff et al. compared nerve root regeneration in chondroitin sulfate hydrogels versus hyaluronic acid hydrogels. Cultured E8 chick dorsal root ganglia in chondroitin sulfate hydrogels exhibited growth than those in hyaluronic acid (i.e, their control). They hypothesized that this was due to stronger affinity of the applied nerve growth factor for hyaluronic acid and that hyaluronic acid chains potentially also serves as a growth inhibitor [336]. Cell culture and regenerative medicine applications for chondroitin sulfate continuously increase due to intrinsically attractive properties and commercial availability [329]. A downside is that chondroitin sulfate varies in concentration and purity depending on its source, and also impurities either from the source (e.g., proteins, nucleic acids) or from the isolation procedure (e.g., chemical solvents, detergents, endotoxins) [329]. Published evidence suggests that chondroitin sulfate from fish (e.g., shark) is a preferred source over mammals due to its sulfation pattern and safety [329]. More recently, microbial fermentation-based production of chondroitin sulfates has been commercialized. *E. coli* fermentation and chemical modification (e.g., sulfation and hydrolysis of fructose monomer) produced an alternative chrondroitin sulfate source and composition [329].

Dermatan sulfate (animal-derived polysaccharide). Dermatan sulfate is structurally similar to chondroitin sulfate, with the difference dermatan sulfate has some D-glucuronic acids

replaced by L-iduronic acid (Figure 3.5). This change distinguishes dermatan sulfate from chondroitin sulfates and more similar to heparin and heparan sulfates, as they also contain iduronic acid residues [337]. Iduronic acid is important for the binding site specificity for glycosaminoglycan (GAG)-binding proteins [337, 338]. The influence of the iduronic acid residue on cellular behavior has been previously reported to show that fibroblast proliferation was strongly inhibited when GAG chains with high amounts of iduronic acid residues were used [339]. Dermatan sulfate is also glycosidically linked by a D-xylopranosylserine to the core protein to form proteoglycans found in fibrous connective tissue, the cornea and some fibrous cartilage [172, 325].

Chen et al. analyzed the effects of adding dermatan sulfate to a previously tested chondroitin-6-sulfate-chitosan scaffold, comparing the two scaffold types after seeding chondrocytes. Dermatan sulfate was found to increase scaffold-cell interactions, and influence cell morphology, gene expression, GAG and collagen production positively [317]. Not many studies report in vitro cell culture data with dermatan sulfate materials, possibly due to sourcing and cost issues.

Heparin/Heparan sulfate (animal-derived polysaccharide). Structurally, heparin and heparan sulfate are very similar (Figure 3.5) [340], comprising glucosamine saccharides alternating with glucuronic acid or iduronic acid units in linear GAG chains that span polydisperse molecular weights ranging from heparin's 15kDa to heparan sulfate's 30kDa. While substantial structural heterogeneity exists in both molecules, heparan sulfates contain more glucuronic acid while heparin contains more iduronic acid in their respective disaccharide repeats with glucosamine. Key to their bioactivity seems to be their relative degrees of sulfation, with heparin bearing more anionic sulfate charge density and correlated abilities to bind growth factors and peptides [337, 338, 341]. A heparin disaccharide averages ~2.7 sulfate groups, whereas heparan sulfate disaccharide bears ≥1 sulfate group [342]. Heparan sulfates exist primarily as proteoglycans in extracellular matrix and expressed on many cell membrane surfaces, while heparins are secreted from mast cell granules and can dissociate from proteins to present extracellularly as GAGs [172, 325].

Feijen's group used heparin-tyramine conjugates and dextran-tyramine conjugates to form hydrogels for 3D cell chondrocyte culture. They observed optimal cell proliferation and viability in

gels with a 50/50 ratio of heparin-tyramine and dextran-tyramine, which made them promising scaffolds for injectable cartilage regeneration studies [343]. Tae et al. developed a modified heparin hydrogel by thiol modification of the heparin and then cross-linking with poly(ethylene glycol) diacrylate. They used this gel to successfully encapsulate fibroblasts and observe cell proliferation within the gel, with 5-fold higher cell proliferation after adding fibrinogen to the gel [344]. Further, they encapsulated hepatocytes in heparin-PEG diacrylate gels and maintained hepatocyte cultures with high levels of albumin and urea synthesis over a 3-week in vitro period [345]. Heparin-hyaluronan hydrogels were used to improve survival of stem/progenitor cells in transplantation. Two different neural progenitor cell lines, derived either from embryonic stem cells or embryonic cortex, in these hydrogels exhibited extended survival, attributed to cell stress reduction in the hydrogel compared to cell culture without hydrogel encapsulation [346]. Benoit et al. used poly(ethylene glycol) gels functionalized with heparin to encapsulate human mesenchymal stem cells. The cells remained viable in the hydrogel and underwent osteogenic differentiation over a study period of 5 weeks [347]. A different approach using heparin-mimetic peptide nanofiber scaffold demonstrated effective simulation of natural ECM heparan sulfates and allowed for spatial presentation of important growth factors [348]. Roberts et al. used a poly(vinyl alcohol)-heparin hydrogel for simultaneous encapsulation of basic fibroblast growth factor and vascular endothelial growth factor and were able to show controlled release of both growth factors which lead to a significantly higher human umbilical vein endothelial cell outgrowth with their model cell line, BaF32 [349].

Hyaluronic acid (animal-derived polysaccharide). Hyaluronic acid (HA) is the only GAG which is not a proteoglycan – not covalently bound to a core protein. Hyaluronic acids consist of linear repeats of a β-1,4-glucuronic acid-1,3-N-acetylglucosamine disaccharide unit (Figure 3.5) with wide ranging molecular weights. They are found naturally in vitreous humor, synovial fluid, skin, and diverse connective tissue, often as a high mass-fraction component. HA is the primary component in cartilage and central to many proteoglycan aggregates [172, 325]. It has normal biological activities in wound healing, angiogenesis, and embryonic development [350, 351].

HA was originally isolated for biotechnology and biomedical use from animal sources,

mainly rooster combs, hen crests, synovial fluid, vitreous humor, and umbilical cords [352]. More recently, several in vitro bioreactor, scalable microbial fermentation technologies exploit *streptococcus* bacteria to produce HA [353]. This fermentation approach yields higher concentrations of HA while reducing unit costs and allowing for more effective downstream processes [329, 354, 355]. As with other natural polysaccharide biomaterials, complete, validated removal of impurities and endotoxins prior to use is essential for HA use in hydrogels for cell culture applications [356, 357].

HA is ubiquitous in human tissues and has an important role in cellular events including cell motility, cell adhesion, cell proliferation, and tissue structuring, mainly due to HA interactions with two major signal-transducing cell surface HA-receptors: CD44 and RHAMM [358]. Many cells express specific cell surface binding proteins, or receptors, for hyaluronan. Hyaluronan receptors are reported for chondrocytes [359, 360], endothelial cells, macrophages, SV-40-transformed 3T3, BHK, and human bladder carcinoma cells [361-363]. These putative hyaluronan receptors comprise related hydrophobic membrane proteins, named hyaladherins [364], with biochemistries and functional structures distinct from integrin receptors. Hyaluronan receptors are grouped by similar physical and functional properties including high affinity binding for hyaluronan (K_d -10^{-9}M) that increases with increasing ionic strength and is off-competed with hyaluronan oligosaccharides of minimum size of six monosaccharides (i.e., hyaluronan hexasaccharide, HA_6), as well as high specificity for hyaluronan. Importantly, these and other properties distinguish hyaluronan binding proteins/receptors from other hyaluronan-binding proteins, including aggrecan and link proteins that require minimally 10-12 monosaccharides for effective binding competition [176, 365-367].

Cellular hyaluronan receptors are related to the CD44 family of receptors expressed by many cell types and varying widely in their glycosylation, oligomerization, and protein sequences [368, 369]. Many cells also express the cell surface receptor and hyaluronan binding protein, RHAMM (receptor for hyaluronan-mediated motility) involved in cell motility and cell transformation. RHAMM induces focal adhesions to signal the cytoskeletal changes required for elevated cell motility seen in tumor progression, invasion, and metastasis. CD44 and RHAMM are involved in growth factor-regulated as well as hyaluronan signaling and can be involved in different aspects of

cell signal regulation: e.g., CD44 is involved in endothelial cell adhesion to hyaluronan as well as proliferation regulation while RHAMM is needed for migration and activation of the protein tyrosine kinase cascade of endothelial cells in response to hyaluronan [370-372]. Endothelial cells of the lymph node and liver sinusoids remove hyaluronan via specific receptors LYVE-1 (a CD44 homolog) and HARE (hyaluronan receptor for endocytosis).

Structurally, many hyaluronan-binding proteins and receptors commonly share a protein motif called the link module, first described in cartilage link protein [373]. Link proteins belong to the subfamily of hyaluronan and proteoglycan link proteins (HAPLN) found in many tissues. Four hyaluronan binding receptors have extracellular domains with link module motifs: CD44, LYVE-1 (lymphatic vessel endothelial hyaluronan receptor), HARE/STABILIN-2 (hepatic hyaluronan clearance receptor), and STA-BILIN-1, all expressed on discontinuous endothelial cells and some activated macrophages.

Functionally, hyaluronans are proposed to exhibit important roles in cell proliferation, migration, and invasion, and pathologically in inflammation and tumorigenesis. To produce these signals, hyaluronan receptors serve to bind cell membranes with extracellular glycosaminoglycans [370]. Previous studies have shown that the effect of hyaluronan is strongly dependent on cell type as well as the size of the hyaluronan [370, 374, 375]. With its high natural abundance in most connective tissue, hyaluronic acid is commonly used in cultures for cell encapsulation in the context of extracellular matrices rich in hyaluronic acid (e.g., chondrocytes) [67, 376].

This cell engagement with HA imparts HA with requisite materials properties attractive to exploit for 3D cell culture constructs [350, 351, 377]. As a weakly acidic biopolymer, HA does not effectively gel with calcium ions but can be gelled with other polyvalent cations, like iron [378]. Acidic HA and basic chitosan, for example, form complex polymer-polymer coacervates that yield nanoparticles, hydrogels, microspheres, sponges, and films [379]. HA is often chemically modified to effectively gel or polymerize in vitro [19]. Such cross-linking efforts include physical, ionic, or covalent HA network formation [378]. To improve cell encapsulation, multiple HA studies incorporate covalent polymerizable groups, for example, methacrylates [380-382] or thiols [383, 384], forming gels from these materials by direct polymerization or with diverse crosslinkers. Some

HA gels can be degraded into diverse oligosaccharide fragments by disulfide reducing agents or using hyaluronidase enzymatic activity [381, 384]. Master et al. showed that cell-mediated HA degradation improved heart valve tissue growth [381].

Crosslinked HA hydrogels are also created using photopolymerization [380, 385, 386]. Chung et al. reported that implantation of photocrosslinked HA gel-encapsulated articular chondrocytes into subcutaneous pockets showed better tissue growth in HA gels of lower macromer concentration having lower crosslink density. They also showed that HA molecular weight had less influence on tissue growth [382].

Acrylated HA reacts in aqueous media with derivatized PEG-tetrathiol [387] or, conversely, thiol-modified HA can analogously react with PEG diacrylate (PEGda) [383, 384, 388] both via Michael addition. Using these approaches, Kim et al. used HA hydrogels formed by Michael addition to encapsulate mesenchymal stem cells (MSC), claiming increased bone regeneration and growth after implantation compared to “blank” HA hydrogels [387]. HA Michael addition-type gels allowed adipose-derived stem cells to better differentiate compared to decellularized protein matrix surfaces [388]. Similarly, elevated neurite outgrowth was reported for HA encapsulation of dorsal root ganglia [389]. Specific to drug toxicity screening in vitro, a recent 3D kidney proximal tubule culture model improves toxicity predictive capacity compared to current 2D kidney cell monocultures on plastic [13, 47, 60]. Viable mouse kidney-derived proximal tubule fragments (PTs) are embedded in a commercial biomedical grade HA-based crosslinked hydrogel matrix. Encapsulation of PT fragments in this semisynthetic hydrogel mimics ECM and encourages endogenous PT epithelial cells to remain in their native tertiary tissue-like PT structure to maintain differentiated states and cell functionalities in vitro for extended periods [12, 47, 60]. PT cells therefore reflect toxicity states with more fidelity when interacting with drug compounds [13, 60].

Another approach to HA hydrogels for cell encapsulation is using click chemistry. HA derivatives containing azide and alkyne chemistry can react together to form crosslinks in aqueous media [390, 391]. DeForest et al. used this HA chemistry and successfully encapsulated 3T3 fibroblasts [392].

Similar to approaches with other natural polysaccharide gels in cell culture, HA is also

combined with other natural or synthetic materials in gel networks to increase cell engagement and enhance cell culture properties. Thiol-modified HA was combined with thiol-modified gelatin to create an ECM-like environment when crosslinked with diacrylated PEG [383]. This combined matrix provided advanced tissue regeneration with cartilage, similar to native architecture with encapsulated MSCs [393-395]. A different approach combines HA and collagen in a semi-interpenetrating network to achieve mechanical robustness with bioadhesive properties. Brigham et al. showed fibroblasts seeded inside this scaffold maintained high levels of viability and that the scaffold supported both cell adhesion and proliferation [396, 397]. Suri et al. embedded Schwann cells in a similarly engineered collagen/HA interpenetrating polymer network to show that cells spread out and proliferated over a 14-day study. Furthermore, these cells were functional and actively secreted nerve growth factor and brain-derived neurotropic factor [398].

Synthetically modified HA is commercially available under different brand names, e.g., Hyaff® (Fidia Advanced Biopolymers) and Glycosil® (ESI Bio). A combination product of thiol-modified HA, thiol-modified gelatin, and PEG-based crosslinker is available under the brand name, HyStem™ (ESI Bio). Overall, HA gels demonstrate excellent chemical versatility, good biocompatibility and optical properties, and readily modified mechanical properties (using molecular weights and crosslinking variables) suitable for in vitro 3D cell culture as well as for regenerative medicine [399].

Synthetic polysaccharides

All glycosaminoglycans are biosynthetic products of native glycan-specific enzymes (e.g., hydrolases, oxidoreductases and transferases) that selectively utilize carbohydrate substrates: polysaccharides are formed by repeated enzyme-catalyzed, highly enzyme-specific glycosylation reactions between glycosyl donor and glycosyl acceptor substrates of the enzyme. Unlike all natural proteins, no polysaccharides are encoded by genes. Mammalian polysaccharides for example comprise only ten different monosaccharide monomer units, most frequently encountered in nature as glycoconjugates (i.e., glycol-peptides, -proteins, and -lipids). In these natural products, the oligosaccharide component is more chemically complex than either peptides or oligonucleotides

are as families of analogous bioderived polymers. In polymerizing glycan monomers, each glycosidic bond produces a new stereogenic center. This chemistry is unlike amide and phosphate diester linkages in protein and nucleotide polymers, respectively. Copying this unique stereochemical control in polysaccharide glycosidic bond formation remains largely an unsolved challenge. The array of reactive amine and hydroxyl groups decorating each glycan ring is not yet effectively addressed by protective group strategies for automated synthesis [400]. While most well-studied natural glycosaminoglycans comprise controlled, polymerized repeats of a few chemically distinct glycan monomer units in alternate sequence or short blocks, simplified and automated approaches to prepare synthetic analogs, or more ambitiously, exotic “designer carbohydrates”, are lacking.

To date, however, the most powerful methods reported for polysaccharide total synthesis combine chemical and enzymatic approaches. This provides access to many different shorter oligosaccharides of mammalian origins, in addition to some glycolipids and simpler glycoproteins [401]. Kobayshi et al. achieved the first chemical synthesis of cellulose using enzymatic polymerization with cellulase and a fluorinated cellulose monomer derivative (β-CF) as a substrate [402]. Success with this enzyme–substrate polymerization of starch then stimulated other polysaccharide polymerization efforts using hydrolases, oxidoruductases and transferases as catalysts [403-406]. Kobayashi’s group subsequently reported using a hydrolase enzyme to polymerize synthetic glycan-like monomers designed as “transition-state analogue substrates” (TSAS), fluoridated glycan monomers for polycondensation and oxazoline-based sugar monomers suited for ring-opening polyaddition reactions. This enzymatic polymerization was shown to yield in vitro synthesis of several natural polysaccharides including cellulose, xylan, chitin, hyaluronan and chondroitin, and also of unnatural polysaccharides such as a cellulose–chitin hybrid, a hyaluronan–chondroitin hybrid, and others [407]. His further efforts were using ring-opening polymerization of bicyclic anhydro sugar derivatives and via enzyme-catalyzed polymerization with phosphorylases [408].

Native proteins and nucleotides both represent linear biopolymers assembled from either twenty different amino acids monomers or four unique nucleotide monomers, respectively. By

contrast, evolving the library of glycan monomers available in nature, and their unique coupling stereogenic chemistry is more daunting. In particular, growing techniques such as native chemical ligation (NCL), sugar-assisted ligation, Staudinger ligation, expressed protein ligation (EPL), and pathway engineering are now shown to effectively produce homogeneous glycoproteins with reliable glycan content. In a protein polymer-analog synthetic approach, Wong et al. showed that unnatural amino acids containing a keto group could be site-specifically incorporated into a target protein by exploiting the amber nonsense codon [409]. Aminooxy saccharide derivatives were then selectively coupled to this genetically encoded keto group in the expressed protein. The resulting saccharide core was transformed to full glycan chemistry with glycosyltransferases. Alternatively, aminooxy analogues of more complicated glycans were prepared and directly attached to the keto group. This represents a general approach for synthesizing homogeneous glycoprotein mimetics containing well-defined reactive saccharide substituents.

Significantly, improvements in glycan synthesis and coupling strategies, including chemo-enzymatic, one-pot and solid-phase synthetic methods have created improved processes that yield various pure glycans in quantities feasible for more than exotic carbohydrate research in biopolymer synthesis. Seeberger et al. demonstrated the combination of an automated carbohydrate synthesizer and photolabile linkers cleaved in a continuous-flow photoreactor to synthesize two chondroitin hexasaccharides as examples for a general polysaccharide method [410]. Other glycan oligosaccharides (e.g., heparin, heparin sulfate, dermatan sulfate, or keratin sulfate) might follow suit with this approach. Seeberger et al. also developed a generalized and modular strategy claiming the first completely stereoselective synthesis of defined heparin oligosaccharides, producing stereochemical control of α-glucosamine glycoside formation as a precedent [411].

Nonetheless, despite monomer feedstocks in limited quantities and some success in oligosaccharide synthetic hallmark examples, long stereochemically controlled glycan-based polymers analogous to natural hyaluronan, alginic acids and other polysaccharides escape modern synthetic approaches. Instead, glyco-mimetic polymers based on protein- or polymer- glycan coupling [412] or polymerization of vinyl- or acryl- derivatized glycan monomers is reported in

several forms [413, 414]. These approaches are generally limited in biomimetic heterogeneity and diversity by polymerization method limitations on monomer compositional and sequence control, polymer blockiness, or alternating chemistry and resulting product stereochemistry. Production of monomer precursors that impose requisite stereochemical regularity on high molecular weight glycan polymer products is simply not affordable or practical currently.

Perspectives and future outlook

Polysaccharides represent an increasingly popular materials choice for 3D cell culture studies, but the reasons for their selection are more pragmatic than biomimetic. Most available polysaccharides are gentle, benign biomaterials convenient for cell encapsulation using aqueous encapsulation methods and crosslinking by diverse physical and chemical means to control mechanical integrity, morphologies, and hydrogel properties. Some glycan-based materials are commercially available in high-purity forms suitable for biomedical studies and many are optically transparent to permit external interrogation using microscopy and spectroscopy. From this record, proven benefits for 3D cell culture include nontoxic matrix formation and degradation profiles, general biocompatibility in culture, commercial materials availability in quantity and quality at reasonable cost, optical transparency of noninvasive monitoring, and structural support for cells and organoids to allow for in vivo-like cell differentiation, attachment, proliferation and cell-cell and cell-matrix interactions. These matrix factors combine to produce successful cell culture systems that show in vivo-like gene expression profiles and toxicity responses. Hence, the requirements for 3D culture matrices shown in Tables 3.1, 3.3, and 3.4 are often satisfied by a diverse array of chemically unrelated polysaccharide biomaterials in 3D gels. This reflects perhaps more general properties attributable to hydrogels, nonspecifically supporting cell-matrix interactions.

Several polysaccharides are derived from their native presence in mammalian extracellular matrix and as natural products, require no synthesis. Other materials have nonmammalian origins (e.g., seaweed/algae and plant-derived biopolymers) yet exhibit suitable properties and structural homologies sufficiently similar to mammalian polysaccharides to serve as suitable surrogate gel materials for 3D cell culture. Notably, no polysaccharides mentioned exhibit complete ECM cell-

support equivalence in either their structure or function: modes of specific cell engagement with polysaccharides are weak and rare (e.g., CD44 for HA). Specific ECM ligands (i.e., for cell membrane integrins) are often missing. Cell encapsulation within polysaccharide 3D gels provides cells with a hydrated, porous, soft matrix with some similarity to ECM physically. Chemically, this 3D matrix is often nonoptimal to promote normal cell function, and therefore, hybrid and blended gel matrices with matricellular proteins with cell-specific binding motifs (e.g., gels with gelatin, laminins, collagens) are used to enhance polysaccharide physical gel properties in cell cultures.

Other suboptimal polysaccharide materials properties are primarily in batch-to-batch materials variability, endotoxin purity and variable final gel mechanical properties. Additionally, downstream in vitro testing including ex situ optical issues and cell assay interference, remain to be vetted.

A different approach to optimize structure of 3D cell cultures is the use of 3D printing technologies. This fabrication method is used and studied now in several different formats to produce new materials scaffolds from natural polysaccharides [415-417]. Additionally, the printed approach also allows the precise combinations of different polysaccharides and biopolymer blends to optimize different properties from each polysaccharide. He et al. recently successfully analyzed the printability of alginate/gelatin hydrogels and the effects on cell viability of L929 mouse fibroblasts [418]. Axpe et al. reviewed the use of alginate for 3D bioprinting, currently the most commonly used material for bioinks [419]. Overall bioink use in 3D printed matrices opens new doors into the options of possible shapes and structures of future in vitro 3D cell culture designs from natural polysaccharides,

No one single technique/material will be optimal in satisfying all needs of different 3D cell cultures; users should select and validate the most appropriate model for their specific cell-based needs and requirements. Overall, fabrication of hydrogels from natural polysaccharides has already proven experimentally versatile and successful. Many attributes attractive to in vitro 3D cell studies, drug and toxin screening assays and tissue engineering, and advanced fluidics and co-culture designs are identified. Such novel 3D matrix-based culture systems exhibit greater similarity to actual tissue constructs (i.e., organoids, micro-tissues, spheroids, and cell/gels) [19] and enable

platform technologies currently sought for drug development, developmental biology studies, improved disease models, and regenerative medicine research and development beyond the scope of this review.

Despite substantial precedent use and history of development, a number of technical challenges represent significant barriers to rational use of polysaccharides in 3D cell culture systems in vitro. Few available polysaccharide biomaterials are mammalian sourced – most are from algal or plant sources (e.g., alginates, agaroses, gums and cellulosics). Most glycosaminoglycans lack known cell receptor adhesion ligands that trigger cell signaling and normal phenotypic behaviors known from native ECM. For example, few polysaccharides compete with collagen, a popular cell culture protein substrate, for availability and pricing, as well as known cell receptor binding behaviors. No glycan analogies to well-known cell-ECM engagement through integrin-receptor interactions exist. As a result, many polysaccharide materials in 3D culture provide a highly hydrated, permeable and noninteractive culture environments, and lack specific receptor-mediated cell interactions important to cell phenotypic stability, differentiation and renewal. To overcome this deficit, many polysaccharides are blended with ECM proteins to provide the advantages of both materials in culture, including the mild physical and tailored processing advantages of polysaccharides as hydrogels with the biochemical cell engagement specificities of ECM matricellular proteins. Future research should work to identify cell-specific glycan ligand biochemistry and receptor biochemistry in order to define chemistries important to future synthetic biomimetic polysaccharide-like materials for 3D cell culture. This is also important to distinguish important 3D cell culture properties in natural polysaccharide materials from other traditional hydrogel classes. This glycan-specific cell culture evidence to date is not that distinguishing.

Obtaining this evidence of interaction and cell engagement would also benefit current efforts to design synthetic polysaccharides with the proper stereochemical features to emulate natural biopolymer properties important to 3D cultures. This should focus on what features are necessary versus what are sufficient to adopt from ECM prototype materials for effective 3D use. While synthetic methods are still challenged to couple a limited library of sugar-based monomers in native configurations, an essential challenge to the 3D cell culture field is to define polymer

chemical features important to cell phenotypic stability and proliferative capabilities. These then identify the unknown chemical and structural design features currently unavailable in synthetic polysaccharide mimetic polymers.

A remaining challenge is a materials sourcing issue: improving both the ability to procure and produce pure natural polysaccharides at a lower cost of goods and greater batch-batch quality control. This could result from shifts away from current natural materials batch-wise production from natural extraction (i.e., from algae and plants) to biosynthetic or enzyme-facilitated biochemical routes.

Table 3.1 Cell characteristics and performance benefits desired in 3D cell culture systems.

Cell Characteristics	3D cell culture benefits	References
Morphology	In vivo-like cell shape	[10, 20, 21]
Proliferation	Cell type and 3D model dependent	[25, 26]
Motility	Cell type and 3D model dependent	[63]
Cell-cell communications	3D paracrine and autocrine signaling	[64]
Drug/medium/O_2 exposure	Potential penetration gradients toward center	[10, 66, 67]
Cell cycle staging	Cells of different stages (proliferating, hypoxic, quiescent and necrotic) possible	[10, 11, 16]
Gene expression	More similar to in vivo expression profiles	[12, 25, 77, 78]
Toxicity responses	Better predictive values to in vivo compound responses	[13, 25, 79]

Table 3.2 Current 3D cell culture methods including commercially available products.

3D cell culture method	Commercial source	References
Spheroids/ scaffold-free platforms • Forced-floating • Hanging drop • Agitation-based approach ○ Spinner flask bioreactors ○ Rotational culture systems	PrimeSurface (Sumitomo Bakelite) Lipidure-coated plates MicroWell MiniTray (Nunc) 3D Biomatrix (http://3dbiomatrix.com) InSphero (www.insphero.com) Wheaton Spinner Flask (Wheaton) Spinner Flasks (Corning) Synthecon (www.synthecon.com) Rotary Cell Culture Systems	[10, 27-33]
Matrices, gels and scaffolds	Matrigel (BD Biosciences) PathClear Grade Basement Membrane Extract (Amsbio) ECM gel (Sigma-Aldrich) ECL Cell Attachment Matrix (Millipore) Geltrex (Invitrogen) HuBiogel (Vivo Biosciences) Cytodex 3 microcarrier (GE Healthcare) ProNectin F (Solohill)	[37-40]
Microfluidic cell culture platforms/ microchips (organ-on-a-chip)	MiCA plate (CellASIC) Iuvo Microconduit Array Platform (BellBrook) Quasi Vivo (Kirkstall) Organovo (ONVO) HepatoPac (Hepregen) 2-OC and 4-OC (TissUse)	[1, 48-51]

Table 3.3 Gel/matrix general technical requirements for use in 3D culture systems. [1, 2]

Maintenance of organ features critical for their function and tissue-tissue interfacing
Control of gradients of media, chemicals and oxygen essential for 3D viability
Mechanically active microenvironment important for organ functionality
Duplication of matrix microstructure that yields normal tissue microarchitecture
Incorporation of versatile biochemical cues recapitulating the natural ECM microenvironment
Endotoxin free
Scalable in mass and volume
Highly reproducible material properties and compositions batch-to-batch and location-to-location
User-friendly in preparation and deployment in culture
Manufacturable to a quality standard
Approvable, possibility of regulatory approval
Affordable, competitive cost/economy
User-initiated degradability (enzymatically, nonenzymatically) under mild conditions (biodegradable)
Sterilizable, low bioburden
Low contraction and expansion
Usable and cross-linkable under physiological conditions (e.g., temperature, pH)
Optically transparent
High-throughput screening (HTS) applicable with fluidics interface and stability under fluid shear
Potential for translational applications beyond in vitro culture
Nontoxic degradation

Table 3.4 Common advantages and disadvantages of natural polymer matrices used for 3D cell culture systems. [3-19]

Advantages	***Disadvantages***

• Natural origin
• Complex geometric structure and shapes
• Structural support for cells/organoids
• Support in vivo-like cell differentiation (functional and morphological)
• Encourage cellular attachment
• Encourage cell proliferation
• Encourage intercellular and cell-ECM interactions
• Promote cell diversity
• More in vivo-like gene expression profiles and cellular behavior
• Simple to use
• HTS compatibility
• Bioreactor applicability
• Economical
• Abundant commercial providers
• Bridges gap between in vitro and in vivo drug screening needs
• Possible decreasing the use of animal models
• Nontoxic degradation
	• Optical issues due to:
	  ○ Density
	  ○ Light scattering
	  ○ Curvature (non-line-of-sight)
	  ○ Assay interference
	  ○ Signal-to-noise ratio
	• Assay read out
	  ○ Termination of culture needed
	  ○ Culture disassemble needed
	• Lack of ECM complexity
	  ○ Limitation of adhesion molecules
	  ○ Limitation of cellular ligands
	• Lack of tissue-like organization
	• Lack of vasculature
	• Diffusion/transport issues (necrotic core)
	• Batch-to-batch variability
	• Contamination risks
	• Endotoxin and impurities removal
	• More expensive than 2D cell culture
	• Risk of absorption/interaction of compounds or assay chemistry

Native ECM consists of covalent and noncovalent heterogeneous molecular interactions between matrix proteins (primarily collagens), glycoproteins, and diverse glycosaminoglycans (GAGs) [2], like chondroitin and heparan sulfates. The resulting ECM network contains both essential physical and chemical cues that engage cell receptors and provide proper context for native cell behaviors in three dimensions. Native ECM spatially displays, stores and secretes growth factors, provides physical structure and mechanical context, and enables cellular communications. ECM has an important role in controlling the distribution of nutrients and gases. The ECM hereby creates signal gradients essential for cell processes (e.g., migration, homing and tissue organization and patterning) [21, 35, 36]. More detailed information on ECM's complex structure, importance and use are found in recent reviews [42, 43].

Figure 3.1 Extracellular matrix (ECM): A brief description for 3D native matricellular context

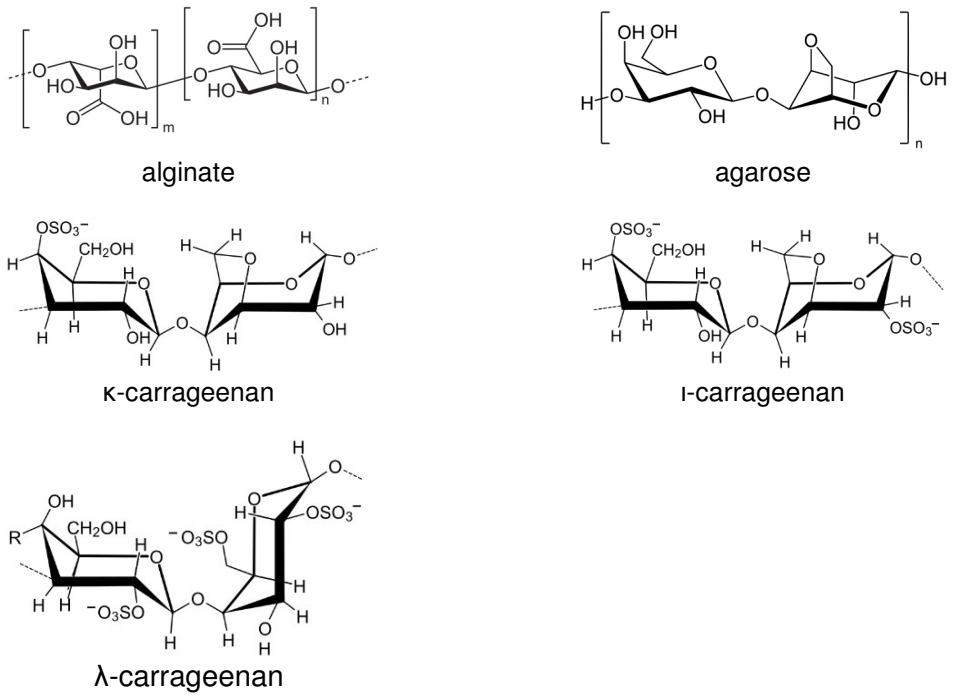

Figure 3.2 Chemical structures of algal/seaweed-derived polysaccharides

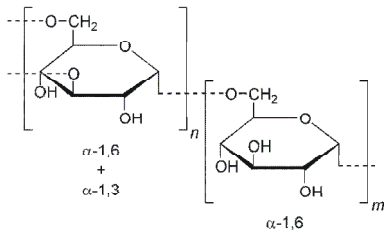

dextran

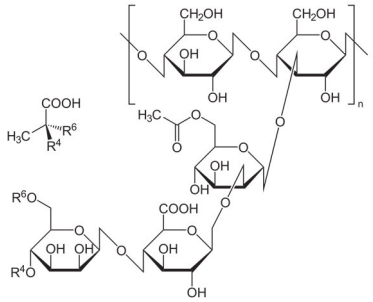

xanthan gum

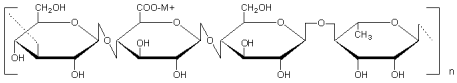

gellan gum

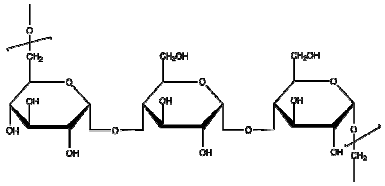

pullulan

Figure 3.3 Chemical structures of microbial-derived polysaccharides

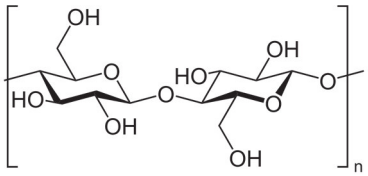

cellulose

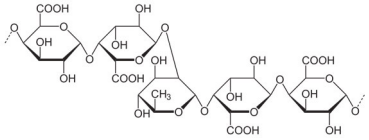

pectin

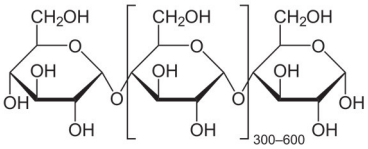

amylose

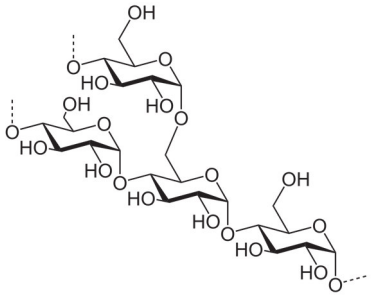

amylopectin

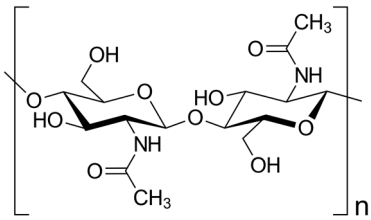

chitin

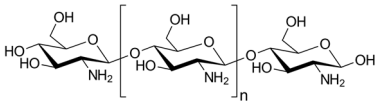

chitosan

Figure 3.4 Chemical structures of plant-derived polysaccharides and others

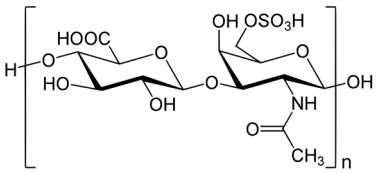

chondroitin sulfate C

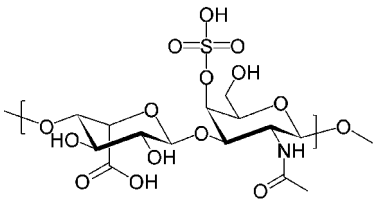

dermatan sulfate

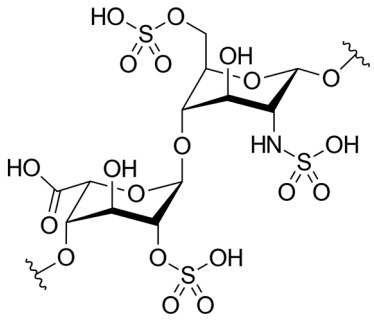

heparin

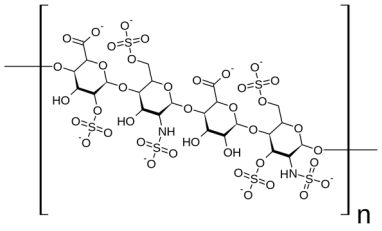

heparan sulfate

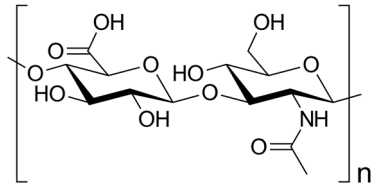

hyaluronic acid

Figure 3.5 Chemical structures of animal-derived polysaccharides

CHAPTER 4

DRUG TRANSPORTER EXPRESSION PROFILING IN A THREE DIMENSIONAL KIDNEY PROXIMAL TUBULE IN VITRO NEPHROTOXICITY MODEL[2]

Abstract

Given currently poor toxicity translational predictions for drug candidates, improved mechanistic understanding underlying nephrotoxicity and drug renal clearance is needed to improve drug development and safety screening. Therefore, better relevant and well-characterized in vitro screening models are required to reliably predict human nephrotoxicity. Because kidney proximal tubules are central to active drug uptake and secretion processes, and therefore to nephrotoxicity, this study acquired regio-specific expression data from recently reported primary proximal tubule three-dimensional (3D) hyaluronic acid gel culture and nongel embedded cultured murine proximal tubule suspensions. Quantitative assessment of the mRNA expression of 21 known kidney tubule markers and important proximal tubule transporters with known roles in drug transport was obtained. Asserting superior gene expression levels over current commonly used two-dimensional (2D) kidney cell culture lines was the study objective. Hence, we compare gel-based 3D proximal tubule fragment culture and their nongel suspensions for up to one week, and demonstrate that 3D tubule culture exhibits superior gene expression levels and profiles compared to published commonly used 2D kidney cell lines (Caki-1 and HK-2) in plastic monocultures. Additionally, nearly all tested genes retain mRNA expression after seven days in both proximal tubule cultures, a limitation of 2D cell culture lines. Importantly, gel presence is shown not to interfere with gene expression assay. Overall, results validate retention of essential toxicity-relevant

[2] Diekjürgen, Dorina and Grainger, David. Drug transporter expression profiling in a three-dimensional kidney proximal tubule in vitro nephrotoxicity model. Under revision 2017

transporters in this 3D proximal tubule model over conventional 2D kidney cell cultures, producing opportunities for more reliable and comprehensive drug toxicity studies relevant to drug development and nephrotoxicity goals.

Introduction

Kidney proximal tubules play a major role in the secretion of xenobiotics and metabolites from the body, and are the primary target sites of drug-induced nephrotoxicity. This results from the action of specialized transporters (e.g., OAT1, OAT3, OCT2) in the proximal tubule that uptake organic compounds and biotransformed metabolites across the basolateral membrane [420-422]. This active transport system results in high levels of toxins within proximal tubule cells, leading to cell damage and necrosis [423, 424]. Additionally, proximal tubule cells have polarized distributions of transporters. Apical side transporters facilitate exit of compounds into the tubule lumen, specifically, the known efflux transporters, MDR1, MRP2, and MRP4 [425-427]. These transporters play a major role in nephrotoxicity models and why proximal tubules are an ideal focus for drug toxicity screening. Previous work has identified drug transporters and their functions [428-431]. However, the mechanistic processes and importance of individual transporters on both sides of the proximal tubule and their effects on nephrotoxicity are largely unclarified. Therefore, a detailed characterization of the transporter expression profiles is critical for developing relevant drug toxicity models. This study focuses on profiling mRNA expression levels of 21 known tubule markers (Table 4.1) as well as important proximal tubule transporters with known roles in drug transport in a 3D tubule culture model (Figure 4.1). These are then compared to routine 2D kidney cell cultures reported in the literature.

Three-dimensional (3D) cell culture has been previously shown to be superior to conventional 2D cell cultures: their cell morphology and physiology differ [432, 433], and 3D cell cultures demonstrate more similar responses to in vivo behaviors than 2D cell cultures [434, 435]. Despite this, 2D cell monoculture on flat, rigid plastic supports remains the current standard for drug screening in the pharmaceutical industry in combination with animal in vivo studies [14]. Currently, immortalized renal epithelial cell lines of nonhuman origin (LLC-PK1 [436], OK [437],

MDCK [436]) or human cell lines (HK-2 [44, 438], Caki-1 [59], RPTEC-TERT [70, 439]) are routinely used in vitro for pharmacological studies (Table 4.2). Two-dimensional primary proximal tubule cells lose their polarization within minutes to weeks of monoculture [102], while secondary (transformed, immortalized) cell lines often are missing important kidney transporters required for drug toxicity [98]. Therefore, recent technologies emphasize a shift away from monolayer-cultured cells on plastic plates to 3D matrix-based culture systems more resembling in vivo tissue mechanics, hydration and architecture (i.e., organoids, micro-tissues, spheroids, and cells in gels) [39, 103, 104].

A recently developed 3D kidney organoid toxicity model [60] fulfills many of these requirements and improves on current 2D kidney cell monocultures on plastic by using viable mouse kidney-derived intact proximal tubules embedded in a commercially available hyaluronic acid-based hydrogel matrix [105]. Within these gels, encapsulation of harvested viable proximal tubule organoid fragments preserves the natural kidney tubule extracellular matrix, allowing proximal tubule epithelial cells to remain within their native tissue structures while suspended in highly hydrated 3D biopolymer culture media. Furthermore, these gels facilitate cell-matrix and natural cell-cell communication, maintain differentiated states and cell functionalities [104, 440], and allow for similar cellular heterogeneities seen in vivo [25, 441, 442]. Proximal tubule cells in these cultures therefore reside and interact in their more natural 3D extracellular matrix environment, and are proposed to produce toxicity responses to soluble species with more fidelity when interacting with drug compounds [47, 60, 103].

In this study, we characterize intact cultured proximal tubule transporter mRNA expression levels to determine how this proximal tubule model might be able to better retain and recapitulate drug transport and nephrotoxicity responses in vitro. Results provide more insight into the reliability of this in vitro model beyond functional equivalence evidence reported previously for a select nephrotoxic proof-of-concept demonstration of this model [47, 60]. Understanding the expression profiles for critical kidney tubule transporters should facilitate future in vitro-in vivo correlations (IVIVC) and interspecies comparisons to validate nephrotoxic assays. Data for transport expression in vitro in 3D cultures to 7 days supports the value of this in vitro culture system for toxicity screening

of compounds that are substrates or inhibitors of known specific kidney transporter proteins.

Materials and methods

Murine proximal tubule harvest and isolation

Male C57BL/6 mice were purchased (age 6-8 weeks, Charles River Laboratories International, Inc., Wilmington, USA). All animals were euthanized using carbon dioxide (CO_2) in accordance with University of Utah Institutional Animal Care and Use Committee (IACUC)-approved protocols. Kidneys were harvested and proximal tubules were isolated using a mechanical technique followed by enzymatic digestion as previously described [60, 443]. Briefly, kidneys were removed surgically under standard aseptic conditions in a BSL2-certified laminar flow hood. The kidney capsule, ureter and blood vessels were removed and the isolated kidneys were mechanically disrupted by using a sterilized razor blade followed by enzymatic digestion in 2 mg/ml hyaluronidase (Worthington Biochemical Corporation, USA), 3 mg/ml collagenase IV (Worthington Biochemical Corporation, USA), and 0.1 mg/ml DNase I (Sigma Aldrich, USA) KREBS solution (145 mM NaCl, 10 mM HEPES, 5 mM KCl, 1 mM NaH_2PO_4, 2.5 mM $CaCl_2$, 1.8 mM $MgSO_4$, 5 mM glucose, pH 7.3) at 37 °C [444]. To isolate the proximal tubules from the digested sections, sequential 250 µm and 70 µm sieving was used [443]. Proximal tubules were pelleted by centrifugation and yields were estimated using a hemocytometer.

Proximal tubule cultures

Nonembedded proximal tubule cultures (nongel PT). Proximal tubules were resuspended in proximal tubule media comprising Dulbecco's Modified Eagle Medium/Nutrient Mixture F-12 with 4-(2-hydroxyethyl)-1-piperazineethanesulfonic acid and L-glutamine (Invitrogen, USA). Additionally, 1% fetal calf serum (Invitrogen, USA), 5% sodium pyruvate (Invitrogen, USA), 10% nonessential amino acids (Invitrogen, USA), 10% insulin/transferrin/selenium (Invitrogen, USA), 1% antibiotic-antimycotic (Invitrogen, USA) and 0.9 µg hydrocortisone (Invitrogen, USA) were added [443]. Finally, 100 µl proximal tubule media containing approximately 5000 proximal tubules was added to each well of a 96-well plate well. Plates were then incubated for up to 7 days

in cell culture incubators under 5% CO_2 and 95% air at 37 °C. Media was exchanged every 2 days for maximum cell viability.

3D gel proximal tubule cultures. Proximal tubules were encapsulated immediately after isolation within a 1.5% semisynthetic, thiol-modified biomedical-grade carboxymethylated hyaluronic acid (CMHA-S, SentrX Animal Care, Salt Lake City, USA) and 7.5% poly(ethylene glycol) diacrylate (PEGDA, SentrX Animal Care, Salt Lake City, USA) hydrogel (4:1 v/v). PEGDA is used as a bifunctional electrophile in situ cross-linker to produce in situ gelation in PBS with proximal tubules [105, 445, 446]. Hyaluronic acid-PEGDA 3D tubule organoid culture constructs (HA gel PT) were made with approximately 5000 proximal tubules/well in a 50 µl total volume HA gel matrix. Gel-tubule constructs in 96-well plates were allowed to gel for 30 min in a cell incubator at 37 °C (5% CO_2, 95% air). After gelation, 100 µl proximal tubule media (vide supra) was added onto gel constructs [60]. Constructs were incubated for up to 7 days in cell culture incubators under 5% CO_2 and 95% air at 37 °C. Media was exchanged every 2 days for maximum cell viability.

RNA extraction

Total tubule RNA was isolated and purified from cultures using the PureLink® RNA Mini Kit (Ambion® by Life Technologies, Carlsbad, USA) according to manufacturer's protocol. Final RNA elution was done in 30 µl of RNase-free H_2O. The quality and quantity of each RNA sample was determined using a NanoDrop 2000 Spectrophotometer (Thermo Scientific, Carlsbad, USA).

cDNA preparation

cDNA was synthesized using High-Capacity cDNA Reverse Transcription Kit (Applied Biosystems® by Life Technologies, Carlsbad, USA) according to manufacturer's protocol on the ProFlex™ Base PCR System (Applied Biosystems®, Life Technologies, Carlsbad, USA) using the following program: step 1: 10 min at 25 °C, step 2: 120 min at 37 °C, step 3: 5 min at 85 °C, step 4: 4 °C. 50 ng of cDNA was preamplified using the TagMan® PreAmp Master Mix Kit (Applied Biosystems®, Life Technologies, Carlsbad, USA) with 14 cycles (holding stage: 10 min at 95 °C, cycling stage: 14 cycles of 15 s at 95 °C and 4 min at 60 °C). Preamplification linearity was

successfully verified previously.

Quantitative real-time RT-PCR (qPCR)

Gene sets representing key important classes of cation, anion, protein endocytosis, glucose transporters, and metabolizing enzymes with known roles in drug transport or proximal tubule function were selected. Quantitative Real-Time RT-PCR was performed using a 1:30 dilution of the PreAmp product on the StepOnePlus™ Real-Time PCR System (Applied Biosystems®, Life Technologies, Carlsbad, USA) using the following program: 2 min at 50 °C followed by 10 min at 95 °C (holding stage), then a cycling stage of 40 cycles with 15 s at 95 °C and 1 min at 60 °C. TaqMan® Gene Expression Assays (Applied Biosystems®, Carlsbad, USA) were used for all genes of interest and endogenous controls (Table 4.1).

Relative expression analysis

Quantitative Real-Time RT-PCR data were analyzed using the StepOne™ Software (Applied Biosystems® by Life Technologies Corporation, Carlsbad, USA) and relative gene expression was analyzed using the $2^{-\Delta\Delta Ct}$ method [447]. Potential endogenous control genes were tested for their stability by commonly used software methods: BestKeeper [448], NormFinder [449], GeNorm [450], and comparative delta-Ct method [451], as well as for their potentially statistically significant differences. Using these methods, the three most stable endogenous controls were chosen (GAPDH, RPL19, and PPIA) and their geometric mean and standard deviation of the entire reference gene sample size was calculated for further quantification of all genes of interest.

Data analysis/ statistical analysis

All data were analyzed with Microsoft Excel® 2013 (Microsoft Corporation, Redmond, USA) and GraphPad Prism 6 software (GraphPad Software Inc., San Diego, USA). All experiments were performed on three independent biological samples with three technical replicates each. All data are shown with mean (average) and standard deviation (SD). One-way analysis of variance (ANOVA) followed by Tukey's multiple comparison post-hoc test or unpaired Student's t-test were

performed to analyze statistically significant differences. Results were considered as statistically significant differences with a confidence interval of 95% ($p<0.05$).

Results

Validation of reference genes

Quantitative RT-PCR indicates no statistically significant differences between the three time points of each reference gene (Figure 4.2). Furthermore, no statistically significant difference is observed between the two culture conditions at each time point for each reference gene (Figure 4.3).

To determine which reference gene to apply for data analysis, Bestkeeper, geNorm, and NormFinder Software were used to analyze reference gene Ct values [448-450]. Each analysis method consistently ascertained GAPDH, PPIA, and RPL19 as the most stable genes in proximal tubule fragments across the two different culture conditions and three culture time points used. Therefore, the geometric mean of these three reference genes is an appropriate choice for an accurate normalization strategy in proximal tubule expression analysis and was used for gene normalizations in this study.

Transporter xpression in murine proximal tubule fragments

Quantitative RT-PCR results showed that twenty (95%) of the 21 transporter genes tested from Table 4.1 were expressed in the harvested proximal tubule fragments after 3 days of culture and 19 (90%) were expressed after 7 days of culture. These results, normalized to endogenous control and expression at day 1 using the $2^{-\Delta\Delta Ct}$ method, are consistent for both culture conditions: proximal tubule fragments embedded in 3D modified HA gel and suspended in liquid media (Figure 4.4).

Comparison of mRNA expression in 3D proximal tubule HA gel versus nongel PT suspension cultures

Figure 4.4 compares proximal tubule fragment gene expression as quantified for Table 4.1 transporters for tubules cultured in 3D modified HA gel versus liquid media suspension. With the exception of MRP4, all genes were significantly downregulated when normalized to the geometric mean of the endogenous control genes GAPDH, PPIA, and RPL19. All genes show no statistically significant differences between the different culture conditions (analyzed by unpaired Student's t-tests, 95% confidence interval). Correlation of these data for the two proximal tubule culture systems is shown in Figure 4.5 (linear correlation factor shown is R^2=0.97).

Time-dependent changes in proximal tubule mRNA expression in different culture conditions

Expression of OCT3 and PepT1 are significantly reduced (as analyzed by unpaired Student's t-tests, 95% confidence interval) from the 3-day time point to the 7-day time point (Figure 4.6). Similar down-regulation of gene expression over this time can be observed in all genes, though not statistically different from each other.

Discussion

Proximal tubule cell differentiation and transporter expression functionality is essential for validation of proximal tubules as screening tools for drug screening and toxicity testing. Therefore, gene expression profiles for 21 important proximal tubule transporters with known roles in drug transport or normal proximal tubule function [429, 452-455] are compared in 3D gel versus nongel cultures for proximal tubule isolates from murine primary kidney harvests. As 3D cell culture techniques are increasingly asserted to improve cell culture translational relevance for toxicity screening [1, 14], few studies actually compare critical phenotypic functional aspects of these models. Previous reports describe limitations or lack of equivalence between 2D cell monocultures with actual in vivo conditions and cell phenotypes [14, 58, 434, 435]. For example, HK-2 and Caki-1, commonly used 2D cell lines [44, 59] for nephrotoxicity assays, lack expression of important

uptake transporters OAT1, OAT3, and OCT2 [58, 59]. Lack of phenotypic fidelity has been asserted to be an important limitation to the accuracy and predictability of in vitro cell-based toxicity assays [16, 25, 456, 457]. Hence, retention of key functional and phenotypic markers linked to relevant cell, tissue, and organ toxicity must be proven for model systems used for such screening. Cell source (e.g., primary versus immortalized), passage number, culture time, media-dependence and culture type all contribute to phenotypic fidelity and stability for such assays [16, 457, 458].

Hydrogel and extracellular matrix mimicking polymer supports are often proposed to support cells and organoids in culture to preserve or enhance cell functional performance over standard 2D culture methods [16]. While many such 3D culture matrices are described, and even commercially available [14, 19, 103], few are validated to show improvements over 2D cell culture analogs [77, 78], including both existence and preservation of functional cellular markers relevant to each toxicity assay/cell type.

Previous studies recently reported the 3D hydrogel-based murine proximal tubule drug toxicity assay and select responses to known nephrotoxic drugs [60, 65]. While demonstrating the value of this new culture concept to improve predictability of nephrotoxicity screening in general, those studies did not provide comprehensive analyses of key genes associated with known proximal tubule transporters and associated nephrotoxicity. This study's mRNA expression data for the same system now support the longevity of the 3D HA gel and nongel, media-based proximal tubule models up to 7 days. Moreover, the similarities of 3D HA gel gene expression with nongel expression indicates that gel embedding does not affect gene expression in these constructs. Expression of functioning, encoded proteins for these 21 genes is not reported due to the difficulties in quantifying membrane protein abundance – a major technical challenge for proteomics. mRNA expression data remains the most qualified alternative and studies have shown correlations between mRNA and protein expression levels [459, 460].

Results in Figure 4.4 show that after 3 days in both culture systems, 95% of the 21 transporter genes remain expressed in the proximal tubule fragments, and 90% after 7 days but at reduced levels. This shows superiority of these proximal tubule models to traditional 2D kidney cell lines, like HK-2 and Caki-1 that do not exhibit relevant gene expression profiles. Hilgendorf et al.

showed that transporter expression levels are not only lower in Caki-1 cell lines, but also that these cell lines showed narrower transporter expression profiles than kidney tissue [59]. On a statistical basis, their rank correlation analysis between kidney tissue expression levels and Caki-1 cell line expression levels shows only a coefficient of k'=0.12 [59] due to a general trend of lower expression levels in 2D cell line cultures. Similarly, Jenkinson et al. found that HK-2 cells, commonly used for nephrotoxicity studies [44] have limited value due to their low mRNA expression profiles of important drug transporters compared to renal cortex samples [58]. Their results show that mRNA expression of the SLC22 transporter family (OAT1, OAT3, and OCT2) is absent in HK-2 cells [58].

In contrast, the primary proximal tubule models demonstrate significant expression of these transporters for up to a week, and perhaps longer. Significantly, expression of important efflux transporters MDR1, MRP2, and MRP4 located at the tubule apical membrane surface and also uptake transporters OAT1, OAT3, and OCT2 on the basolateral membrane surface is shown, improving on the limited retention of proximal tubule characteristics reported by Jenkinson et al. for HK-2 cells [58]. OAT1, OAT3, and OCT2 in particular are key transporters in kidney drug transport and filtration [431, 461, 462] and highly expressed in human tissue samples [58, 59]. Lack of their expression in HK-2 cells [58, 463] as well as in Caki-1 cells [59] limits the relevance and predictive value of these culture models for nephrotoxicity studies. More relevant nephrotoxicity models that represent functional equivalents to proximal tubules in vivo are therefore required. Data presented here support the presence of requisite kidney transporters in an intact proximal tubule organoid-type 3D model, and therefore further completes our previous characterization data for this model [47, 60]. This also improves the knowledge that supports the importance of this model in further validation against known nephrotoxic drugs so that a meaningful translation/correlation between this model's data and human in vivo data can be made. We assert that this model can yield important information about potential mechanisms of toxicity, one of the most important criteria for useful in vitro toxicity models [464, 465].

To enable this proximal tubule in vitro model for handling in high throughput screening formats (e.g., multiwell plates, robotics fluid handling systems, screening platforms), we previously investigated encapsulation of harvested proximal tubule fragments in a modified, biomedical-grade

hyaluronic acid and PEG-diacrylate hydrogel [47, 60]. This 3D matrix encapsulation provides several culture enhancements, including direct gel formation in the presence of added proximal tubules, improving downstream handling of cultures through fluidics dispensing into 96-well plates, media exchange and drug candidate additions and dispersion of known amounts of proximal tubules within a viscous 3D matrix without settling, or compromising tubule integrity or amount. Additionally, this hyaluronic acid hydrogel limited the out-migration of proximal tubule cells from fragments into the gel matrix in culture, a complication of using collagen-based gels for this application [151, 466, 467]. The result of this approach was retention of several important nephrotoxic-relevant attributes in these proximal tubule 3D hydrogel cultures in toxicity assays compared to secondary kidney cell line 2D cultures [47, 60].

This study now adds additional veracity to these previous claims for functional and more reliable nephrotoxicity improvements to this culture method, showing that intact proximal tubules retain relevant gene expression profiles for kidney transport and toxicity processing, and addition of the 3D hydrogel embedding matrix does not compromise or alter gene expression profiles (see Figures 4.3-4.5). Analysis of the gel matrix on the endogenous mRNA expression controls (Figures 4.2 and 4.3) also shows that the gel matrix has no observable influence on reference gene stability, and therefore risks of data artifacts or falsification from varying reference gene expression are minimized (Figure 4.3). The correlation analysis for the two different proximal cell culture conditions supports their comparable expression profiles (correlation factor of R^2=0.97, Figure 4.5). The plot's y-intercept close to zero (-0.86) and the plot slope close to one (1.07) indicate that there is no difference between the relative gene expression profile of the HA gel embedded PT cultures and the nongel PT cultures.

Although most nephrotoxicity screens are performed within 24 h, mRNA expression levels for critical transporters are shown here to be measurable to 7 days in these cultures (e.g., see Figure 4.4) – further time points might even be possible. Figure 4.6 shows an overall trend of down-regulation of expression levels from 3 to 7 days and, with the exception of OCT3, all genes retain expression to 7 days. In vitro drug toxicity studies in these proximal tubule cultures could therefore be conducted up to 7 days depending on the genes of interest, and the drug or toxin applied.

In conclusion, this study extends earlier assertions of functional equivalence of primary 3D gel-based proximal tubule cultures for improving the predictability and reliability of in vitro nephrotoxicity screening over existing 2D kidney monocultures [47, 58-60]. Broad proximal tubule cell transporter expression known to be critical for nephrotoxicity is shown over extended culture times. While it is known that some transporters in rodents are different than in humans [455], these phenotypic and genotypic comparisons are essential to validate these (and any) in vitro assay system seeking to improve the quality and reliability of nephrotoxicity predictions from in vitro models to humans by using predictive correlation, and not a 1:1 identical response. Further 3D nephrotoxicity assay enhancements might include fluidics interfacing, miniaturization, and interfacing with other in vivo-mimicking biotransformation pathways (e.g., cytochrome p450 metabolic processing from gut and liver microsomes). Additionally, the 3D kidney-based model can be extended to understand the impact of new drug candidate structure-activity relationships in proximal tubule pharmacology and exploiting proximal tubule mutations in driving mechanism for drug toxicity.

Acknowledgements

This work was supported by AstraZeneca UK Limited, London, England. We thank Matthew Wagoner at AstraZeneca Pharmaceuticals, USA, for valuable discussions. DWG is grateful for support from the George S. and Dolores Doré Eccles Foundation (USA).

Table 4.1 TaqMan® Gene Expression Assays used for qPCR analysis in this study. The table provides an overview of the assays used, common gene symbols and systematic gene nomenclature [34].

Gene abbr.	Gene name	Gene symbole	TaqMan® Gene Expression Assay	Sequence Accession ID	UniGene ID	Entrez Gene ID	NCBI Location Chromosome	Exon Boundary	Assay Location	Amplicon Length
GAPDH	glyceraldehyde-3-phosphate dehydrogenase	Gapdh	Mm99999915_g1	NM_001289726.1	Mm.304088	14433	Chr.6: 125161338 - 125166511	2-3	117	107
PPIA	peptidylprolyl isomerase A	Ppia	Mm02342429_g1	NM_008907.1	Mm.5246	268373	Chr.11: 6415870 - 6419810	3-4	232	112
RPL19	ribosomal protein L19	Rpl19	Mm02601633_g1	NM_001159483.1	Mm.10247	19921	Chr.11: 98023080 - 98030493	5-6	517	69
OCT1	solute carrier family 22 (organic cation transporter), member 1	Slc22a1	Mm00456303_m1	NM_009202.5	Mm.594	20517	Chr.17: 12648874 - 12675838	3-4	856	69
OCT2	solute carrier family 22 (organic cation transporter), member 2	Slc22a2	Mm00457295_m1	NM_013667.2	Mm.17322	20518	Chr.17: 12583958 - 12628488	9-10	1596	85
MDR1	ATP-binding cassette, sub-family B (MDR/TAP), member 1B	Abcb1b	Mm00440736_m1	NM_011075.2	Mm.146649	18669	Chr.5: 8798147 - 8866315	20-21	2624	70
OCTN1	solute carrier family 22 (organic cation transporter), member 4	Slc22a4	Mm00457739_m1	NM_019687.3	Mm.274590	30805	Chr.11: 53983123 - 54028662	8-9	1568	73
OCTN2	solute carrier family 22 (organic cation transporter), member 5	Slc22a5	Mm00441468_m1	NM_011396.3	Mm.42253	20520	Chr.11: 53864542 - 53891799	5-6	1109	74
OCT3	solute carrier family 22 (organic cation transporter), member 3	Slc22a3	Mm00488294_m1	NM_011395.2	Mm.99252	20519	Chr.17: 12419972 - 12507704	9-10	1879	70
MRP2	ATP-binding cassette, sub-family C (CFTR/MRP), member 2	Abcc2	Mm00496899_m1	NM_013806.2	Mm.39054	12780	Chr.19: 43782308 - 43838332	29-30	4238	64
MRP4	ATP-binding cassette, sub-family C (CFTR/MRP), member 4	Abcc4	Mm01226381_m1	NM_001033336.3	Mm.40537	239273	Chr.14: 118482692 - 118707620	30-31	3978	99
OAT1	solute carrier family 22 (organic anion transporter), member 6	Slc22a6	Mm00456258_m1	NM_008766.3	Mm.30090	18399	Chr.19: 8617996 - 8628299	8-9	1644	95
OAT3	solute carrier family 22 (organic anion transporter), member 8	Slc22a8	Mm00459534_m1	NM_001164634.1	Mm.285294	19879	Chr.19: 8591254 - 8611835	5-6	983	63
SGLT2	solute carrier family 5 (sodium/glucose cotransporter), member 2	Slc5a2	Mm00453831_m1	NM_133254.3	Mm.38870	246787	Chr.7: 128265697 - 128272433	3-4	298	79
Megalin	low density lipoprotein receptor-related protein 2	Lrp2	Mm01328171_m1	NM_001081088.1	Mm.23847	14725	Chr.2: 69424335 - 69586067	77-78	13926	91
Cubilin	cubilin (intrinsic factor-cobalamin receptor)	Cubn	Mm01325077_m1	NM_001081084.2	Mm.313915	65969	Chr.2: 13276338 - 13491876	64-65	10418	64
PepT1	solute carrier family 15 (oligopeptide transporter), member 1	Slc15a1	Mm04209483_m1	NM_053079.2	Mm.155618	56643	Chr.14: 121459621 - 121505254	14-15	1096	80
PepT2	solute carrier family 15 (H+/peptide transporter), member 2	Slc15a2	Mm00451610_m1	NM_001145899.1	Mm.281804	57738	Chr.16: 36750164 - 36785157	5-6	738	69
AQP1	aquaporin 1	Aqp1	Mm00431834_m1	NM_007472.2	Mm.18625	11826	Chr.6: 55336299 - 55348555	1-2	581	64
AQP2	aquaporin 2	Aqp2	Mm00437575_m1	NM_009699.3	Mm.20206	11827	Chr.15: 99579056 - 99584545	1-2	458	107
Na,K-ATPase	ATPase, Na+/K+ transporting, alpha 1 polypeptide	Atp1a1	Mm00523255_m1	NM_144900.2	Mm.193670	11928	Chr.3: 101576219 - 101604707	10-11	1622	74
ABCB1	ATP-binding cassette, sub-family B (MDR/TAP), member 1A	Abcb1a	Mm00440761_m1	NM_011076.2	Mm.207354	18671	Chr.5: 8567091 - 8748575	20-21	2610	82
CYP3A11	cytochrome P450, family 3, subfamily a, polypeptide 11	Cyp3a11	Mm00731567_m1	NM_007818.3	Mm.332844	13112	Chr.5: 145854607 - 145879854	10-11	1108	128
GGT	gamma-glutamyltransferase 1	Ggt1	Mm00492322_m1	AK079235.1	Mm.4559	14598	Chr.10: 75564114 - 75586193	3-4	412	98

Table 4.2 Common renal cell sources used in drug screening assays.

Cell Name	Full name	Species	Origins	Cell type	Morphology	References
OK	Opossum Kidney	Opossum	Kidney, proximal tubule	Secondary	Epithelial	[41]
LLC-PK1	Lewis Lung Cancer-Pig Kidney	Pig	Kidney, proximal tubule	Secondary	Epithelial	[44-47]
HEK-293	Human Embryonic Kidney	Human	Embryonic kidney	Secondary	Epithelial	[47, 56]
HK-2	Human Kidney	Human	Kidney, proximal tubule	Secondary (HPV-E6/E7 immortalized)	Epithelial	[44, 57, 58]
Caki-1	Human Renal Cancer Cell Line	Human	Kidney, metastatic skin	Secondary	Epithelial	[59]
Rodent PTEC	Proximal Tubule Epithelial Cells	Rodent	Kidney, proximal tubule	Primary		[60]
hPTEC	Human Proximal Tubule Epithelial Cells	Human	Kidney, proximal tubule	Primary		[57, 61, 62]
NKi-2	N/A	Human	Kidney, Renal epithelial	Secondary (hTERT immortalized)	Epithelial-like	[65]
RPTEC/ TERT1	Renal Proximal Tubule Epithelial Cells	Human	Kidney, proximal tubule	Secondary (hTERT immortalized)	Epithelial-like	[70-72]
MDCK (NBL-2)	Madin-Darby Canine Kidney	Dog	Distal tubule	Secondary	Epithelial	[73, 74]

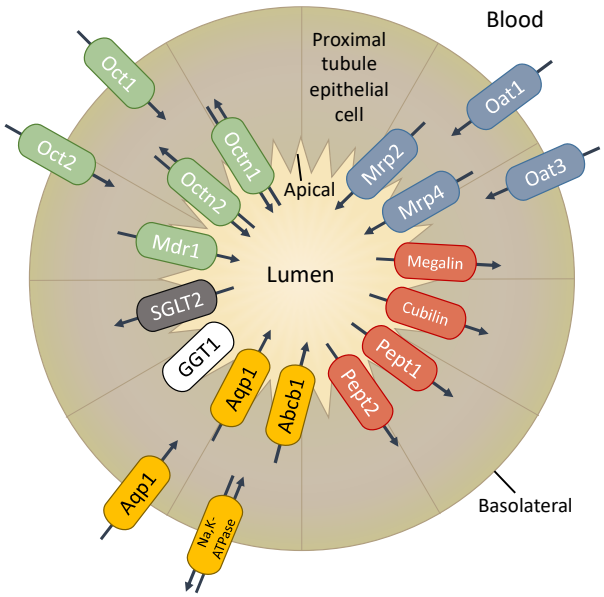

Figure 4.1 PT transporters with known roles in drug transport or PT function and their location. Gene sets used in this study represent important classes of cation (green), anion (blue), protein endocytosis (red), glucose (gray) transporters, metabolizing enzymes (white) and other transporters (yellow). Proximal tubule epithelial cells enclose the lumen in a monolayer of polarized cells. The microvilli-rich, apical membrane is facing the lumen, while the basolateral membrane faces the blood side. (Figure modified with permission from SOLVO Biotechnology (www.solvo.com), Szeged, Hungry, May 2017.)

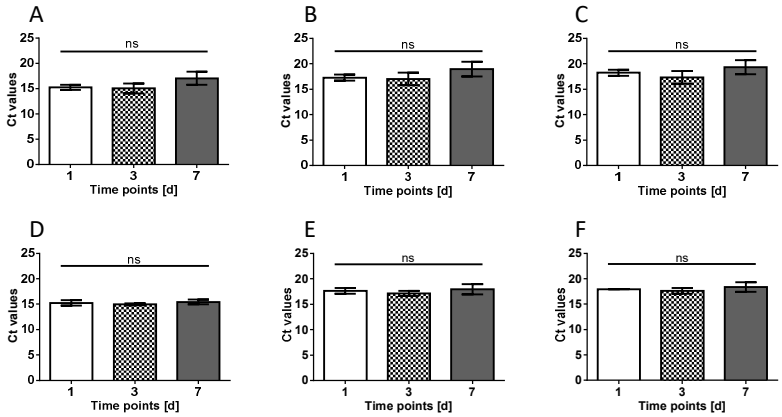

Figure 4.2 Reference gene controls. Endogenous control stability over time (1, 3, and 7 days) determined by qPCR in either nongel media suspension (A-C) or HA gel-embedded (D-F) isolated proximal tubule fragments. Used endogenous controls: GAPDH (A,D), PPIA (B,E) and RPL19 (C,F). Raw Ct values (y-axis) of each reference gene per time point (x-axis) are displayed. Each bar shows mean ± standard deviation (SD) from three individual biological samples (n=3) analyzed in triplicates. One-way analysis of variance (ANOVA) followed by Tukey's multiple comparison post-hoc test between all time points was performed. No statistically significant differences (ns) between time points were observed (p<0.05)

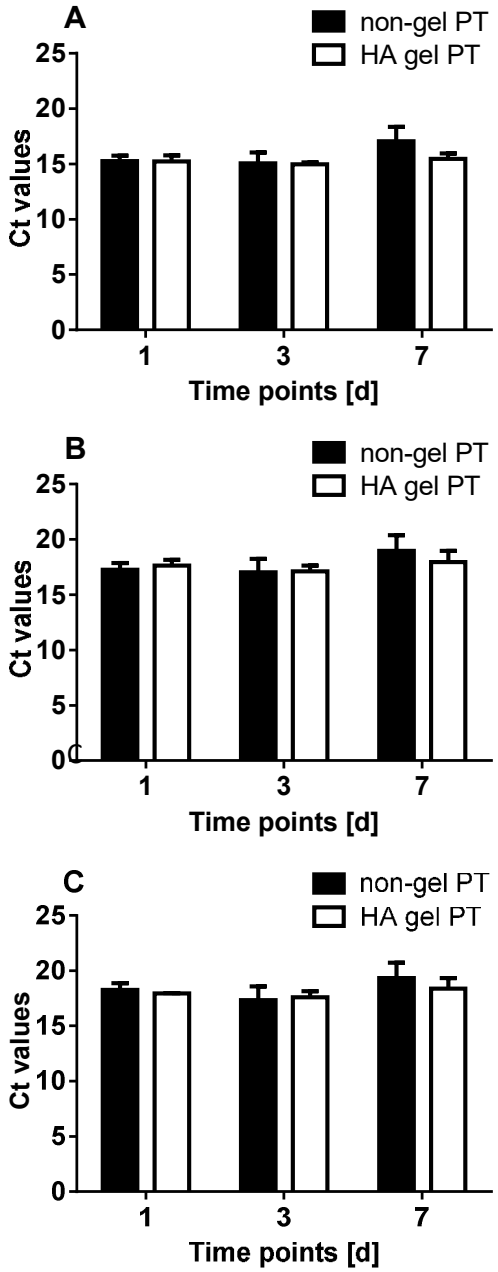

Figure 4.3 Replot of Figure 4.2 data. Comparison of the endogenous control stability between culture conditions (nonembedded proximal tubules shown in black, HA gel-embedded proximal tubule shown in white) determined at different time points.Raw Ct values (y-axis) of each reference gene (GAPDH (A), PPIA (B), RPL19 (C)) per time point (x-axis) are displayed. The bars show the mean ± standard deviation (SD) from three individual biological samples (n=3) analyzed in triplicates. Unpaired Student's t-tests were performed between each culture condition on each time point. No statistically significant differences between cell culture condition were observed (p<0.05)

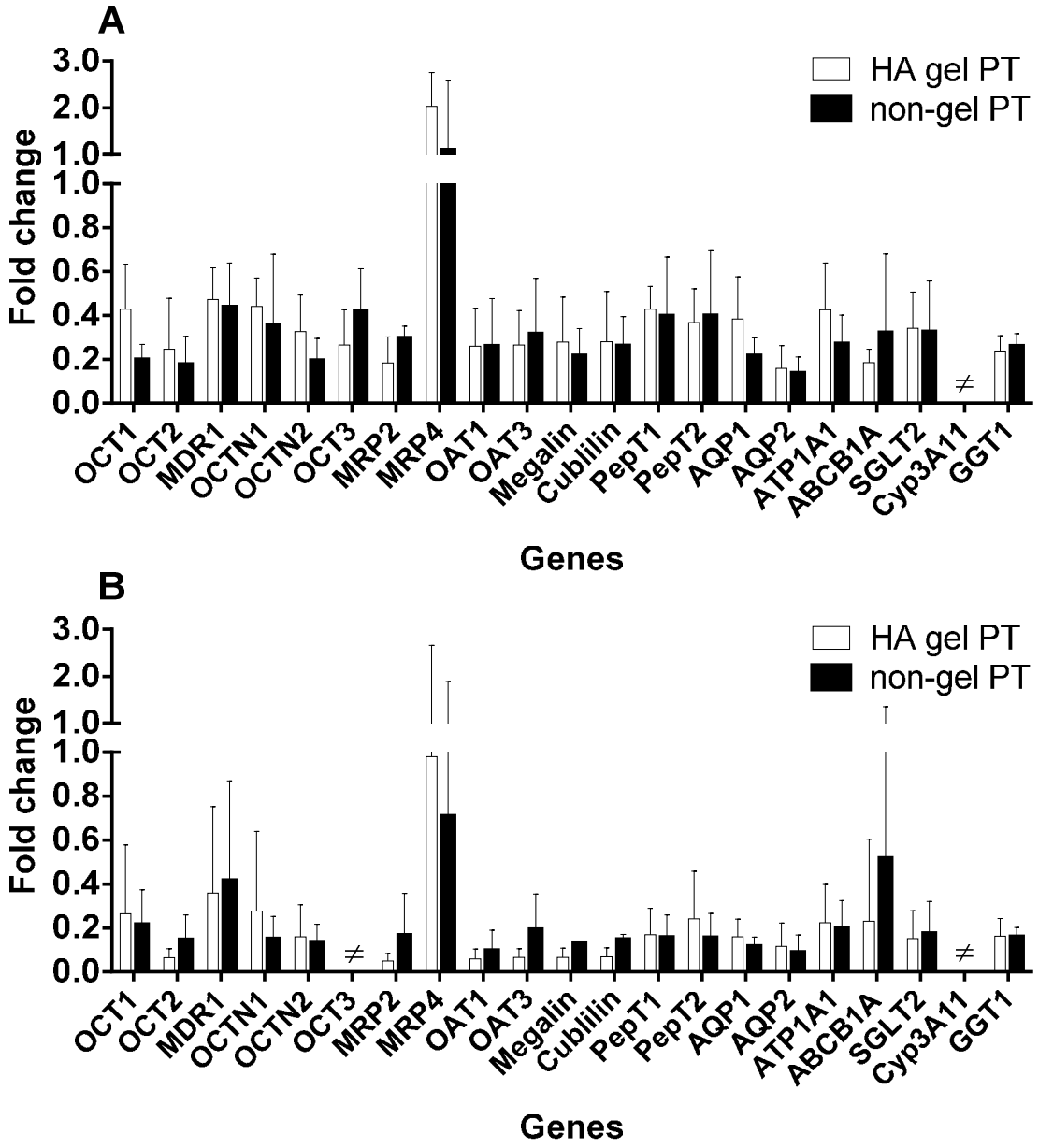

Figure 4.4 qPCR analysis of transporter gene expression in proximal tubule fragments. Relative expression of proximal tubule transporters with known roles in drug transport or proximal tubule function of embedded (shown in white) or nonembedded (shown in black) proximal tubule fragments. Expression levels are shown after (A) 3 days and (B) 7 days in culture. The bars represent the mean relative expression level and the error bars indicate the standard deviation (SD) from three individual biological samples (n=3) analyzed in triplicate. ≠ indicates absence of gene expression. Unpaired Student's t-tests were performed for each gene between the two culture conditions. No statistically significant differences between the embedded and nonembedded culture conditions were detected (p<0.05)

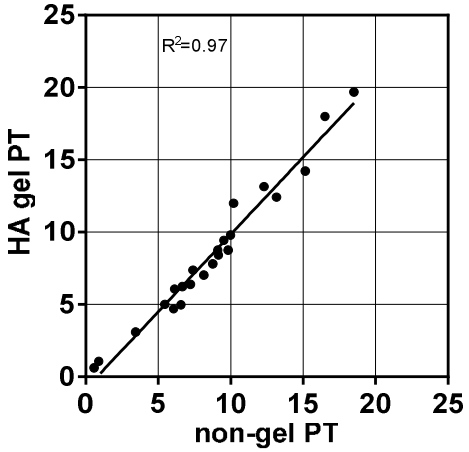

Figure 4.5 Correlation analysis of relative expression levels. Relative expression levels in modified HA gel embedded proximal tubule fragments (y-axis) and proximal tubule fragments suspended in media (x-axis).Correlation coefficient (R^2) is provided

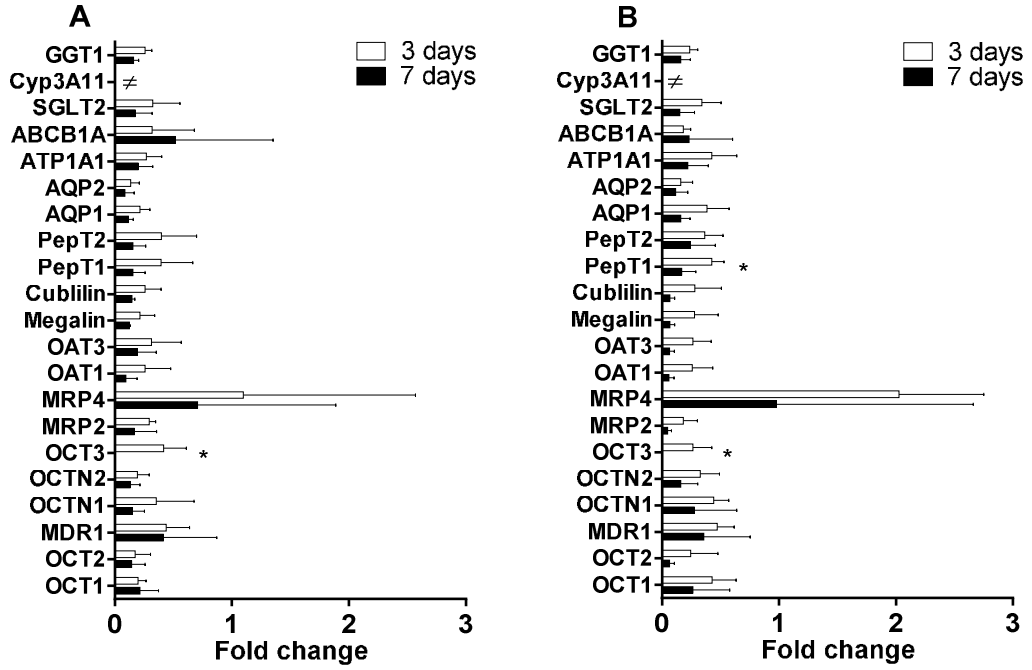

Figure 4.6 qPCR analysis of transporter gene expression in proximal tubule fragments. Relative expression change over time (3 days expression levels shown in white, 7 days expression levels shown in black). Expression levels are shown of (A) in modified HA gel embedded proximal tubules and (B) nonembedded proximal tubules. The bars represent the mean relative expression level and the error bars indicate the standard deviation (SD) from three individual biological samples (n=3) analyzed in triplicate. ≠ indicates absence of gene expression. Unpaired Student's t-tests were performed for each gene between the two time points. Statistically significant differences (p<0.05) between the two different time points are indicated by asterisks

CHAPTER 5

AN EX VIVO 3D KIDNEY PROXIMAL TUBULE MODEL IMPROVES PREDICTIONS OF CLINICAL DRUG-INDUCED NEPHROTOXICITY[3]

Abstract

The inhibitor constant, Ki, is an indication of how potent an inhibitor is; it is the concentration required to produce half maximum inhibition. The inhibitor constant, Ki, is an indication of how potent an inhibitor is; it is the concentration required to produce half maximum inhibition. Drug attrition and clinical product withdrawals due to nephrotoxicity remain a major challenge for pharmaceutical drug development pipelines. Currently, no reliable high-throughput in vitro screening models are available that provide reliable, predictive toxicology data for clinical nephrotoxicity. The fidelity of drug screening assays to predict toxicity and desired pharmacology assessments is compromised by standard two-dimensional (2D) cell monoculture models common to drug development. Here we extend the use of our previously reported murine three-dimensional (3D) kidney organoid proximal tubule model to provide ex vivo drug toxicity data that reliably compare to clinical experiences and that improve nephrotoxicity predictions. Proximal tubule cytotoxicity (via ATP depletion) was monitored for 9 compounds (cimetidine, cidofovir, cisplatin, doxorubicin, gentamicin, polymyxin B, polymyxin B nonapeptide, probenecid, and vancomycin) in the 3D proximal tubule ex vivo model. Drug concentration-response curves and their IC_{50}, LEC, and AUC values were calculated and compared to clinical therapeutic exposure levels (C_{max}). The 100-fold C_{max} threshold demonstrated the most sensitivity (96.6%) and specificity (88.9%) for this assay with a high positive (96.6%) and negative (88.9%) predictive value for nephrotoxicity. These

[3] Diekjürgen, Dorina and Grainger, David. An ex vivo 3D kidney proximal tubule model improves predictions of clinical drug-induced nephrotoxicity. Toxicological Sciences, submitted 2017

results support the model's capability to predict substrate-inhibitor/competitor interactions, in addition to yielding changes in toxicity similar to those in vivo. Our approach demonstrates the utility of 3D proximal tubule cultures in drug screening assays that better predict nephrotoxicity and yield more insight into the complex mechanisms implicated in nephrotoxicity. This study offers a new approach for rapid drug toxicity testing with more reliable clinical comparisons than current 2D cell culture screening models.

Introduction

Kidney toxicity is the second highest cause of new drug failure after liver toxicity, resulting in many adverse pharmaceutical drug performance issues in clinical trials [91]. The lack of reliable drug candidate identification and reliable toxicity screening methods result in costly consequences when drugs fail late in the development process [92]. Currently, only 8% of new pharmaceutical compounds tested in clinical trials receive regulatory approval [65]. This low success rate does not sufficiently balance against drug development efforts (typical timeframes averaging 9 years) and associated expenses (~$1-2 billion) [65]. Hence, improved predictive testing models to screen drug toxicity in early research stages that facilitate more reliable elimination of toxic drug candidates well before clinical trials is required [91].

Besides the liver, the kidney is a primary drug metabolism and elimination site. Therefore, kidney cells are essential components for many systemic drug toxicity models. The currently used screening models for nephrotoxicity eliminate only about 7% of pharmaceutical compounds in preclinical tests, correlating poorly to drug-induced acute renal failure cases estimated between 30-50% [93-95]. This suggests that a considerable validity gap exists between current in vitro screening approaches and physiological responses seen both in clinical trials and after drugs reach the marketplace [93, 96, 97].

Kidney proximal tubules play a major role in xenobiotic secretion and metabolism, and therefore are primary target sites of drug-induced nephrotoxicity. This is attributed to specialized transporters (e.g., OAT1, OAT3, OCT2) within proximal tubules responsible for the uptake of organic compounds on their basolateral membrane [420-422]. This active transport then results in

high levels of toxins within proximal tubule epithelial cells, leading to cellular damage and death [423, 424]. Proximal tubule physiology figures prominently into their practical and predictive utility as drug toxicity screening model, yet is poorly accommodated in cell monocultures on plastic cultureware in vitro.

Previously, many different three-dimensional (3D) cell culture systems have exhibited performance advantages over conventional two-dimensional (2D) cell monocultures in vitro drug screening standards in pharmaceutical industry currently used in combination with animal studies [14]. In 2D cell culture, primary proximal tubule cells lose their apical-basal polarization rapidly, sometimes within minutes of culture [102, 468, 469]. Immortalized kidney secondary cell lines (e.g., HK-2, Caki-1, LLC-PK1, OK) are often missing important transporters relevant to drug toxicity [98]. By contrast, 3D cultures of renal proximal tubule cells demonstrate more abundant and enduring apical and basal transporter expression than transporters in 2D cell lines [12], suggesting their more reliable response to pharmaceutical compounds. 3D cell culture models generally exhibit cell morphology and physiology better resembling in vivo characteristics versus 2D cell culture lines [432, 433]. Furthermore, 3D cell cultures respond with more in vivo-like behaviors than 2D cell cultures [434, 435]. Therefore, recent strategies emphasize a shift away from homogenous monolayer-cultured cells on rigid plastic plates to more promising 3D culture systems with biomaterials architectures similar to tissue constructs (i.e., organoids, micro-tissues, spheroids and cells in hydrogel matrices of various chemistries) [103, 104].

To enhance proximal tubule epithelial cells to retain their native proximal tubule organ structure, we recently developed a murine 3D kidney organoid toxicity ex vivo model fulfilling many functional drug screening criteria and improvements over current 2D kidney cell monocultures on plastic. This model comprises viable mouse kidney-derived proximal tubule fragments in suspension culture amenable to multiwell scaling and screening assays [12, 60]. This 3D approach keeps the proximal tubule extracellular matrix with innate natural cell-cell communications intact, maintains differentiated cellular states, and preserves cell-specific tubule functionalities [60]. Kidney proximal tubule cells therefore reside and interact in these 3D cultures in a more natural environment, reflecting toxicity responses with more fidelity when interacting with administered drug

compounds. Additionally, previous work has shown that known proximal tubule markers and important proximal tubule transporters with known roles in drug transport are retained in this 3D proximal tubule culture model, exhibiting better expression levels and profiles than commonly used 2D kidney cell lines [12].

Given the current high rates and high costs of drug failures, and poor predictive capacities and costs of animal testing, new drug testing models must be highly sensitive to drug concentration, minimize animal use, and be suitable for high-throughput screening modalities. New testing models that respond accurately to pharmaceutical compounds and allow for human clinical comparison must be validated. To do so for our newly developed 3D proximal tubule organoid model [12, 60], 3D proximal tubule fragment cultures were exposed in this present work to known nephrotoxins (cidofovir, polymyxin B, gentamicin, cisplatin, doxorubicin, vancomycin, and polymyxin B nonapeptide) and also nonnephrotoxins (probenecid and cimetidine) and analyzed for toxicity dose-response outcomes. This model is shown to be capable of accurately predicting nephrotoxicity for all tested compounds and produced toxicity responses highly correlated to known human clinical experiences with the same agents. Therefore, the model is most promising for reliable toxicity screening of novel compounds during early phases of drug development. Furthermore, this model could be further used to gain insight into specific drug structural mechanisms that drive toxicity, and facilitate rapid assay of different chemical moieties during structure activity relationship screening.

Materials and methods

Materials

All reagents and compounds were purchased from Sigma-Aldrich (St. Louis, USA) or Invitrogen (Carlsbad, USA). Cell culture consumables were purchased from ThermoFisher Scientific (Hampton, USA) unless noted otherwise. The CellTiter-Glo® 3D Cell Viability Assay was purchased from Promega (Madison, USA).

Compound Classification

Compound nephrotoxin classifications were collected from Micromedex (www.micromedex.com). Classical terminologies for renal injury (e.g., nephrotoxicity, renal damage) were used to identify compounds with reported clinical adverse events. If no reports for nephrotoxicity were evident, then the compound was classified as nonnephrotoxic. Maximum plasma concentrations (C_{max}) and nephrotoxicity incidences were acquired from Micromedex, PubMed, and FDA drug labels for all compounds used here unless otherwise stated. Collected C_{max} values were after single-dose administration at commonly recommended therapeutic doses as previously described [470]. The compounds were selected to represent different therapeutic drug classes.

Murine proximal tubule harvest and isolation

Male C57BL/6 mice were purchased (age 6-8 weeks, Charles River Laboratories International, Inc., Wilmington, USA) and fed and housed and acclimated in climate and light cycle controlled, approved murine vivarium conditions. All animals were euthanized using carbon dioxide (CO_2) in accordance with University of Utah IACUC-approved protocols. Kidneys were harvested and proximal tubules were isolated using a mechanical technique followed by enzymatic digestion as previously described [60, 443]. Briefly, kidneys were removed surgically under standard aseptic conditions in a BSL2-certified laminar flow hood. The kidney capsule, ureter and blood vessels were removed and the isolated kidneys were mechanically disrupted by using a sterilized razor blade followed by enzymatic digestion with 2 mg/ml hyaluronidase (Worthington Biochemical Corporation, USA), 3 mg/ml collagenase IV (Worthington Biochemical Corporation, USA), and 0.1 mg/ml DNase I (Sigma Aldrich, USA) in KREBS solution (145 mM NaCl, 10 mM HEPES, 5 mM KCl, 1 mM NaH_2PO_4, 2.5 mM $CaCl_2$, 1.8 mM $MgSO_4$, 5 mM glucose, pH 7.3) at 37 °C [444]. To isolate the proximal tubules from the digested sections, sequential 250 µm and 70 µm mechanical sieving was used [443]. Resulting proximal tubule fragments were pelleted by centrifugation and yields were calculated using a hemocytometer.

Proximal tubule (PT) cultures

Murine proximal tubule fragments (approximate size range of 70-250 µm) were resuspended in proximal tubule media comprising Dulbecco's Modified Eagle Medium/Nutrient Mixture F-12 with 4-(2-hydroxyethyl)-1-piperazineethanesulfonic acid and L-glutamine (Invitrogen, USA). Additionally, 1% fetal calf serum (Invitrogen, USA), 5% sodium pyruvate (Invitrogen, USA), 10% nonessential amino acids (Invitrogen, USA), 10% insulin/transferrin/selenium (Invitrogen, USA), 1% antibiotic-antimycotic (Invitrogen, USA), and 0.9 µg hydrocortisone (Invitrogen, USA) were added [443]. The media was phenol-red free to avoid possible interference of luminescence signals through the pH indicator alone [469]. Finally, 100 µl proximal tubule media containing approximately 1000 proximal tubules was added to each well of a 96-well plate well. Plates were then incubated in cell culture incubators under 5% CO_2 and 95% air at 37 °C.

Compound preparation and model exposure

All bioactive compounds were dissolved in UltraPure™ Distilled Water (ThermoFisher, USA) to obtain stock solutions (no insolubility or precipitation was seen with any compounds, assessed by visual inspection) and stored according to the manufacturer's information. For all compounds, six concentration dilutions in PT media were prepared fresh prior to addition to cell culture wells to obtain final indicated concentrations. Final compound concentration ranges were 1-1000 µM. Potential compound precipitation was again assessed after dilution in media by visual inspection and no precipitation was seen for any of the compounds. Proximal tubule fragments were exposed to the various compounds at each concentration in PT media replicates for 24 h in cell culture incubators under 5% CO_2 and 95% air at 37 °C.

To analyze the 3D assay model's ability to reveal kidney tubule epithelial cell substrate-inhibitor competitive interactions, the toxic drug alone and the same drug in combination with a potent, receptor-specific inhibitor/competitor selected from the 9 compounds was tested. In this case, each concentration over the full concentration range (1-1000 µM) of toxic drug was co-administered with 30 µM of the selected, matched inhibitor/competitor in PT media replicates for 24 h in cell culture incubators under 5% CO_2 and 95% air at 37 °C. This 30 µM concentration was

chosen as each inhibitor/competitor alone did not exhibit a toxic response at this concentration (Figure 5.1). This indicates that any change in toxicity would reflect the coadministration and not that from the selected inhibitor/competitor alone. Assays with compounds, controls of vehicle only (media), and positive control (1% Triton X-100 in PT media) were screened in biological triplicate with three technical replicates.

Cytotoxicity (ATP depletion) assay

For compound testing, proximal tubule (PT) fragment cultures were seeded at 1000 PT fragments/well in solid white 96-well plates in 100 µl PT media and allowed to recover from harvest at 37 °C under humidified atmosphere and 5% CO_2 and 95% air for 24 h before test compound addition/exposure. After 24-h compound exposure, cellular adenosine triphosphate (ATP) concentrations were assessed using the CellTiter-Glo® 3D Cell Viability Assay following manufacturer's protocols (Promega, USA): Briefly, an equal amount (100 µl) of assay reagent was added to proximal tubule cultures cooled to room temperature, followed by orbital shaking of the plate for 5 min and additional 10 min of incubation in the dark. Wells were then read for luminescent light intensity using a Synergy 2 Multi-Mode Reader (Biotek, USA). The luminescence assay is based on the luciferase/luciferin reaction that determines the number of viable cells based on ATP levels. No interference between the test compounds and the assay itself was observed (data not shown).

Toxicity assay output parameter profiling

Three different toxicity output parameters were used to evaluate this model's ex vivo toxicity from the ATP assay concentration-response curves for each compound. The molar concentration of each test compound producing 50% inhibition (IC_{50}) was calculated using three-parameter nonlinear regression with a Hill slope of -1 and upper and lower values constrained to 100 and 0, respectively. The lowest effective concentration (LEC) of each drug was determined as the first compound concentration producing toxicity outside the normal viable cell population (mean ± 3 standard deviations (SD)) for the negative controls. Area Under the concentration-response

Curve (AUC) as well as under the Receiver Operating Characteristic (ROC-AUC) curve were calculated and expressed unitless as at least one of the axes is expressed in percent.

Data analysis/statistical analysis

All data were analyzed with Microsoft Excel® 2013 (Microsoft Corporation, Redmond, USA) and GraphPad Prism 6 software (GraphPad Software Inc., San Diego, USA). Concentration-response curves were plotted for each test compound and expressed relative to vehicle (no drug) control ±SD. All experiments were performed on three independent biological samples with three technical replicates each. All data are shown with mean (average) and standard deviation (SD). One-way analysis of variance (ANOVA) followed by Tukey's multiple comparison post-hoc test or unpaired Student's t-test were performed to analyze statistically significant differences. Results were considered as statistically significant differences with a confidence interval of 95% (p<0.05). To consider an assay response as positive, the following criteria had to be fulfilled: 1) statistically significant change compared to vehicle control (no drug), 2) unless the statistically significant response change was seen at the highest concentration, the compound had to follow a concentration-response relationship, and 3) a biologically meaningful (e.g., decrease in mitochondrial function, decrease in ATP level) result had to be shown. If a response did not meet these criteria, it was considered to be negative.

Therapeutic index (TI) was calculated by dividing the acquired cytotoxicity parameter (IC_{50}, LEC and AUC) by each compound's maximum therapeutic plasma concentration (C_{max}). F-tests to compare the concentration-response curves were performed in Graphpad Prism. The Z'-factor, a measurement of assay quality (signal dynamic range and data variation) [471] was derived from the raw data using Microsoft Excel® 2013. A Z' value between 0.5 and 1 indicates good, robust and reliable assay quality [471]. Receiver operator characteristic (ROC) curves were plotted using Graphpad Prism and used to examine paired true positive (sensitivity) and false-positive (specificity) rates for all TI thresholds of the model [472]. True positives (TP) are defined as nephrotoxic compounds that provide positive 3D assay results, while true negatives (TN) are those for nonnephrotoxic compounds that provide negative results in the 3D culture model. Assay

sensitivity was calculated by dividing the TP value by the total number of nephrotoxins used in this study. Specificity was calculated by dividing the TN value by the total number of nonnephrotoxic compounds used in this study. The Youden's index was calculated to determine the optimal cut-off value, which is defined as the maximum value of the index [473]. The ROC curves were generated by plotting sensitivity against 1-specificity at different C_{max} threshold levels. Additionally, the positive predictive value (PPV) was calculated by dividing the TP value by the total number of positive results and the negative predictive value (NPV) was calculated by dividing the TN value by the total number of negative results [474].

Results

3D proximal tubule model for ex vivo toxicity profiling

The cellular ATP-based CellTiter-Glo® 3D Cell Viability (Promega, USA) assay is used to determine ex vivo drug-induced nephrotoxicity testing in the 3D proximal tubule fragment culture model. To validate the linear range of the assay to avoid saturation of signal intensity or other artifacts, assay signal versus proximal tubule seeding density was first determined and analyzed using Z'-factor calculation (value between 0.5-1.0 required [471]) prior to testing selected compounds (data not shown). Subsequently, compound concentration-response curves (Figure 5.1) for 9 different drugs (nephrotoxic and nonnephrotoxic) and respective IC_{50}, LEC, and AUC values were calculated as described in Materials and methods (Table 5.1). While it has been previously recommended that drugs in such in vitro assays be tested at 30-100 times the human therapeutic C_{max} [470, 475, 476], all drugs were tested at fixed concentrations ranging from 1-1000 µM to account for the observation that in early drug development phases, clinical C_{max} values are unknown. This facilitates seamless adoption of the model for routine ex vivo toxicity screening in early drug development stages. A full overview of the results from validation of this drug set is shown in Table 5.1.

Correlation of different toxicity output parameters and zone classification of compounds with similar toxicity profiles based on IC50 and LEC

To compare different toxicity output parameters commonly used in ex vivo toxicity studies, three different parameters (IC_{50}, LEC, AUC) are calculated. Figure 5.2 compares the C_{max}-normalized IC_{50} against the C_{max}-normalized LEC values, exhibiting a good correlation (0.9998-1 linear correlation factor, Figure 5.2). Additionally, IC_{50} (Figure 5.3 A) and LEC (Figure 5.3 B) results are plotted against the clinical C_{max} values, and the model identifies one zone that only includes nephrotoxic drugs (i.e., below the divider line shown in each plot). Therefore, the model correctly identified compounds in this validation set as nephrotoxic (e.g., cidofovir, cisplatin, polymyxin B, polymyxin B nonapeptide, doxorubicin, and gentamicin) and nonnephrotoxic (e.g., cimetidine and probenecid) within the tested concentration range using the IC_{50} toxicity output parameter (Figure 5.3 A) and one false negative outlier is observed when using the LEC toxicity output parameter (Figure 5.3 B).

Determination of safe drug exposure values based on different toxicity output parameters

To determine safe drug exposure values from our model, TI threshold analysis was performed. Visualization of the relationship between the IC_{50} and C_{max} for each tested compound is shown in Figure 5.4: the higher the IC_{50} value the less toxic a compound is. Additionally, Figure 5.4 shows that very toxic drugs either demonstrate similar IC_{50} and C_{max} values (e.g., polymyxin B and cisplatin) or very low C_{max} values (e.g., doxorubicin). Use of multiplied C_{max} values leads to more robust and predictive toxicity assessments, especially the 100x C_{max} [470, 475-477]. Using this approach, a drug producing an in vitro response below 100x of its in vivo C_{max} is considered toxic [470, 475-477]. To determine if the 100x C_{max} threshold is also appropriate for the 3D proximal tubule nephrotoxicity model (or if perhaps a different threshold is more applicable), the assay sensitivity and specificity for multiple different-fold increases of C_{max} (range 1-1000-fold) was determined. This analysis was performed for two different toxicity output parameters: IC_{50} and LEC (calculated as previously described in Materials and methods). These predictions are shown in

Table 5.2. Overall, at high TI thresholds, classification of nephrotoxic compounds by the 3D assay is more correct (i.e., higher number of true positives), while at lower TI thresholds the correct classification of nonnephrotoxic compounds dominates (i.e., lower number of false positives).

ROC curves for the two output parameters (IC_{50} and LEC) were then generated in Figure 5.5. The ROC curve for IC_{50} is closer to the upper-left corner, indicating that this parameter offers better predictive value for nephrotoxicity in the 3D ex vivo kidney model. The calculated ROC-AUC values of 0.9638 and 0.9400 for the IC_{50} and LEC, respectively, are shown in Table 5.3. The higher the ROC-AUC, the more predictive the toxicity model (i.e., values >0.5 indicate predictability greater than chance [472]).

ROC curves can be also used to determine the appropriate cut-off levels for compound toxicity. In this 3D proximal tubule ex vivo model, a 100-fold C_{max} provided the highest combination of sensitivity and specificity, calculated by the Youden's index, and therefore, the optimal cut-off value. Using this threshold, the assay sensitivity was 96.6% for both IC_{50} and LEC values, and assay specificity was 88% and 66.7% for IC_{50} and LEC, respectively. Comparing between different C_{max} TI cutoff values, assay sensitivity increases significantly from 6.9% at 1x C_{max} to 75% at 30x C_{max} and finally 96.6% at 100x C_{max} for IC_{50}. Assay specificity decreases from 100% at 1x and 30x C_{max} to 88% at 100x C_{max}. A similar trend was seen for LEC: sensitivity increases significantly from 37.9% (1x C_{max}) to 93.1% (30x C_{max}) to 96.6% (100x C_{max}), and specificity decreases from 100% (1x C_{max}) to 77.8% (30x C_{max}) to 66.7% (100x C_{max}) – see Table 5.2. Therefore, both toxicity output parameters achieved good assay sensitivity values at 100x C_{max} (96.6%) but the IC_{50} parameter showed better specificity (88%) compared to that for the LEC parameter (66.7%). Additionally, the positive predictive value (PPV, defined as the probability that the compound is toxic when the 3D model result is positive) and negative predictive value (NPV, defined as the probability that the compound is nontoxic when the 3D model result is negative) were also determined. These values also show better results for the IC_{50} parameter (96.6% PPV, 88.9% NPV) compared to the LEC parameter values (90.3% PPV, 85.7% NPV) at 100x C_{max} (Table 5.2).

Validation of the 3D proximal tubule model for compound nephrotoxicity testing

To validate whether nephrotoxicity can be reliably predicted with this 3D proximal tubule ex vivo model, the calculated IC_{50} values were normalized by different clinical C_{max} literature data and plotted against documented clinical nephrotoxicity incidences at that specific C_{max} concentration (Figure 5.6). Each dot represents data from a different clinical drug exposure level and the resulting toxicity incidence percent (y-axis) compared to normalized IC_{50} values from the 3D toxicity model (x-axis). This correlation provides a valuable comparison of the outcomes of the 3D toxicity model parameters with known human effects in vivo. The closer the dot is located to the top right corner, the higher the risk of clinical nephrotoxicity, indicated by the arrow (Figure 5.6).

Mechanistic (substrate-inhibitor) insights from the 3D proximal tubule model using paired compounds

The influence of coadministration of selected clinically relevant inhibitors/competitors with single compounds reveals kidney tubule epithelial substrate-inhibitor interactions. To analyze the 3D model's ability to discriminate kidney tubule epithelial cell substrate-inhibitor interactions, the toxic drug alone and the drug combined with a potent, receptor-specific inhibitor/competitor selected from the 9 compounds was tested: Figure 5.7 shows the concentration-response curves for A) cidofovir (OAT1 substrate) alone versus in combination with probenecid (OAT1 inhibitor), B) cisplatin (OCT2 substrate) alone versus cisplatin in combination with cimetidine (OCT2 inhibitor), and C) polymyxin B (megalin substrate) versus the combination of polymyxin B with polymyxin B nonapeptide, a known, less-toxic polymyxin B analog [478]. All three plots show shifts in the concentration-response curves to the right in the presence of the inhibitor/competitor compared to curves of each compound alone, equating to reduced toxicity. The respective IC_{50} values from each compound condition were calculated, with these data expressed as the ratio of IC_{50} of toxic drug co-administrated with inhibitor/competitor to IC_{50} of toxic drug alone (Figure 5.7 D). A ratio of ≥ 1 indicates that the inhibitor is protective against the compound's nephrotoxicity or that a competitor (i.e., the case of polymyxin B/polymyxin B nonapepetide) can reduce toxicity by competing for the same receptor. In all three cases, the specific inhibitor/competitor displays nephron-protection to

varying degrees.

Discussion

Kidney proximal tubules play a major role in xenobiotic and metabolite secretion from the body, and are the primary target site of drug-induced nephrotoxicity. Active transport of toxin into the proximal tubule cells concentrates the toxin, producing cell damage and necrosis [423, 424]. Reliable active transport is important to recapitulate in kidney epithelial cell models to reproduce clinical toxicity effects. Previous work has shown that 2D primary proximal tubule cells lose their polarization sometimes within minutes of monoculture [102] and that secondary, immortalized cell lines are often missing important kidney transporters needed for drug toxicity responses [98]. This led to a shift away from monolayer-cultured 2D cells on plastic to 3D cell culture systems that more closely resemble in vivo tissue conditions (i.e. organoids, micro-tissues and spheroids) [39, 103, 104].

The 3D ex vivo murine kidney organoid toxicity model used here [12, 19, 60] out-performs the current 2D kidney cell cultures on plastic, as relevant drug transporter expression and maintenance in this system was recently shown to be superior to 2D cultures [12]. This present study focused on leveraging these transporter profiles and prior proof-of-concept for this 3D culture to analyze drug toxicity prediction by this model using the CellTiter-Glo® 3D Cell Viability Assay (Promega, USA). ATP is a marker of mitochondrial function, and therefore cell viability [479]. Beyond the high-throughput screening (HTS) compatibility, low fluorescence interference issues and excellent sensitivity and reproducibility [470], the CellTiter-Glo® 3D Cell Viability Assay exhibits an intensified cell lytic capability important to assure lysis of the 3D proximal tubule fragments and facilitating stronger, more sensitive signal generation compared to normal CellTiter-Glo® Cell Viability Assay (data not shown). Assay validation showed consistent mean values and low standard deviations for assay responses under test conditions. Various toxicity assay output parameters (e.g., IC_{50}, LEC, AUC) were previously shown to provide more accurate insight into drug toxicity [480]. All of these parameters are derived from the Hill equation [481] and commonly used in toxicity assessments. IC_{50} is considered the classical measurement parameter for drug

potency, and LEC is used to determine drug efficacy. AUC is the combination of potency and efficacy [480]. As all of these parameters are commonly used, we calculated and analyzed all three values in our model from compound concentration-response curves (Figure 5.1).A good correlation between the C_{max}-normalized IC_{50} and LEC values was produced (R^2=0.9998-1, Figure 5.2).

As it is important for a reliable drug toxicity model to avoid excluding potentially promising compounds early in development, a low false positive rate is essential for assay reliability. The zone classification attempt based on the IC_{50} or LEC and C_{max} values (shown in Figures 5.3 A, B) identified an area with only toxic drugs and no false positive answers. While it can be seen that the IC_{50} parameter also produces a zone with only nonnephrotoxic compounds (Figure 5.3 A), the LEC parameter includes a false negative outlier (Figure 5.3 B). This can be explained by the less sensitive nature of the LEC determination compared to the IC_{50} parameter. While the IC_{50} parameter is defined by the Hill equation and therefore a curve fit value with a lot of statistical precision, the LEC is dependent on the amount of chosen concentration test points in the assay and therefore increases in precision with increased test concentrations per compound. Therefore, the false negative outliner is an artefact of the LEC determination and the IC_{50} zone classification plot is more precise and accurate.

An important factor for toxicity assessment is determining proper thresholds to assess a compound as nephrotoxic or nonnephrotoxic at therapeutic concentrations. Previous studies determine a toxicity threshold from the determined therapeutic index (TI), defined as the toxicity-indicating parameter from the in vitro study divided by the therapeutic maximum plasma concentration (C_{max}) from clinical data. This method has been shown to reliably classify a drug as toxic or nontoxic [470, 475-477, 482].

Notably, in the absence of any clinical C_{max} experience (i.e., early preclinical drug development), others have reported that in vitro efficacious concentration can be used to normalize the IC_{50} values [483, 484]. Also, C_{max} values from animal studies could be used in preclinical stages. If these kind of data are absent, IC_{50} values can only be used to rank the compounds [470, 475, 483].

For our model the best sensitivity was evident at a threshold of 100x C_{max} while maintaining

a low false positive rate. While sensitivity values are the same, the false positive rate values are superior for the IC_{50} parameter over LEC. Data in Table 5.2 indicates that 100x C_{max} is the most appropriate threshold in the 3D model for both toxicity parameters, demonstrating a high positive predictive value of 96.6% for IC_{50} (90.3% for LEC) and also a high negative predictive value of 88.9% for IC_{50} (85.7% for LEC). This high predictive value is important so that potential drug candidates can be identified correctly early in the development process. At this 100x C_{max} cut-off value the 3D proximal tubule model correctly identified nephrotoxic (cidofovir, cisplatin, polymyxin B, polymyxin B nonapeptide, doxorubicin, gentamicin), and nonnephrotoxic (cimetidine, probenecid) drugs within the concentration range of 1-1000 µM using the IC_{50} toxicity output parameter. The 100x C_{max} threshold is consistent with that found in other studies [475-477]. The ROC-AUC values (Figure 5.5, Table 5.3) in both parameter cases are high (i.e., 0.9638 for IC_{50} and 0.94 for LEC), much higher than the 0.5 value for random probability, validating their predictive accuracy for toxicity in the 3D proximal tubule model. Comparisons to parameters from other cell culture models (Table 5.4) indicate that our models ROC-AUC values are superior to porcine LLC-PK1 cells (ROC-AUC of 0.73) [62] and human-derived cell line HK-2 (ROC-AUC of 0.71) [62]. Human primary cells (HPTC1, HPTC-like and HPTEC) show ROC-AUC values around 90% [62, 107, 485] but still less than the ROC-AUC values for the 3D model (Table 5.4).

Our 3D assay also shows higher sensitivities for toxic compound detection than previously reported in cell lines in adherent 2D monoculture [486]. Cisplatin, an antineoplastic agent well known for dose-limiting nephrotoxicity [487] showed little relevant cytotoxicity in HK-2 cells (i.e., lowest cytotoxic concentration fulfilling the positive response was 1000 µM) [486], compared to the 3D ex vivo model (i.e., cisplatin IC_{50} of 11 µM and LEC of 1 µM), a clinically much more realistic value (Tables 5.1 and 5.4). This prior 2D study [486] also reported no cytotoxicity after 24 h of gentamicin exposure, while the 3D proximal tubule model determined a gentamicin IC_{50} of 0.4 mM and a LEC of 100 µM. Also, a complete lack of gentamicin cytotoxicity detected in the 2D assay of cell line LLC-PK1 [488] counters the well-known human aminoglycoside (gentamicin) acute nephrotoxicity with clinical incidence rates as high as 30% [489]. The sensitivity value of these 2D toxicity models are only between 50 and 64% and their positive predictive values only reach 73%

(HK-2) and 74% (LLC-PK1), respectively, with even lower negative predictive values of 60% and 67%, respectively (Table 5.4), compared to higher positive and negative predictive values in our 3D model (96.6% and 88.9%, respectively).

A recent study analyzed the nephrotoxicity screening potential of primary human proximal tubule epithelial cells, reporting high performance metrics with the exception of a low negative predictive value of 57% [485]. Even though the predictive performance values looked very promising, the amount of toxic drug required to induce nephrotoxic effects was higher than in our 3D model: their IC_{50} values for cisplatin was ~8x higher and for gentamicin 23x higher than those in our 3D model (Table 5.4) [485]. These findings suggest that the OAT1 transporter expression in these 2D cultures for cisplatin, and megalin expression for gentamicin, respectively, are less sufficient, slowing the rate of toxicity and explaining the need for higher drug amounts or longer drug exposure times.

Figure 5.4 data support a general observation that known cytotoxic drugs tested here exhibit IC_{50} values below 1.4 mM in this 3D proximal tubule model (Table 5.1), with much lower values for known highly nephrotoxic drugs like cisplatin (IC_{50}=11 µM). Comparing published studies IC_{50} values in Table 5.4, only doxorubicin values are higher in the 3D model than the other 2D toxicity studies in cell lines. As an anthracycline used in chemotherapy, doxorubicin is general known to be highly cytotoxic by generating reactive oxygen species (ROS) [490]. Resulting oxidative stress-induced cytotoxicity is reported in various cell types [46, 65, 469, 490]. Doxorubicin endocytic cell uptake requires no specific transporters [46, 65, 469, 490]. Based on this and the higher cell surface area exposure in 2D cell culture (i.e., spread, flattened cell morphology) facilitating drug access and permeability, lower levels of this compound might plausibly produce toxicity in 2D cultures compared to the more morphologically protected 3D proximal tubule fragment cultures.

Another study tested nephrotoxicity using 41 nephrotoxic and nonnephrotoxic drugs in HK-2 and LLC-PK1 cells, showing that the sensitivity in both cell lines is no better than chance probability [62]. These discrepancies could be due to the lack of proper transporter functionality in cultured 2D cell lines: in vivo proximal tubule toxicity is highly dependent on transporter expression,

drug-transporter uptake and increased toxin levels within proximal tubule cells [423, 424]. Previous work on the 3D proximal tubule model showing superior transporter expression levels and profiles in 3D culture compared to 2D cell lines such as HK-2 and LLC-PK1 supports this assertion [12].

Predictive drug nephrotoxicity assay validation in humans must correlate to human clinical experience with these drugs and in vitro cytotoxicity assays. To probe such a correlation, 3D toxicity data were normalized with clinical C_{max} values and plotted against their nephrotoxicity incidence reported from clinical trial data at different exposure levels. Figure 5.6 shows a scatter plot correlating the 3D ex vivo model predictions against actual human clinical nephrotoxicity reports where nephrotoxicity risks increase towards the upper right corner. The C_{max}-normalized cytotoxicity responses correlate with observed adverse event rates in clinical studies.

Another important factor for early toxicity screen reliability is the capability to easily analyze new chemical moieties that might make new compounds safer and also identifying mechanisms driving drug nephrotoxicity, and therefore determine their human clinical relevance. These structure-activity relationships facilitate more rapid development of safer and more effective drug candidates in small scale models more economically and in early drug development stages. Also investigating potential treatment options for patients with a particular drug-induced nephrotoxicity is a plausible, more specific clinical use for these validated ex vivo nephrotoxicity models. In this regard, different substrate-inhibitor combinations were tested coadministered with the compounds and compared to assay results for toxic drugs alone. Figure 5.7 data show that for the substrate/inhibitor pair of cidofovir and probenecid (OAT1 transporter specific) as well as the cisplatin and cimetidine (OCT2 transporter specific) pair, a shift of the drug concentration-response curve to the right is seen. These shifts indicate that the toxicity of the compound in the 3D proximal tubule model was reduced, and that the IC_{50} values increased. In the clinic, probenecid, a known OAT1 inhibitor, is commonly co-administered with cidofovir to reduce nephrotoxic effects of cidofovir, a dose-limiting factor [491], by blocking cidofovir proximal tubule uptake and toxic consequences. These 3D assay data suggest that the substrate-inhibitor interactions seen in vivo can be modulated and emulated by this 3D model. Additionally, the 3D ex vivo model demonstrated reduced toxicity by co-administering a potent toxic drug, polymyxin B, and a related, less toxic

derivative of polymyxin B, polymyxin B nonapeptide [492-494]. Figure 5.7 also shows a shift in the concentration-response curve to the right for this pairing, indicating that the model is capable of reflecting substrate competition for the same kidney epithelial drug transporter.

Conclusion

This 3D ex vivo kidney proximal tubule assay exhibits high predictive value for a group of clinically relevant agents known to be either nephrotoxic or nontoxic in vivo. The approach yields assay responses with high sensitivity and specificity, and high correlative value to known clinical experiences with the same agents. Importantly, the assay format shown here in multiwell plates is amenable to high throughput (i.e., robotics dispensing) in high-density multiwell plates and even manifold-interfaced microfluidics designs. It also preserves essential kidney epithelial cell transporter functions and phenotypic states in 3D culture much more reliably than 2D kidney cell cultures widely used for similar toxicity assessments currently.

The ex vivo approach currently requires murine sacrifices to yield the kidney proximal tubule cultures, but the convergence of this approach with new functional kidney in vitro organoids derived from stem cells [106-109] may enable hybrid systems combining the benefits of both strategies without proximal tubule supplies from animal or human sources. Taken together, these results and those published previously for this 3D ex vivo model [12, 60], prove beneficial for improving drug development and structure adjustment studies, and rapid dose-response toxicities in vitro, helping to minimize unexpected toxic effects in late stage human drug clinical trials. Comparing the results from the 3D proximal tubule assay to known in vivo effects for each drug used clinically, 3D proximal tubule cultures are shown to be an improved model over standard 2D cell monocultures for predicting nephrotoxicity at therapeutically relevant concentrations.

Acknowledgements

This work was supported by AstraZeneca UK Limited, London, England. We thank Matthew Wagoner at AstraZeneca Pharmaceuticals, USA for valuable discussions. DWG is grateful for support from the George S. and Dolores Doré Eccles Foundation (USA).

Table 5.1 Compounds used in this study and their multiparametric data after 24h of drug exposure.

Compound	Pharmacologic Category	IC_{50}	SD	LEC [µM]	AUC	C_{max} [µM]
Cidofovir	Antiviral	1.1 mM	0.2	1000	531.0	11.5
Cimetidine	H_2- Antagonist	5.9 mM	1.9	1000	574.3	2.0
Cisplatin	Antineoplastic	11.0 µM	3.6	1	284.8	9.2
Doxorubicin	Antineoplastic	45.0 µM	2.4	1	344.6	0.6
Gentamicin	Antibiotic	0.4 mM	0.05	100	474.3	23.0
Polymyxin B	Antibiotic	10.5 µM	1.0	10	304.5	13.9
Polymyxin B Nonapeptide	Antibiotic	0.7 mM	0.1	100	501.3	13.9
Probenecid	Uricosuric	4.3 mM	0.8	1000	585.6	35.0
Vancomycin	Antibiotic	1.4 mM	0.2	316	534.1	30.0

Table 5.2 Important nephrotoxicity prediction performance metrics at 1x C_{max}, 30x C_{max} and 100x C_{max} cutoff from the 3D proximal tubule model.

	Nephrotoxicity prediction with IC_{50}			Nephrotoxicity prediction with LEC		
C_{max} TI	<1x	<30x	<100X	<1x	<30x	<100X
Sensitivity [%]	6.9	75	96.6	37.9	93.1	96.6
Specificity [%]	100	100	88.9	100	77.8	66.7
Positive predictive value [%]	100	100	96.6	100	93.1	90.3
Negative predicitive value [%]	25	56.2	88.9	33.3	77.8	85.7

Table 5.3 ROC-AUC values from ROC curves shown in Figure 5.4.AUC values from the two assay toxicity output parameters were used to construct ROC curves. ROC-AUC values >0.5 represent a predictive model (0.5 is considered chance).

Toxicity parameter	ROC-AUC
IC_{50}	0.9638
LEC	0.9400

Table 5.4 In vitro studies on drug-induced nephrotoxicity and their important performance metrics.

Cell type	Species	IC_{50} values						Performance metrics					References
		Cisplatin	Doxorubicin	Gentamicin	Polymyxin B	Polymyxin B Nonapeptide	Vancomycin	Sensitivity	Specificity	PPV	NPV	ROC-AUC	
PT	murine	11 µM	45 µM	0.4 mM	10.5 µm	0.7 mM	1.4 mM	0.97	0.89	0.97	0.89	0.96	this study
NRK-52E	rat	> 300 µM [+]	0.3 µM [+]	25.96 mM [*] > 300 µM [+]	288.7 µM [*]		>300 µM [+]	0.73 [+]	0.78 [+]	0.65 [+]	0.84 [+]		[*][495] [+][470]
MDCK	canine			16.98 mM	1.01 mM								[495]
HEK293	human	2.7 mM [+]	2.3 µM [+]	12.77 mM [*]	360.97 µM [*]								[*][495] [+][47]
hRPTEC	human	39.6 µM	11.2 µM										[469]
HK-2	human	> 1 mM [*]	1 µM [*]	> 1 mM [*] > 2.1 mM [¥]	20 µM [+]	> 1 mM [+]	> 673 µM [¥]	0.5 [¥]	0.79 [¥]	0.73 [¥]	0.6 [¥]	0.71 [¥]	[*][486] [+][478] [¥][62]
NKi-2	human	17 µM	> 20 µM	22 mM									[65]
NKi-2 tissue	human	25 µM	2 µM	9 mM									[65]
HPTC1	human	2.96 mM		> 2.1 mM			> 673 µM	0.91	0.9	0.91	0.94	0.94	[62] [107]
LLC-PK1	porcine	2.0 mM [+]	1.9 µM [+]	> 2.1 mM [*]			> 673 µM [*]	0.64 [*]	0.74 [*]	0.74 [*]	0.67 [*]	0.73 [*]	[*][62] [+][47]
HPTC-like	human	2.26 mM		> 2.1 mM			> 673 µM	0.68	0.84	0.83	0.70	0.8	[107]
HPTEC	human	84.6 µM		9.2 mM				0.75	1	1	0.57	0.89	[485]

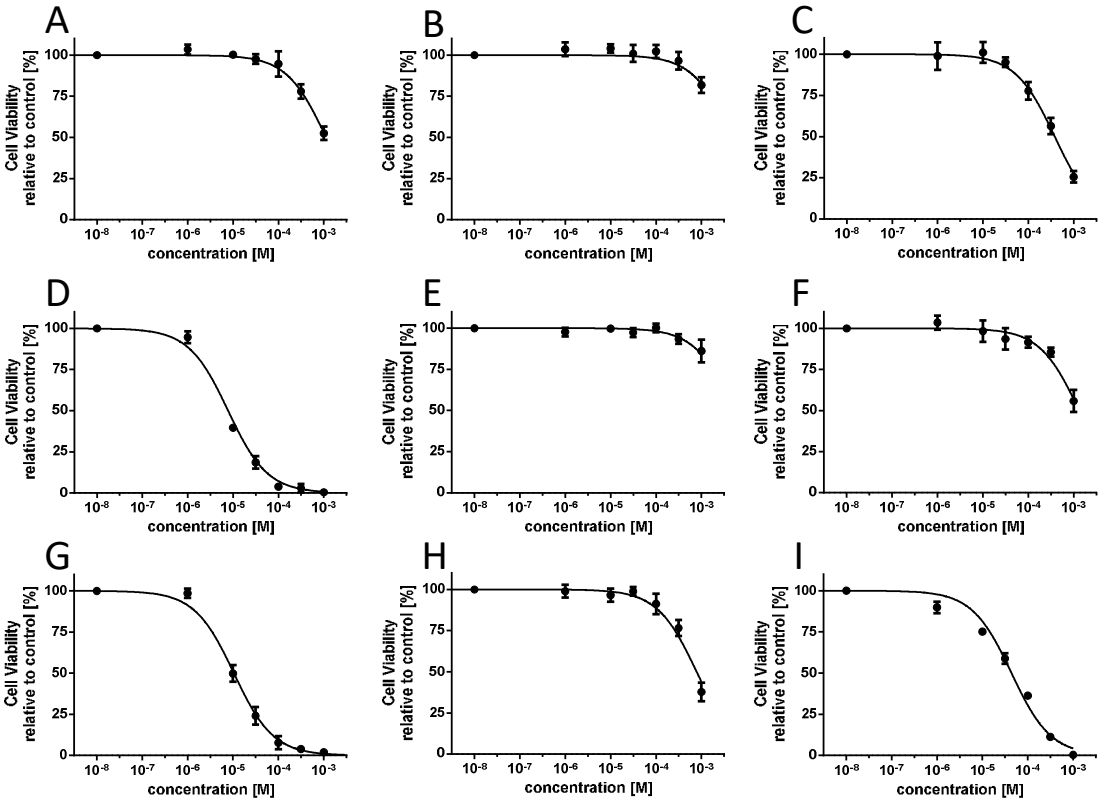

Figure 5.1 Impact of different compounds on 3D murine proximal tubule ex vivo cultures. ATP content was measured after 24h of compound incubation. Compounds were tested over a concentration range of 1-1000 µM per compound: A) cidofovir, B) probenecid, C) gentamicin, D) cisplatin, E) cimetidine, F) vancomycin, G) polymyxin B, H) polymyxin B nonapeptide and I) doxorubicin. Concentration-response curves were plotted (n=3, mean ±SD) and IC_{50} values, LEC and AUC from each compound were calculated. Values associated with each compound are shown in Table 5.1.

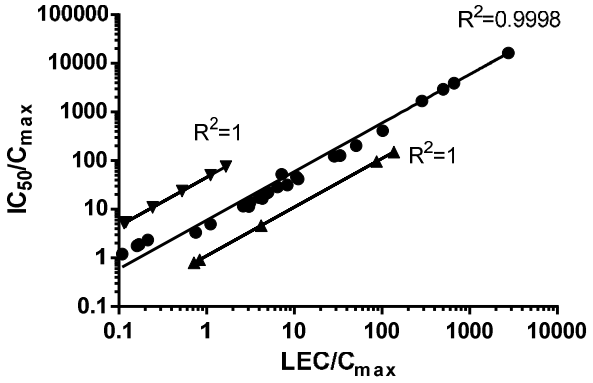

Figure 5.2 Correlation analysis of normalized IC_{50} (y-axis) and LEC (x-axis) values. IC_{50} and LEC values were normalized by many different published C_{max} values from clinical studies (▼doxurubicin, ● cisplatin, genatmicin, vancomycin, probenecid, cimetidine, polymyxin B nonapeptide, ▲ cidofovir, polymyxin B). Correlation coefficients (R^2) are provided.

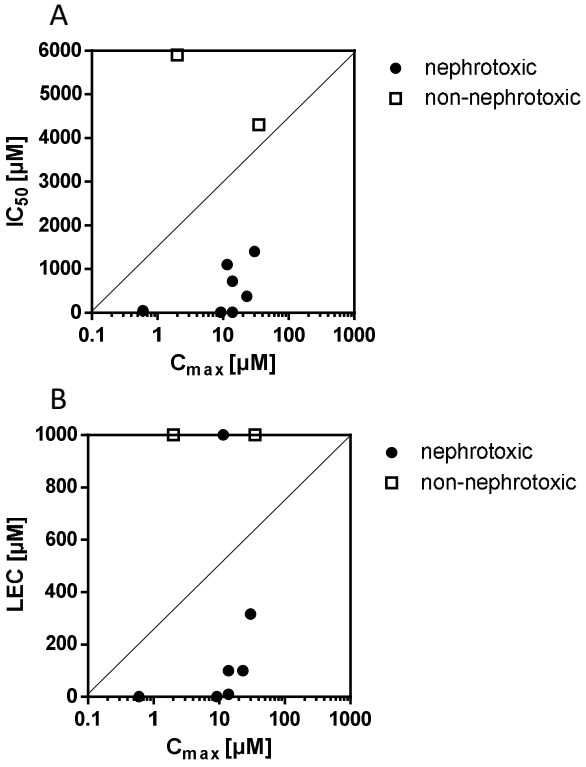

Figure 5.3 Nephrotoxicity classification based on compound IC50 and LEC. IC_{50} (A) and LEC (B) value are plotted against published human therapeutic plasma concentration C_{max}. A simple divider (black line) identifies a zone with only nephrotoxic drugs.

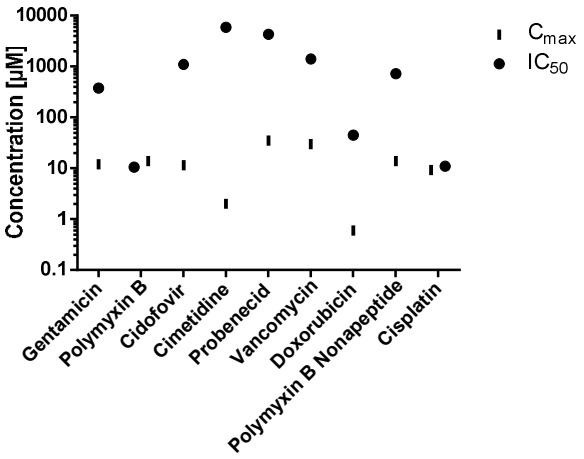

Figure 5.4 Nephrotoxic effects for each compound on the 3D proximal tubule culture. IC_{50} values from concentration-response curves in (Figure 5.1/Table 5.1) were calculated for each compound (black circles) and compared to each compound's individual C_{max} concentration (vertical lines).

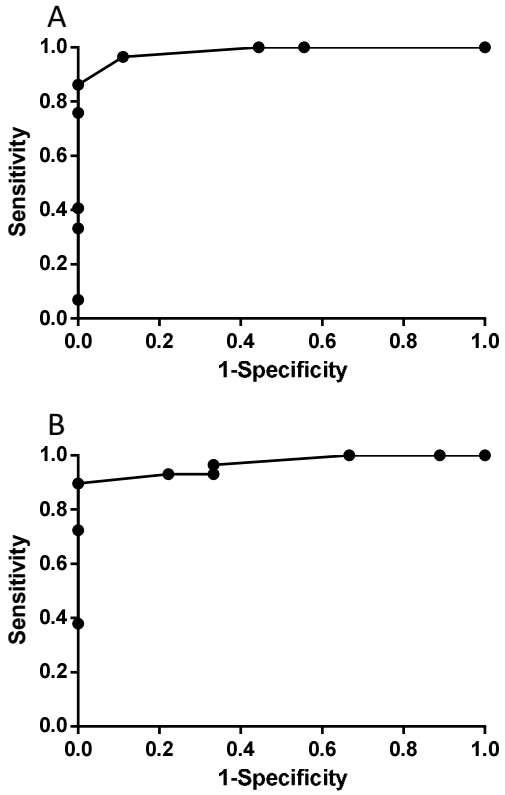

Figure 5.5 Determination of the predictive value of the 3D proximal tubule model by ROC analysis. Two different toxicity output parameters IC_{50} (A) and LEC (B). The respective AUC values are summarized in Table 5.3.

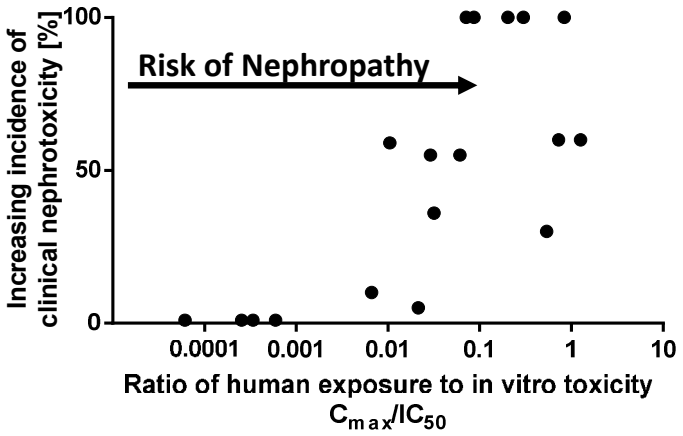

Figure 5.6 Validation of the 3D proximal tubule model for compound nephrotoxicity testing. Each dot represents data from different exposure levels per drug from clinical studies, resulting in different levels of toxicity, compared to IC_{50} values from the 3D proximal tubule model. The arrow represents the increasing risk of nephropathy towards the top right corner of the graph.

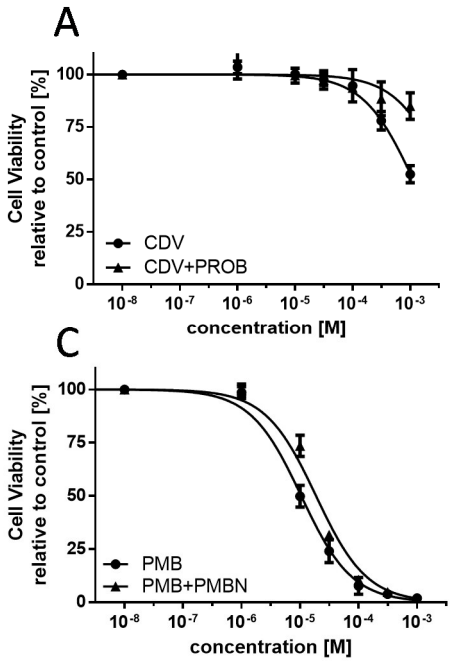

D

Drug pair	Ratio competitor co-administration IC_{50}:compound IC_{50}
Cidofovir/Probenecid	3.64
Cisplatin/Cimetidine	1.18
Polymyxin B/Polymyxin B Nonapeptide	1.82

Figure 5.7 Impact of receptor competitor addition. ATP content was measured after 24h of compound incubation. Full concentration range (1-1000 µM) of toxic compound and 30µM of competitor coadministration: A) cidofovir (CDV) and probenecid (PROB), B) cisplatin (CIS) and cimetidine (CMT), and C) polymyxin B (PMB) and polymyxin B nonapeptide (PMBN). Concentration-response curves were plotted to show the shifts in potency to the right (*n*=3, mean ±SD). IC_{50} values from each compound condition were calculated and the data expressed as the ratio of IC_{50} of toxic drug co-administrated with inhibitor/competitor to IC_{50} of toxic drug alone (D). A ratio of ≥ 1 indicates that the inhibitor/competitor is protective against the compounds nephrotoxicity. In all three cases the specific inhibitor displays nephroprotection to a varying degree.

CHAPTER 6

SUMMARY AND FUTURE DIRECTIONS

Summary

Currently a significant portion of drug molecules fail in clinical studies because the current state of the art in vitro drug toxicity screening tools in combination with animal models do not correlate sufficiently with final human in vivo outcomes. This dissertation aimed to validate the properties of an ex vivo 3D kidney proximal tubule screening model over standard 2D kidney cell cultures to improve the predictability and reliability of kidney toxicity results in drug screening. Differences between 2D in vitro drug exposure data from both immortalized and primary kidney cell monocultures independent of origin and actual clinical toxicity results obtained from human data are likely due limited functional and structural similarities between 2D monocultures and human kidney tissues. Specifically, known deficiencies in expression levels of important kidney drug transporters [58, 59, 98, 463, 496] and metabolic enzymes (Chapter 4) [47, 497], as well as intracellular drug targets [498] in 2D kidney cell culture lines are thought to be problematic, limiting their ability to accurately reproduce clinical toxicity responses.

The model described in this dissertation overcomes the above-mentioned problems by using intact, freshly harvested, and isolated murine proximal tubule fragments. Proximal tubule epithelial cells lining the proximal tubule lumen retain their native in vivo-like context, environment and structure. Data presented in each chapter reflect the importance of this cell native environment with cell-cell and cell-matrix interactions and culture-dependent differences. First, a detailed analysis of known, toxicity-associated kidney tubule cellular transporter expression profiles was reported for 3D cultured proximal tubules. Understanding these expression profiles for critical kidney tubule transporters over time in drug screening conditions should facilitate future in vitro-in

vivo correlations (IVIVC) and interspecies comparisons to validate nephrotoxicity assays. We compare hydrogel-based 3D proximal tubule fragment cultures and their nongel 3D suspension cultures for up to one week, demonstrating that 3D tubule cultures exhibit superior gene expression levels and profiles for key transporters compared to published commonly used 2D kidney cell line monocultures on plastic (Chapter 4). Gel use produced certain limitations, including: 1) interference with certain assays, 2) inability to readily recover biological material, 3) inconsistent distribution of doses drug throughout the gel, 4) inability to utilize nanoparticle or colloidal drugs due to transport limitations and gel binding, 5) possibly incomplete media exchange and catabolic retention problems, and 6) poor oxygen transport and exchange. Therefore, specific advantages would have to be advocated for gel use in order to offset these limitations.

Chapter 5 then provides functional confirmation of the ensemble of these transporters and enzymes in actual clinical relevant drug compound in vitro testing. Nine compounds with either known clinical nephrotoxicity or nontoxicity were assessed in the 3D nongel suspension culture and drug concentration-response curves and their molar concentration producing 50% inhibition (IC_{50}), lowest effective concentration (LEC) and Area Under the Curve (AUC) values were calculated and compared to clinical therapeutic exposure levels (C_{max}). Receiver Operating Characteristic (ROC) analysis was performed and the toxicity validation using this test group yields high sensitivity (96.6%) and specificity (88.9%) as well as high positive (96.6%) and negative (88.9%) predictive values in correlating toxicities for these agents with published clinical experiences (Chapter 5). Given these metrics, validation of the ex vivo 3D proximal tubule model against actual clinical toxicity experience was an important conclusion (Chapter 5). Specifically, the 3D model provided toxicity data similar to those seen in vivo at the best determined threshold of 100x C_{max}. Additionally, benefits from using the 3D proximal tubule model over standard 2D kidney cell monocultures for nephrotoxicity predictions at therapeutically relevant drug concentrations are shown (Chapter 5). By reliably predicting nephrotoxicity for all compounds tested, this screening model should prove useful for more reliable screening of novel compounds during early phases of drug development.

Overall, the findings show that the 3D kidney organoid fragment culture approach preserves essential kidney epithelial cell transporter functions and phenotypic states in 3D culture

much more reliably than 2D kidney cell cultures widely used for similar assessments currently. This collective outcome then validates critical phenotypic and functional aspects of this 3D culture model, providing confidence that it can now move forward to further toxicity testing and be extended to study new drug candidate structure-activity relationships (SARs) on proximal tubule pharmacology. This model can be further used to gain new insights into the mechanisms that drive toxicity from selected toxins and provide rapid screening of different chemical moieties during candidate SAR screenings. Data from this dissertation provides new information critical to understanding the models' functionality and sensitivity. Importantly, the assay format is versatile, amenable to high throughput in multiwell plates and even interfacing with fluidics designs. It can also be adapted to future kidney functional organoid cultures derived from human stem cells, eliminating the need for animal sourcing. Taken together, these data from this 3D ex vivo model support its utility in drug development, candidate screening, and rapid dose-response toxicities in vitro, hopefully better predicting the current unexpected and costly, toxic effects in late-stage human drug clinical trials and increasing postmarket drug product withdrawals.

Future directions

The use of novel clinical predictive markers for drug toxicity

Most common currently used toxicity markers in clinical trials are blood urea nitrogen (BUN) and serum creatinine. The major drawback for these markers is that they are rather insensitive: a 50-70% reduction in glomerular filtration rate (GFR) must occur to observe increases in BUN and serum creatinine levels [100]. This slow response and the lack of better available markers prompted the FDA's Critical Path Initiative call for development of better tools and more predictive, early phase nephrotoxicity markers [84, 91]. Based on this initiative, the following novel predictive markers were developed and remain under investigation [54, 84]: KIM-1 [68], NGAL [75], GST [69] and cytokines IL-6 and IL-8 [86, 132] (see Table 6.1). All of these markers show increased sensitivity towards nephrotoxicity and present earlier than BUN and serum creatinine. To facilitate developing of more reliable models and to increase the usability/functionality of our 3D proximal tubule model to detect drug toxicity at early stage, it would be a great advantage to assess these

markers in 3D culture systems. To do so would require the capabilities to evaluate gene expression of these markers in 3D cultures in general, and specifically in the 3D kidney proximal tubule model, and analyze their toxicity predictive values when exposed to known nephrotoxic and nonnephrotoxic drugs over time and concentration. Those data would then be comparable to human clinical toxicity responses and ideally, allow sufficient correlations to be seen. With this validation, these markers can then be used in combination with cell viability assays described in this dissertation for even more reliable and predicable toxicity screenings in early drug development phases.

Exploiting a genetically modified mouse for improved nephrotoxicity assays

A significant technical obstacle in using the 3D proximal tubule model was finding and optimizing assays reliable for 3D cell culture. Most current cell toxicity and metabolic assays and procedures are developed for flat 2D cell culture applications in plasticware plates, often using line-of-sight or other optical assay read-outs. Assay use in more complex and voluminous 3D structures, especially those without optical transparency, has not been systematically developed or validated [39]. Specifically, the two most important technical issues were 3D matrix cell lysis capacity and signal detection. The commercial CellTiter-Glo® 3D assay (Promega, USA) used in this study has an enhanced cell lytic capability that improves ATP extraction, the assay's optical signal strength, and therefore, the assay sensitivity. Nonetheless, 3D matrix interference with either cell extraction or assay reagents (e.g., poor reagent dispersibility, diffusion, exchange, matrix binding, poor stringency, cell interference), suboptimal time-dependence or kinetics for assays and matrix optical heterogeneity that corrupts assay fidelity or reporting, all produce unresolved issues for 3D cell culture assays. Figure 6.1 shows the outcome of three different assays for cell viability/cytotoxicity testing that were tested in our 3D proximal tubule system (with and without HA gel). It can be seen that the HA gel-embedding of the proximal tubules narrows the assay range dramatically and that way better signal-to-background ratios are seen when the 3D proximal tubules are used without the matrix (Figure 6.1). Beyond simple end-point cell viability, other desired assay reporting features would be real-time and noninvasive feedback on cell phenotype, metabolic information, proliferation

rates and cell cycles, and subcellular organelle visualization (e.g., mitochondria, Golgi, endosomes, lysosomes, phagosomes). Current 3D culture formats are not yet integrated with these assays, or the requisite analytical instrumentation or algorithmic processing, to make them readily amenable to these reporters.

A different approach would be the use of genetically modified signal pathways in mammalian cells where toxicity indicators are up-regulated genetically in responses to a given specific assault. The KIM-1 reporter C57BL/6 mouse (AstraZeneca, unpublished) upregulates GFP and luciferase in response to KIM-1 activation. Since KIM-1 is a primary kidney toxicity marker [52, 499], the resulting GFP signal produced in the kidney is related to nephrotoxicity. Kidney proximal tubule epithelial cells in the KIM-1 mouse express GFP and also secrete luciferase under control of the KIM-1 promotor. Therefore, the KIM-1 data should be collected to support initial feasibility for exploiting GFP and luciferase expression after exposure to nephrotoxins and calibration against the specific toxicity data presented in this dissertation for 3D proximal tubule in vitro assays derived from kidneys from the related C57BL/6 wild-type mouse.

The exploration of the KIM-1 reporter mouse can then be further extended: GFP appearance can be tracked using real-time fluorescent imaging of cultured proximal tubule fragment harvests both without and with 3D gel matrix, and simultaneous serial sampling of media for excreted luciferase activity. Dynamic reporting range, limits of detection, time-to-response (i.e., signal up-regulation) and assay fidelity as a function of kidney harvest time, animal-animal variation, and assay variables would be vetted. Both of these markers, KIM-1 GFP signal and luciferase secretion, could broaden the usability of the PT in vitro assay to permit serial, real-time assessment of cell response and viability in live proximal tubules, and therefore also dramatically reduce the number of plates and therefore also animals needed to run the assay.

An additional value would be to compare the ex vivo KIM-1 reporter mouse 3D proximal tubule toxicity response data with in vivo KIM-1 reporter mouse response to tail-vein injected and orally ingested compounds and dosages. To do so, the KIM-1 reporter mice would be injected with different concentrations of known nephrotoxic and nonnephrotoxic drugs and their urine would be collected (e.g., metabolic cages or manually) after different time points and analyzed for luciferase

activity. This could be done with a commercially available kit (i.e., ONE-Glo™ Luciferase Assay System, Promega), producing a stable luminescent signal that then can be read on a normal plate reader (e.g., Synergy 2 Multi-Mode Reader from Biotek). These in vivo data then could be compared to the ex vivo KIM-1 reporter mice 3D proximal tubule data (i.e., GFP optical response, CellTiter-Glo® viability, etc.) and an IVIVC can be produced. The urine collection data can furthermore be used to identify drug effects depending on exposure times and the strongest nephrotoxic time point for each drug can be determined. At specific time points, the mice could be euthanized and the kidneys would be harvested and used for histopathological GFP signal determination of in vivo drug responses.

Preliminary data for the GFP signal from harvested KIM-1 reporter mouse 3D proximal tubules after drug exposure ex vivo shows that GFP signal is upregulated depending on drug concentration and that a concentration-response curve based on the GFP signal can be produced (Figure 6.2). GFP signal was detectable visually using normal microscopy as well as using the Synergy 2 Multi-Mode reader (Biotek). Overall, the assay range is narrower than that seen with the CellTiter-Glo® 3D assay (Promega) and further optimization of PT seeding density must be done in order to produce the normal expected assay figures of merit (LOD. LOQ, S/N, reliability, reproducibility, dynamic range, specificity, sensitivity).

Further evaluation of ex vivo 3D PT models amenable for mechanistic toxicity studies using RNAi

In Chapter 5, I showed the potential of this ex vivo 3D proximal tubule model for mechanistic toxicity studies by comparing the concentration-response curve and IC_{50} results of known nephrotoxic drugs (e.g., cidofovir) alone versus coadministration of the nephrotoxic drug with a known inhibitor (e.g., probenecid). The shift of the concentration-response curve to the right as well as the higher IC_{50} values indicated that agent coadministration inhibits kidney uptake of the nephrotoxic drug and correlates with known clinical applications. To validate the mechanistic hypotheses of this model further and to see if this model may be used with RNAi agents to specifically knock out known toxicity pathways, siRNA against a specific receptor or signal molecule

driving kidney PT drug accumulation (e.g., OAT1) could be administered, followed by exposure of the 3D proximal tubules with a known nephrotoxic drug substrate for this specific transporter (e.g., cidofovir). Kidney PTs can be evaluated for their altered drug susceptibility which will provide further insight into toxicity mechanisms. Other alternative methods to achieve the same technical objective include CRISPR/Cas9 cell transfection, iPS cell selection, and TALEN modified cell cultures.

Harvest optimization to improve the HTS potential of the ex vivo 3D proximal tubule model

Use of genetically modified KIM-1 reporter mice should allow use of a previously published sorting method to speed up the PT harvesting process and make the model more valuable for HTS. Miller et al. developed an automated method to isolate collective ducts of digested kidneys from genetically modified mice expressing GFP [444]. They used a complex object parametric analyzer and sorter (COPAS) instrument (Union Biometrica, Somerville, USA), commonly known as *C. elegans* "worm sorter," to sort GFP-expressing collective duct cells from other parts of the nephron. The same method could be used with KIM-1 reporter mice with GFP-expressing proximal tubule cells to allow automated sorting, as conventional flow cytometry is not possible due to the excessive size of the PT organoid fragments (70-250 µM). This process could drastically speed up isolation and eliminate the need to identify PTs in the extraction step. Success here would increase the HTS potential as currently the isolation process is the main rate-limiting step of the ex vivo 3D proximal tubule model. If we focus only on the 96 well plate assay, then throughput could be clearly affected by an efficient fluidics interface capable of changing between media, drug and rinsing steps to control transport and allow reuse of each well.

Development of an ex vivo 3D human model

Another future approach would be the expansion of the knowledge gained through the development and characterization of the murine ex vivo 3D proximal tubule model to an analogous human ex vivo 3D proximal tubule model. To achieve this, prescreened human kidneys from a clinical collaborator with IRB approval for research use of discarded kidneys (e.g., from renal

carcinoma or transplant discards) could be used. To harvest healthy proximal tubules only kidneys with localized, nondisseminated tumors will be used and diseased tissue will be dissected away. This would allow direct comparisons of the model and highlight potential interspecies differences known to be a problem for toxicity responses [500, 501]. As use of murine proximal tubule fragments is less expensive and easier to approach, the ideal case would be that comparable data will be retrieved, the mouse-to-human translational relevance validated and that human tissue discards would NOT be required to employ the assay. An additional aspect would be that the human model could be modified to analyze proximal tubules from diseased kidneys and compare to healthy proximal tubules to monitor differences in nephrotoxicity responses as a function of human pathology or disease co-morbidities.

Elimination of animal or human PT sources by using stem cell-derived organoids

The ex vivo approach described in this dissertation currently requires murine sacrifices to yield the kidney proximal tubule cultures. To eliminate the need for animal sacrifices in this model, a future approach could focus on new functional kidney-like in vitro organoids derived entirely from stem cell 3D cultures [106-109]. Over the last 4 years, multiple groups are competing on the development of kidney organoid structures from stem cells and multiple protocols were published to differentiate pluripotent stem cells into self-organizing kidney organoids in 3D matrices in multiwell plates [106, 108]. These stem cell-derived kidney organoids must be further characterized and important functionality in toxicity assays must be validated. This approach then may enable hybrid systems combining the benefits of both strategies without proximal tubules supplied from animal or human sources.

Concluding remarks

Our 3D PT model is one of multiple current approaches seeking to create more reliable and predictive nephrotoxicity models (Table 6.2). While the current setup is under static fluidics conditions, applying flow would be a future direction to make the model even more efficient, perhaps more relevant, and high-throughput applicable. Applying flow conditions by, e.g., seeding harvested

PT fragments on membrane transwell plates will allow for more in vivo-like conditions as well as rapid media and drug solution exchange and transport control. This would also possibly allow reuse of the same PT fragment culture for different drugs and concentrations by including a rinse-recovery period in complete PT media. Effects of adding protective agents or transporter inhibitors could be studied seamlessly in a flow setup. The benefit of kidney-on-a-chip models is in retaining their functional complexity, and therefore ideally establishing more in vivo-like designs could facilitate this goal [61, 133, 134, 502].

Current results are promising even though more thorough transporter expression as well as drug concentration response curve studies need to be performed to get more reliable data to support assay sensitivity, specificity, NPV, PPV parameters. Current studies are all currently lacking these and are only focusing on a small amount of test compounds for model validation. Full performance metrics are necessary to move all current approaches forward to approved nephrotoxicity testing systems. While the more complex kidney-on-a-chip models look promising, they are also more cost- and labor-intensive. Importantly, that more complicated designs are necessary to obtain data that allows accurate toxicity correlations to human in vivo results remains to be shown. The higher cost and labor intensity of these experimental systems are reasons why only small numbers of test compounds were analyzed and tested in these systems so far [61]. Therefore, our simpler PT approach is competitive and also interesting for pharmaceutical industries as they pursue rapid, inexpensive, and more reliable toxicity assay methods.

Different assay approaches could also be used strategically at different times in the drug development process: a simple, inexpensive, high-throughput system could be used early, when scanning a large quantity of candidates or compounds, while later in the process, a more complex, and therefore, more expensive in vivo-like approach could be used to identify toxicity results in an already narrowed group of compounds. These microfluidic kidney-on-a-chip approaches could also identify toxicity responses of different cell types as they are normally resident in vivo in multicellular systems in a combined or serially staggered exposure sequence [133, 134, 502]. Currently, all toxicity testing models proposed and published - 3D PT cultures [60], kidney-on-a-chip [1, 61, 134, 502] and stem cell derived organoids [106, 133, 137-139] remain to be tested and validated in

large-scale studies and using different drug classes to obtain accurate, reliable predictability and reliability data for new drug development.

Table 6.1 Known predictive biomarkers for drug-induced nephrotoxicity in proximal tubules.

Biomarker	Abbr.	General attributes	Proposed mechanism	Physiological level	Acute Kidney Injury levels	Additional Comments	Source
N-acetyl-β-D-glucosamine	NAG	Lysosomal enzyme	Secreted from lysosomes of damaged cells	<2 µg/g creatinine	50 µg/g creatinine		[22-24]
γ-glutamyl-transferase	GGT	Brush-border membrane protein	Released in response to injury				[22]
Kidney Injury molecule-1	KIM-1	Transmembrane glycoprotein	Expressed in response to injury	0.0-0.1 ng/g creatinine	3.3 ng/g creatinine		[52-55]
Heme oxygenase-1	HO-1	Cellular protein	Expressed in response to injury			Oxidative stress responsive gene	[22, 23]
Glutathione-S-transferase	GST	Soluble cytosolic enzyme	Expressed in response to injury	5 µg/l	10 µg/l	Participates in detoxifying of many compounds	[68, 69]
Neutrophil gelatinase-associated lipocalin	NGAL	Cellular protein	Expressed in response to injury	0.0 µg/l	>5µg/l	Binds to gelatinase in particular neutrophil granulocytes	[55, 68, 75, 76]
Tissue inhibitor of metallo-proteinases-1	Timp-1	Glycoprotein	Expression induced in response to upregulated cytokines				[80]
Clusterin	CLU	Widely distributed heterodimeric glycoprotein	Expressed in response to injury				[54]
Osteopontin	OPN	phosphoprotein	Expressed in response to injury		20 mg/g creatinine or 2 µg/ml		[81]
Monocyte chemoattractant protein-1	MCP-1	Proinflammatory chemokine	Released in response to injury				[82, 83]
Tumor necrosis factor alpha	TNFα	Proinflammatory cytokine	Released in response to injury			Stimulates IL-6 release & TIMP-1 expression	[84, 85]
Interleukin-6	IL-6	Predominant cytokine in kidney, glycoprotein	Released after stimulation by TNFα			Involved in cell growth, differentiation and regeneration	[68]
Interleukin-18	IL-18	Pro-inflammatory cytokine, induced and cleaved in PT	Released in response to injury	<10 pg/ml	>20 pg/ml	Early predictive biomarker of AKI	[55, 86]
Interleukin-1beta	IL-1β	Proinflammatory cytokine	Released in response to injury				[68]
Cytochrome P450	CYP	Drug-metabolism enzyme					[87-90]

Table 6.2 Comparison of current in vitro approaches for drug-induced nephrotoxicity screening.

	2D cell culture	**Kidney-on-a-chip**	**Stem cell-derived kidney organoids**	**3D PT model**
Key drug transporter expression	limited	Depends on cell line used and specific design	yes	yes
Cell phenotype fidelity	Different than in vivo phenotype	Different than in vivo phenotype	In vivo-like	In vivo-like
Microfluidic application possible	yes	yes	yes	Yes
Cost	low	high	Higher than 2D cell culture	low
High-throughput application	yes	yes	yes	yes
Reliable in vivo-like toxicity responses	No as shown in multiple publications	Promising, early-phase, but not validated	Promising, early-phase but not validated	Promising, with small-scale validation

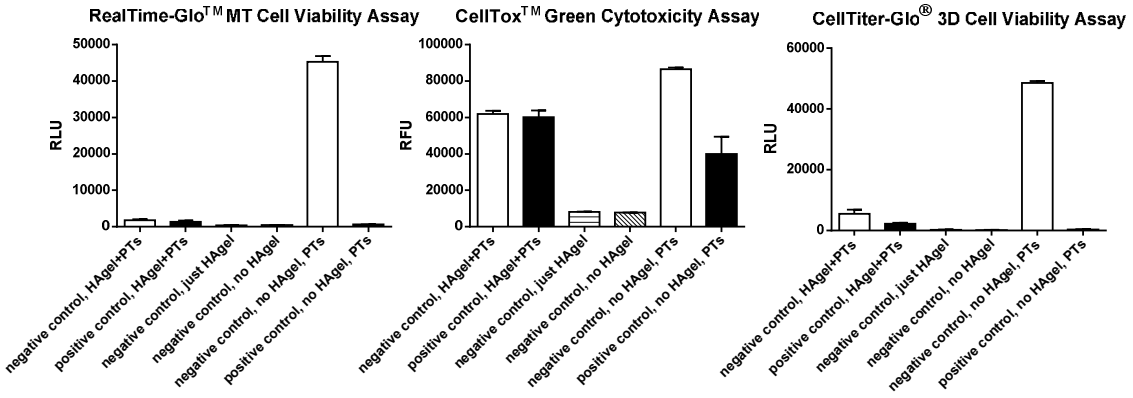

Figure 6.1 Cell viability assay signal strength and assay dynamic range. Three different cell assays are shown: RealTime-Glo™ MT Cell Viability Assay, CellTox™ Green Cytotoxicity Assay and CellTiter-Glo® 3D Cell Viability Assay. Effect of the 3D matrix on the assay is shown. Negative control: PT media, no lysis buffer. Positive control: PT media with lysis buffer.

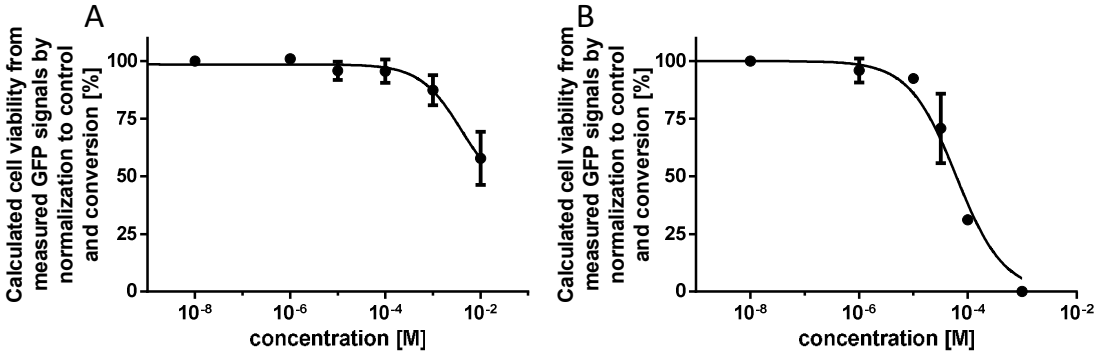

Figure 6.2 Impact of different compounds on 3D KIM-1 reporter mouse PT ex vivo cultures. GFP signal in cultures was measured after 24h of compound incubation and the GFP signal was converted to a concentration-response curve by normalization to no drug control and conversion of cytotoxicity to viability. This allows for comparison to ATP assay concentration-response data (Figure 5.1). Compounds were tested over a concentration range of A) 1-10000 µM for gentamicin and B) 1-1000 µM for polymyxin B. Concentration-response curves were plotted (n=1 (2 technical replicates), mean ±SD).

APPENDIX

A RECOMBINANT HEPARIN-BINDING MAJOR AMPULLATE SPIDROIN 2 (MASP2) SILK PROTEIN[4]

[4] Diekjürgen, Dorina, Kurtzeborn, Kristen, Ngo, Kim, Balasubramanian, Narayanaganesh, Grainger, David and Brooks, Amanda. A recombinant heparin-binding major ampullate spidroin 2 (MaSp2) silk protein. Under revision 2017

Abstract

Peptide units comprising major ampullate spider silk confer a balance of strength and extensibility with established structure-property relationships. Small peptides correlated to specific functionalities can be recombined within these units to create designer silk fibers. In this study, a small basic peptide (ARKKAAKA) known to both bind heparin and mimic an antimicrobial peptide, was genetically linked to a protease-resistant, mechanically robust silk peptide, MaSp2, endowing spider silk with new properties. Purified silk fusion proteins (two or four silk domains and four heparin-binding peptide repeats) were expressed in *E. coli*. Successful fusion of a MaSp2 spider silk peptide with this heparin-binding motif was shown with analytical and functional assays. This strategy can link combinations of the two individual genes to create designer recombinant fusion proteins, including mechanically robust proteins that alter blood-contacting responses.

Introduction

Major ampullate spider silk's intrinsic balance of dichotomous mechanical properties, unrivaled strength and impressive recoverable deformation, is provided by structural hierarchy rooted in the biochemical composition of two proteins, MaSp1 and MaSp2 [503, 504]. Phylogenetic analyses of these major ampullate sequences revealed an evolutionarily conserved sequence of repetitive amino acid motifs thought to correlate to specific structural and functional features [505]. The component amino acid motifs of major ampullate spider silk have been well-studied by producing clones of simplistic monomer motifs [506, 507] to identify and establish overarching structure-property relationships [505]. In addition to mechanical properties that can be engineered by genetically combining motifs correlated with specific properties [503, 505], several recombinant spider silk fusion proteins have been explored to date (i.e., silk-uranium binding proteins [508], silk-antibiotic [509], silk-silica binding proteins [510, 511], silk-bone sialoprotein [512], silk-elastin [513], etc.), providing additional biological functions. Silk was also recently complexed with heparin and chitosan to create an anticoagulant, antimicrobial, dual functional protein [514]; however, the application is contemplated to capture endogenous heparin from circulating blood, allowing for repeated heparin-surface association and disassociation, and endowing intrinsic antimicrobial

properties based on the same amino acid motif. Heparin, a hydrophilic, highly sulfonated negatively charged polysaccharide copolymer comprising glucosamine and glucuronic acid, is endogenously found in the human body (approximately 20 µg/ml in adult plasma) and commonly used as an extracorporeal anticoagulant at therapeutic concentrations over 50 nM [515]. Importantly, heparin is naturally bound by a diverse family of heparin-binding proteins [516-518], based on electrostatic interactions where positively charged, basic amino acid residues in the heparin binding amino acid motif (HBM) of these proteins interact through ionic and hydrogen bonds with the strongly negatively charged sulfate and carboxylate groups on the heparin polysaccharide [518, 519]. Furthermore, the tertiary structure of the HBM is analogous to an antimicrobial peptide (AMP) [520, 521], with the overall structure XBBBXXBX (X – hydrophobic or uncharged amino acid, B – basic amino acid). Previous work has sought to exploit surface-bound HBM to create heparinized surfaces [522, 523]. These efforts were able to successfully bind solution-phase heparin, with the best binding affinity based on four concatenated repeats of the synthetic motif (ARKKAAKA, 42 ± 15 nm) [524]. This peptide is analogous to the LL-37 antimicrobial peptide, which can be proteolytically degraded by human neutrophil-produced elastase as well as *P. aeruginosa* elastase and *S. aureus* V8 metalloproteinase and aureolysin [525]. Thus, bound heparin bioactivity was shown to be reduced by proteolytic cleavage [526, 527]. Therefore, utilizing a heparin-binding motif as a surface capture agent for circulating heparin necessitates embedding the protease-susceptible peptide into a protective polymer background. A biological and structural biopolymer fusion, such as that using major ampullate spider silk with HBMs, may provide such a suitable background to permit heparin capture and stability for possible further technological use in biomaterials.

In this context, we sought to genetically embed a small heparin-binding amino acid motif (HBM) into a recombinant protease-resistant silk peptide, MaSp2 [523, 528-530], to ultimately create a chimera with new biomedical properties as conceptually described in Figure A.1. Although many other silk fusion proteins have been explored [531] (e.g., antibiotics [522, 532], chitosan [514], elastin [513], silica [510, 533, 534], RGD [511], etc.), the recombinant fusion protein target seeks to uniquely combine silk's mechanical properties with the biological activity of the HBM, creating a robust naturally heparin-binding biomaterial. By genetically embedding four concatenated repeats

of the heparin-binding motif, ARKKAAKA, in a background of MaSp2 amino acid motifs, a mechanically robust protein material is created, capable of 1) binding heparin for blood anticoagulation properties and also for 2) resisting pathogen colonization and infection [535]. Here we report the design and production of a heparin-binding silk recombinant protein chimera as well as characterization of the heparin-binding ability of the fusion product.

Experimental section

Gene construction

All enzymes were obtained from New England BioLabs or Fermentas, unless otherwise noted.

Cloning design

The Argiope aurantia MaSp2 consensus repeat amino acid sequence was designed and synthesized as a 179 base pair oligonucleotide (including restriction sites) while an analogous oligonucleotide for the consensus heparin-binding motif (HBM) (105bp including restriction sites, stop and start codons, and 6X-histidine tag) was synthesized. Regardless of the specific gene, oligonucleotide sequences were optimized for the codon bias of *E. coli* codon and included restriction sites (Figure A.2) to facilitate all downstream cloning steps. Each oligonucleotide was synthesized at the University of Utah DNA Sequencing Core Facility and annealed (annealing buffer) 10 mM Tris, 50 mM NaCl, 1 mM EDTA) to its complementary strand to create minigenes, which were subsequently cloned into pBlueScript II SK(+) (pBSK - Stratagene) (Figure A.2) and multimerized using a compatible, nonregenerable cloning strategy, as previously described [536]. Concatenated silk repeats, multiple HBM repeats, or HBM/silk combinations were produced and transferred to pET 30a (Novagen). Transformants were analyzed by PCR colony screening (95 °C 2 min; 30 cycles of 95 °C for 30 s, 60 °C for 30 s, and 72 °C for 30 s; final extension at 72 °C for 5 min). Colonies that screened positive *via* PCR were subsequently sent for DNA sequencing (University of Utah Core Facility, Salt Lake City, UT) using either the M13 or T7 primer sets (Figure A.3). Alternatively, the complete genetic sequence ($silk_2$ or $silk_4$ linked with HBM_4) was synthesized

and cloned directly into pET 30a by GenScript (USA) (Figure A.4).

Protein Expression and Purification

All proteins were expressed in *E. coli* BL21(DE3)pLysS cells (Promega, USA). Cultures were grown in 37 °C LB medium containing 100 µg/ml kanamycin with shaking to an OD_{600} between 0.8 and 1.0. Isopropyl-β-D-1-thiogalactopyranoside (IPTG, Sigma-Aldrich, I5502) was added at a final concentration of 1 mM to induce the expression. After 2 h the culture was centrifuged at 8000 rpm for 10 min and the media was decanted. Cell pellets were resuspended in 100 mM HEPES buffer (1/10 of the final culture volume). To achieve better yields and higher purity, 50 µg/ml DNase I (Sigma), and 1 µL of protease inhibitor cocktail (Sigma)/100 µL of harvested expression culture was added prior to sonication (30 s at 40 % power) and purification. Proteins were purified using nickel affinity chromatography. To identify the highest yield clones from each construct, the Maxwell® 16 Polyhistidine Protein Purification system (Promega) was used according to the manufacturer's instructions for the prefilled nickel affinity reagent cartridge (Promega) [537]. Purified protein was dialyzed against water overnight and lyophilized [538].

Protein Characterization

Sodium dodecyl sulfate polyacrylamide gel electrophoresis (SDS-PAGE). Purified proteins were analyzed for size and purity by SDS-PAGE. Importantly, solution from each well of the Maxwell purification cartridge was also analyzed on SDS-PAGE to assess the efficacy of the purification. Each sample was heated with NuPAGE LDS sample buffer (Invitrogen) briefly (<5 min) at 95 °C and then loaded into a precast Bis-tris 4-12 % polyacrylamide gradient gel (Invitrogen). Protein bands were visualized under white light on a BioRad Chemidoc XRS imaging system after AcquaStain Protein Gel Stain (Bulldog Bio. Inc).

Western blot. The identity of purified protein products were confirmed *via* western blotting. Purified proteins were run on a denaturing SDS-PAGE and transferred to a nitrocellulose membrane at 40 V for 60 min using a standard transfer protocol [536]. After proteins were transferred to the nitrocellulose membrane using Invitrogen's XCell™ Blot Module, the SNAPi.d.

protein detection system (Millipore) was used for immunodetection with a 1:4000 dilution of a HRP-conjugated 6x-His Epitope Tag Polyclonal Antibody (Thermo, PA1-23024) in Tris buffered saline plus Tween 20 (0.05 %) (Fisher, TBST, ionic strength = 175mM). Amersham™ ECL™ PrimeWestern blotting detection reagent (GE Healthcare Life Sciences, RPN2232) was used as detection reagent according to manufacture concentration and the bands were visualized using the Bio-Rad ChemiDoc™ XRS camera under varying exposure.

Mass spectrometry (MS). Liquid chromatography electrospray ionization mass spectrometry (LC-ESI-MS) was performed at the Core Synthesis and Analytical Services Facility (Center for Protease Research, North Dakota State University, USA) on purified protein samples. Briefly, the intact mass analyses of the specific proteins was performed after desalting them through a desalting cartridge followed by LC-ESI-MS analysis on a Waters Synapt G2-Si HDMS. UPLC was performed on an Acquity UPLC- I class with Waters BEH C18 (2.1 mm X 100 mm) 1.7 µm column. The column was maintained at 35°C throughout the analyses. A linear gradient was performed over 7 min shifting the ratio of A (0.1 % formic acid in water) to B (0.1% formic acid in acetonitrile) shifted from 90/10 (A/B) to 10/90 (A/B). The total gradient run was 13 min. Desalted protein solution (100 µL) was mixed with 200 µL of 0.1% TFA in water/acetonitrile (50/50) and 10 µL was injected at a rate of 0.5 mL/min. Mass spectrometric analysis was performed on a Waters Synapt G2-Si HDMS. The collected mass spectrum data in continuum format were processed using MaxEnt1 software (Waters Corporation) to obtain the protein mass. The peak width parameter used to obtain the result was between 0.45 Da to 0.6 Da depending on the sample. Spectra were processed between 5000 to 50,000 Da at 1 Da/Channel.

Heparin-binding characterization

Heparin affinity column chromatography. Affinity column chromatography was performed with HyperD resin (Pall) according to the manufacturer's protocol to determine the affinity of each protein for heparin. Briefly, the column was washed with five column volumes of wash buffer (20 mM Tris HCl, 0.3 M NaCl, pH 7.4.) prior to application of the protein. Based on the binding capacity of the column, approximately 100 µg of protein in a 2 ml volume of Maxwell elution buffer

(500mM imidazole and 100mM HEPES, pH 7.5, ionic strength ≈ 0.73M [539]) was applied to the column and allowed to elute drop-wise (flow-through fraction). The column was then washed with 3 column volumes (6 ml) of wash buffer followed by 2 column volumes of elution buffer (20 mM Tris HCl, 2 M NaCl, pH 7.4). Each chromatography fraction was collected separately for analysis.

Heparin affinity dot blot. Purified proteins (10 µl at approximated 100 µg/µl) were applied to a nitrocellulose membrane (Sigma) and allowed to adsorb for 30 min. The membrane was blocked on a rotating platform for an hour in block solution (5 % solution of nonfat instant milk (Carnation) in Tris buffered saline plus Tween 20 (0.05%) (Fisher, TBST) ionic strength = 0.175M). The membrane was subsequently probed with a biotinylated heparin (Calbiochem) ligand diluted at 1:100 in the blocking solution for one hour on a rotating platform. After washing the membrane three times for 15 min each in TBST (approximately 75 ml), the blot was probed with HRP-tagged streptavidin (Fisher Scientific) at a 1:100 dilution in the blocking solution for one hour on a rotating platform. After washing the membrane three times for 15 min each in TBST (approximately 75 ml), the membrane was reacted with enhance chemiluminescence reagents (Pierce) for 5 min prior to imaging on an Aplegen Omega Lum G over 5 min, acquiring images at varying exposure times. IL-2 (PeproTech, Rocky Hill, New Jersey) was spotted as a positive control and BSA was spotted as a negative control. Additionally, a blot was probed with secondary streptavidin – HRP only using an analogous protocol without the addition of biotinylated heparin.

Heparin affinity enzyme-linked immunosorbent assay (ELISA). Protein samples were aliquoted and one aliquot was processed through a Zeba desalt column (pierce, USA). Biotinylated heparin (Calbiochem) was diluted 1:1000 in TBS and incubated for 2 h at room temperature in a Thermo Scientific™ Pierce™ High Binding NeutrAvidin™ Coated Plate (Fisher Scientific). Subsequently, wells were washed three times with TBST (0.05 % Tween 20) and blocked overnight at 4°C with a 5% nonfat instant milk solution (Carnation) in TBST. Protein (100 µl of 15 µg/ml $silk_2$, S_4H_4, or IL-2 (positive control)) was incubated in the prepared wells for 1 h at room temperature. Wells were washed three times with TBST and incubated with an HRP conjugated antihistidine 6x (Fisher Scientific) diluted 1:2500 in 5% nonfat instant milk solution (Carnation) in TBST for 1 h at room temperature. Wells were once again washed and 75 µl TMB substrate (Fisher Scientific) was

added and allowed to incubate for 18 min at which time the reaction was stopped using 2M HCl according to the manufacturer's instructions. Sample optical absorbance was read at 480 nm on a Biotek Epoch plate reader.

Results

Capitalizing on the molecular hierarchy of spider major ampullate silk, the repetitive sequence for Argiope aurantia major ampullate spidroin 2 (MaSp2), one of the key structural spider silk proteins, was genetically linked with the consensus sequence for binding heparin (HBM) (Figure A.2), thereby endowing MaSp2 with the ability to bind heparin. MaSp2 (silk) and HBM sequences were designed and engineered in a cloning plasmid not only to optimize expression in *E. coli*, but also to facilitate the genetic linkage and polymerization of each gene individually (HBM *n*=1, 2, and 4 repeats, and silk *n*=1, 2, 4 and 6 repeats) using a compatible nonregenerable cloning strategy (Figure A.2 A-C). $Silk_2$ constructs were genetically polymerized to HBM_4 constructs to create a silk/heparin fusion protein (S_2H_4, Figure A.2). All produced clones were screened *via* colony PCR (Figure A.2 D) and sequence confirmed by the University of Utah core sequencing facility (Figure A.3). Subsequently, genes were PCR-cloned into pET30a for protein expression. After constructs were transferred into pET30a, expression was induced in BL21-DE3 *E. coli* using IPTG. Alternatively, $silk_4HBM_4$ (S_4H_4) fusion constructs were synthesized and cloned into pET30a by GenScript. Fusion protein production was confirmed by: (1) the slight shift in molecular weight upon addition of the HBM_4 peptide ($Silk_2$ = 14766 Da, S_2H_4 = 15146 Da, S_4H_4 = 16355 Da, Figure A.5), (2), mass spectrometry (Figure A.5) and (3) the reaction with an anti-histidine – HRP conjugated antibody (Figure A.6).

Following confirmation that the HBM_4 peptide was in fact attached to the $silk_2$ or the $silk_4$ peptide (Figures A.5 and A.6), functional assays were used to determine the capability of fusion peptide to bind heparin in both solid phase (Figure A.7) and from solution as a surface-bound protein film (Figure A.8). In each assay, bovine serum albumin (BSA) was used as negative control, having no reported ability to bind heparin [540], while antithrombin III (ATIII) or IL-2 was used as the positive control [541, 542]. HyperD heparin affinity resin has heparin covalently bound to the

column solid phase, allowing interaction with recombinant proteins under flow through the column. Presence of non-HBM containing silk protein in the eluted unbound wash fraction (Figure A.7) confirms that recombinant silk solution alone has limited affinity for immobilized heparin. Alternatively, when HBM is grafted to the MaSp2 silk repeats, the resulting fusion protein is seen in the elution fraction, reflecting the dramatically increased ability of this recombinant protein to bind immobilized heparin on the column. Despite this result anomalous nonspecific protein affinity interactions can occur in affinity column chromatography; therefore, a dot blot assay on nitrocellulose was used to confirm the ability of surface-adsorbed silk-HBM constructs to bind biotinylated heparin (Figure A.8B). Both IL-2 (positive control) and S_4H_4 were detected by biotinylated heparin; whereas heparin did not bind to either the $silk_2$ or the BSA negative control. An analogous blot was probed with secondary streptavidin – HRP only (data not shown). This assay format exhibited limited sensitivity: approximately 0.3 mg of protein applied to each 10 µl spot was required for subsequent heparin detection. Thus, both kinetic and endpoint Enzyme Linked Immunosorbant Assays (ELISA) were conducted to determine the dissociation constant of heparin with S_4H_4 and silk (Figure A.8A). Although the endpoint ELISA was able to validate the interaction of heparin with S_4H_4 and the lack of significant interaction with $silk_2$, kinetic determination was inconsistent and did not yield significant results (data not shown).

The mechanics of MaSp2 silk protein have been extensively evaluated in the past; however, each protein was dissolved in HFIP and wet spun into methanol to create fibers. The diameter of each fiber and percent birefringence were both assessed via microscopy and image processing.

Discussion

Tailored surface coatings have been used for over four decades to improve materials performance in blood, tissue or biological milieu [543]. Historically, several strategies – either actively or passively pharmaceutical – have been exploited specifically to combat either materials thrombosis or biofilm formation [544]. For over 30 years, heparin's use as a surface-immobilized prophylactic agent has been reported in many forms on to improve hemocompatibility [545, 546] in

vitro and in vivo on numerous commercial medical devices [547, 548]. Recent advances in heparinized surfaces (e.g., Carmeda BioActive Surface, BioInteractions Biba-Hepcoat technology (Tyco Healthcare) licensed by Medtronic) and the relative success of chemically defined polymer surface coatings in providing a versatile cassette for pharmaceutical immobilization is a driving force behind using biological-based biomimetic therapeutics [549-551], or synthetic polymer [552, 553] materials as surface coatings [554]. Furthermore, several groups have recently explored heparin silk complexes by covalently linking heparin to silk (often silkworm silk) or via mixing prior to processing via electrospinning or film casting [555-557]. Unfortunately with all these coatings, once heparin is lost, the surface properties desired for heparinized materials are clinically sub-standard. A “self-renewable” multifunctional coating, such as could be created using the fusion protein described herein, relying on biological mechanisms and thrombosis signaling pathways offers a feasible alternative [558].

Using a compatible nonregenerable cloning strategy [536, 538, 559] $silk_2$ and HBM_4 constructs were created and genetically linked to create the S_2H_4 fusion protein (Figure A.2); whereas S_4H_4 was directly synthesized in pET30a for expression. Based on anticipated intermolecular hydrogen binding, two polymerized MaSp2 silk monomers were predicted to provide a sufficient mechanical background in which to embed a heparin-binding motif and to provide enough flexibility to allow the heparin-binding domain to bind heparin with minimal steric hindrance and potentially even provide antimicrobial efficacy based on its AMP-like residues and structure. It is important to note that while alanine and arginine can promote heparin binding, the presence of proline is disruptive, further necessitating a minimal silk component of the fusion protein [524]. Unfortunately, using only two silk repeats was insufficient to reduce lysine molar fraction in the construct sufficiently to overcome dismal yields (data not shown). It is possible that yields could be increased with the addition of a periplasmic localization signal [560]. Therefore, four silk repeats were genetically linked with the heparin-binding motif, improving the recombinant protein yield.

Based on previous reports of heparin’s dissociation constant with the ARKKAAKA peptide (K_D = 42±15 nm, MW 7298), four uninterrupted heparin-binding motifs were used to optimize possible heparin interactions [524], suggesting that a recombinant silk MaSp2 peptide genetically

fused with four repeats of the HBM peptide would be capable of binding heparin from ionic solutions. Support for this design was evident using a recombinant silk/heparin fusion protein in several heparin-binding assays (Figures A.5 and A.6). Although the genetic sequence of the S_2H_4 clone was confirmed and the peptide was functionally active, mass spectrometry and amino acid analysis were unable to confirm the exact protein identity, attributed to poor yields and concentration. After derivatizing recombinant proteins with o-phthaldehyde, high performance liquid chromatography (HPLC) of S_2H_4, showed the emergence of a new peak, indicating an increase in the number of primary amino acids. Nevertheless, due to this unconventional use of HPLC, this analysis was not considered sequence confirmation of S_2H_4 (Figure A.4). Alternatively, S_4H_4 protein identity was confirmed via mass spectrometry (Figure A.5).

Although antimicrobial peptides receive substantial research interest amidst the rising tide of antimicrobial resistant bacteria and their recombinant production, like most peptides, is cost effective in *E.coli,* it is necessary to proteolytically stabilize them as a fusion peptide [561, 562]. Thus, it was not surprising that bacterial expression was negatively affected by the addition of structurally analogous HBM; nevertheless, the fusion was not thought to be a toxic construct due to the presence of the silk peptide. Observed low but finite levels of protein expression confirmed this suspicion. Expression of the HBM peptide alone in the absence of the MaSp2 silk peptide in any measurable quantity was not feasible (data not shown), likely due to the high molar percent of lysine in the peptide and the bacteria's innate ability to respond to AMPs [561, 563]. Thus, the HBM peptide was expressed only as a fusion with proteolytically stable silk. Unfortunately, expression of the S_2H_4 fusion protein was also significantly hampered apparently by the higher lysine content, indicating that the silk peptide with its extended stretches of alanine, predicted to support heparin binding [524], may not have been of significant length when considering the ratio of the fusion components. This supposition was supported by the increased protein expression when the silk peptide was expanded to four repeats. Recently, Yang et al. produced a Cecropin AD (a cationic AMP) elastin like peptide (ELP) fusion protein similar to that being reported in this study and demonstrated the link between the length of the ELP sequence and the yield of the fusion [564-566]. Thus, efforts to increase levels of recombinant protein expression of S_2H_4 fusion by effectively

"diluting" out the molar percent of lysine using a larger purification tag (GST) (ProMab) (data not shown) demonstrated increased expression, confirming the utility of a large fusion tag. Unfortunately, the GST fusion was unstable to even a single freeze/ thaw cycle, and storage at 4°C also proved susceptible to rapid degradation (within 1-3 days), as indicated by a laddering effect in SDS PAGE. Therefore, the lower expressing 6xHis tag version of the fusion was used for all heparin-binding assays. The fact that expression was significantly increased by the presence of the large GST tag (~25kD) compared to the smaller silk peptide (~15kD) may indicate that the silk peptide was not of sufficient length the mask the cationic heparin binding peptide.

In addition to using a larger fusion tag or additional silk repeats to increase the yield of the heparin-binding motif, evidence suggests that promoting the sequestration of the recombinant cationic fusion protein, such as may occur when using a periplasmic signal peptide, may also improve the yield. A lower induction temperature was also found to improve expression (Figure A.6). Contrary to Luan *et al.* who recently demonstrated the ability of *E.coli* to recombinantly express AMPs as a self-cleaving fusion that was sequestered as aggregates [562], the HBM silk fusion was not sequestered in inclusion bodies in any measurable amount (data not shown) or aggregated. This may have been a detriment to efficient protein production as Zorko *et al*. recently demonstrated the ability to produce large quantities of recombinant AMP by forcing sequestration in inclusion bodies [563]. Considering the chimera protein sequence analogy with an AMP, the resulting fusion protein remains to be evaluated for antimicrobial efficacy although preliminary Kirby Bauer zone of inhibition assays suggest there may be some efficacy against *E.coli* (data not shown). Future work will modify the ratio of the MaSp2 silk to heparin-binding motifs in attempts to optimize both mechanical and biological properties while increasing recombinant protein yield.

The ability of the fusion proteins to bind heparin was utilized as the final distinguishing feature of the silk fusion protein. ATIII or IL2 was used in these assays as a positive control while BSA was used as the negative control [540, 567]. Surface-bound heparin such as presented by HyperD heparin affinity resin was capable of retaining S_2H_4 and S_4H_4 (Figure A.7) although the S_2H_4 fusion did not appear capable of binding heparin with the same robustness as ATIII [567]. This observation was confirmed using dot blot analysis on the elution fractions from the S_2H_4 (data not

shown) and S_4H_4 columns, which also had a more diffuse dot blot signal. Interestingly, S_4H_4 did bind biotinylated heparin with the same intensity as IL-2 (Figure A.8). Additionally, endpoint ELISA indicated that there was no significant difference in heparin binding when compared to the IL-2 positive control.

Even though heparin bound to the fusion protein with very little nonspecific binding to $silk_2$ determining the kinetics of this binding through kinetic ELISA was inconsistent, not allowing accurate determination. Previous indirect efforts using labeled heparin have been used successfully; however, direct label-free kinetic determination is challenging at best [541, 568, 569]. The challenge is two-fold: (1) heparin is an anionic polyelectrolyte and (2) electrostatic binding to heparin is not a specific interaction. Since heparin is polyvalent, it may bind multiple protein partners simultaneously, making it difficult to resolve single binding kinetics. Thus, the observed binding rate will be dependent on the surface density of the protein, yielding a complex profile. In an attempt to decipher and determine kinetic heparin binding profiles, two designs were evaluated via kinetic ELISAs, in which heparin was either the capture ligand and the protein was added in solution, or the protein was the capture molecule and heparin was added in solution. Unfortunately, although this design allowed confirmation that the heparin-binding modified silk can bind heparin, the disassociation constant could not be determined. Additionally, since many proteins bind heparin through charge/charge interactions similar to an ion exchange resin and not specifically, binding site saturation, a key principle for label free affinity measurements, cannot be achieved.

The ionic strength of the various buffers used in all heparin-binding experiments could potentially reduce or disrupt the predominant electrostatic interactions [570] between negatively charged heparin and its positively charged binding partners (i.e., silk and silk fusion constructs) and must be considered during analysis. The ionic strength of the buffer, particularly the wash buffer used in all immunoassays (i.e., dot blot and ELISA), must provide sufficient stringency to prevent nonspecific background interactions. Thus, TBS Tween, with an ionic strength of 0.175M, well below the concentration used to disrupt nonspecific electrostatic interactions in the HyperD heparin column, was used and provided sufficient stringency to reduce nonspecific background interactions at pH 7.5 as evidenced by the minimal or absent signal in the silk and the negative control and the

overall low background of the blot (Figure A.8 B). ELISAs were also run with both desalted and buffered (Maxwell elution buffer) samples with no significant difference in performance (data not shown), indicating that ionic strength based on buffer composition was not a significant factor that altered heparin interactions. Importantly, using Promega's Maxwell 16 system required elution in the Maxwell elution buffer; however, as the interactions being probed are specifically electrostatic interactions, we were concerned that the ionic strength of the buffer may interfere or provide artificial results. Therefore, ELISAs were also run with desalted samples, showing no significant differences between directly eluted samples and those desalted. Furthermore, since all recombinant proteins were purified the same way they all would have experienced the effect of an ionic solution similarly. Finally, the Maxwell elution buffer (500mM Imidazole and 100mM HEPES, pH 7.5) had an ionic strength well below the manufacturer's recommended elution buffer (I=2M) for that of the HyperD heparin column. As a zwitterion, HEPES is proposed not to contribute to solution ionic strength [571]. Imidazole, is partially protonated at pH 7.4, indicating that at physiological pH it has limited ionic strength and is used primarily to stabilize proteins [572]. Therefore, although the potential interference of the buffer in the binding of heparin to its binding partner cannot be completely discounted, experimental and theoretical evidence would suggest that such an effect is limited.

Although a complete stoichiometric analysis and binding pair dissociation constant were not determined, a titration of the protein across the heparin affinity column (data not shown) indicated that at the highest concentration of 100 µg of loaded protein, the reported binding capacity of resin (25-35 µg/ml) was not exceeded, supported by no protein observed in the flow-through fraction of the fusion protein. Furthermore, lack of protein in the flow-through fraction and minimal protein in the wash fraction also indicated that the time to dissociation of heparin and the HBM/silk fusion protein did not exceed the time necessary to perform the column chromatography (~2 hours). This observed robustness of binding may reflect the limited length of the component peptides when compared to the natural full-length protein. Thus, this aspect of the protein fusion could be altered in the future to optimize heparin binding and disassociation events. Future efforts will continue to try to obtain reliable association/disassociation kinetics for this paired affinity.

Conclusions

A new protein fusion comprising spider silk-derived MaSp2 peptides fused with a consensus heparin-binding peptide was cloned, expressed, purified, and shown to bind soluble heparin both at surfaces and in buffer solutions. While fusion protein affinity with heparin was demonstrated under certain in vitro conditions, the precise stoichiometry and binding kinetics remain to be determined as does verification of heparin's bioactivity. Utility of this protein as a biomaterial, exploiting both the recombinant protein-bound heparin and also the intrinsic antimicrobial potential based on its AMP-like structure, represents the next application for this newly engineered recombinant chimera.

Acknowledgements

This research was supported by National Institutes of Health (NIH) grant R21 DK088426-01 and by start-up funds provided to A. Brooks from North Dakota State University Department of Pharmaceutical Sciences. We thank Dr. R. Campbell (Utah) for his input on using biotinylated heparin, K. Hill (NDSU) for assistance with protein production. Funding for the Core Synthesis and Analytical Services Facility used in this publication was made possible by NIH Grant P30 GM103332 (NIGMS). Manuscript contents are solely the responsibility of the authors and do not necessarily represent the official views of the NIH.

Supplementary information

Materials and methods

High performance liquid chromatography (HPLC). Purified proteins were dialyzed against water for 2 days using a 3 kDa-cutoff dialysis membrane and concentration was determined *via* absorbance at 280 nm as well as on SDS PAGE by comparison with BSA protein standards using optical densitometry. Subsequently, silk and silk-HBM recombinant proteins were derivatized with o-phthaldehyde (OPA, Sigma), which binds to primary amines and fluoresces (ex = 360 nm, em = 460 nm) to allow detection [573]. A stock OPA solution was prepared as previously described [573]. Briefly, 50 mg of OPA (powder, Sigma) was dissolved in 4 ml of methanol, 0.5 ml of potassium

borate (0.5 M boric acid adjusted to pH of 10.4 with potassium hydroxide), and 50 µl 2-mercaptoethanol (Sigma) was added. This solution was kept at 4°C in the dark. Working reagent was prepared fresh by adding 50 µl OPA stock solution to 1 ml of 0.5 M potassium buffer. Each reaction contained 100 µl of protein solution in water, 100 µl of isopropanol and 200 µl of OPA reagent. Reactions were allowed to incubate at room temperature protected from light for 30 min prior to injecting on the HPLC column. Each reaction (10 µl) was injected on a C-18 Gold column with an inline guard column (ThermoFisher Scientific). A blend of acetonitrile and phosphate buffer (52:48) was used as the mobile phase (flow rate = 1 ml/min). Column temperature was set to 22°C.

Results and discussion

Since sizes of the MaSp2 silk alone versus that of the silk-HBM fusions were difficult to confidently distinguish by SDS-PAGE alone, each protein was derivatized with fluorescent tag, OPA, for detection with HPLC. OPA reagent derivatizes primary amines, producing a fluorogenic compound, which can then be detected [573]. Pure MaSp2 silk protein is only expected to have a single free amine available for such derivatization on its N-terminus; whereas, the addition of the HBM peptide (ARKKAAKA) provides three lysine residues, equivalent to three additional primary amines (12 primary amines total) available for derivatization. Thus, HPLC was not used to detect a change in the molecular weight of the protein, but merely a change in the sequence of the protein as a confirmation that the HBM peptide was added. Precolumn OPA derivatization followed by separation with a C18 HPLC column provided separation of a new protein peak eluting at approximately 32 min (Figure A.4). The presence of this peak in an S_2H_4 sample is again likely the result of the increased number of primary amines corresponding to an increased molar percent of lysine in the S_2H_4 fusion. Unfortunately, degradation seemed to significantly impact the HBM fraction of the fusion as storing the protein at 4°C for 4 months caused the HPLC peak to not only broaden but also to shift to the left (i.e., retention time = 2-4 min), making it only slightly greater than the minimal peak detected for pure silk (data not shown). Replicate SDS-PAGE analysis run on these protein samples after storage validated the HPLC results, demonstrating not only a slightly higher concentration of silk but also the apparent degradation of the fusion protein, as indicated by

a slight decrease in molecular weight (data not shown). Thus, this OPA fluorogenic detection method exploiting the increase in number of available primary amines for protein product derivatization allowed identification of the recombinant silk-HBM fusion protein.

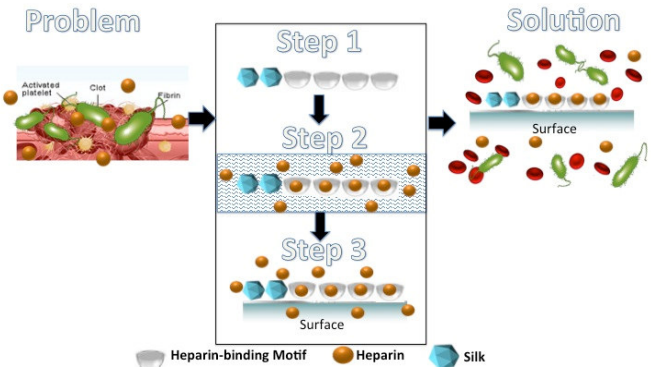

Figure A.1 Infection and thrombosis are intimately connected (problem). This is of particular concern for hemodialysis catheters and other blood-contacting medical devices. The heparin-binding motif (HBM) can both bind heparin to prevent blood clots and also act as an antimicrobial peptide. Thus, genetically linking a heparin-binding motif with a protease-resistant silk protein will bind heparin, both when in solution as well as when bound to a surface (steps 1-3 as described in this dissertation). Ultimately, using this new fusion protein as a medical device coating will not only bind endogenous and exogenous heparin from the blood stream, but will also prevent infection (solution).

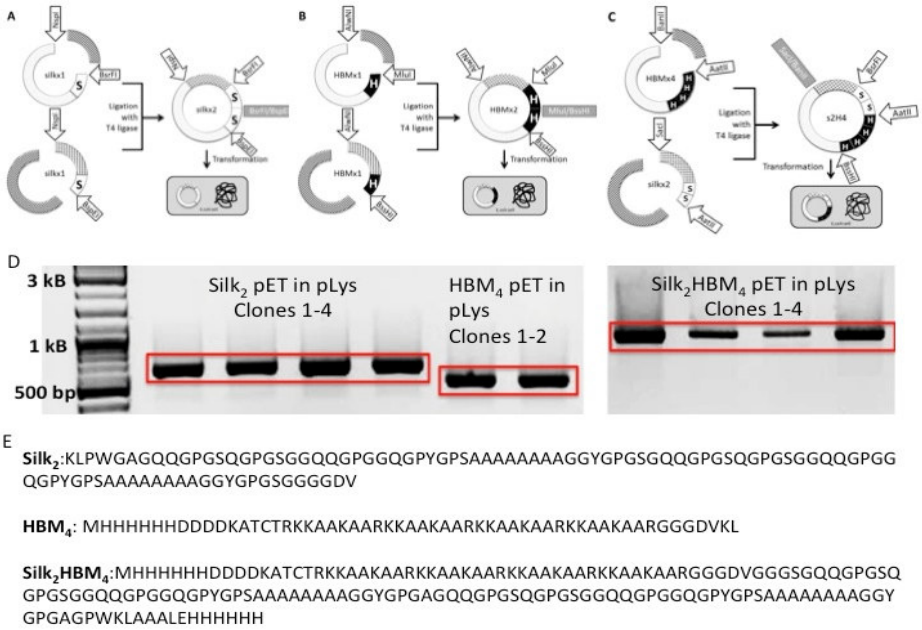

Figure A.2 Schematic showing the compatible nonregenerable cloning design. The design is used to genetically polymerize the A) Argiope aurantia MaSp2 consensus repeat motif using BsrFI and BspEI to produce compatible ends, which after being ligated together cannot be cleaved by either BsrFI or BspEI; B) HBM consensus repeat motif using MluI and BssHI to produce compatible ends, which after being ligated together cannot be cleaved by either MluI or BssHI; C) the Argiope aurantia MaSp2 consensus repeat motif concatenated with the HBM consensus repeat motif using BanII and SacI. D) Agarose gel electrophoresis showing the successful linkage of silk2 and HBM4. Bands of interest are highlighted by the boxes. Each band represents a different clone. E) Amino acid sequences for each clone. Note that a 6xHis tag was included in each construction for purification and detection.

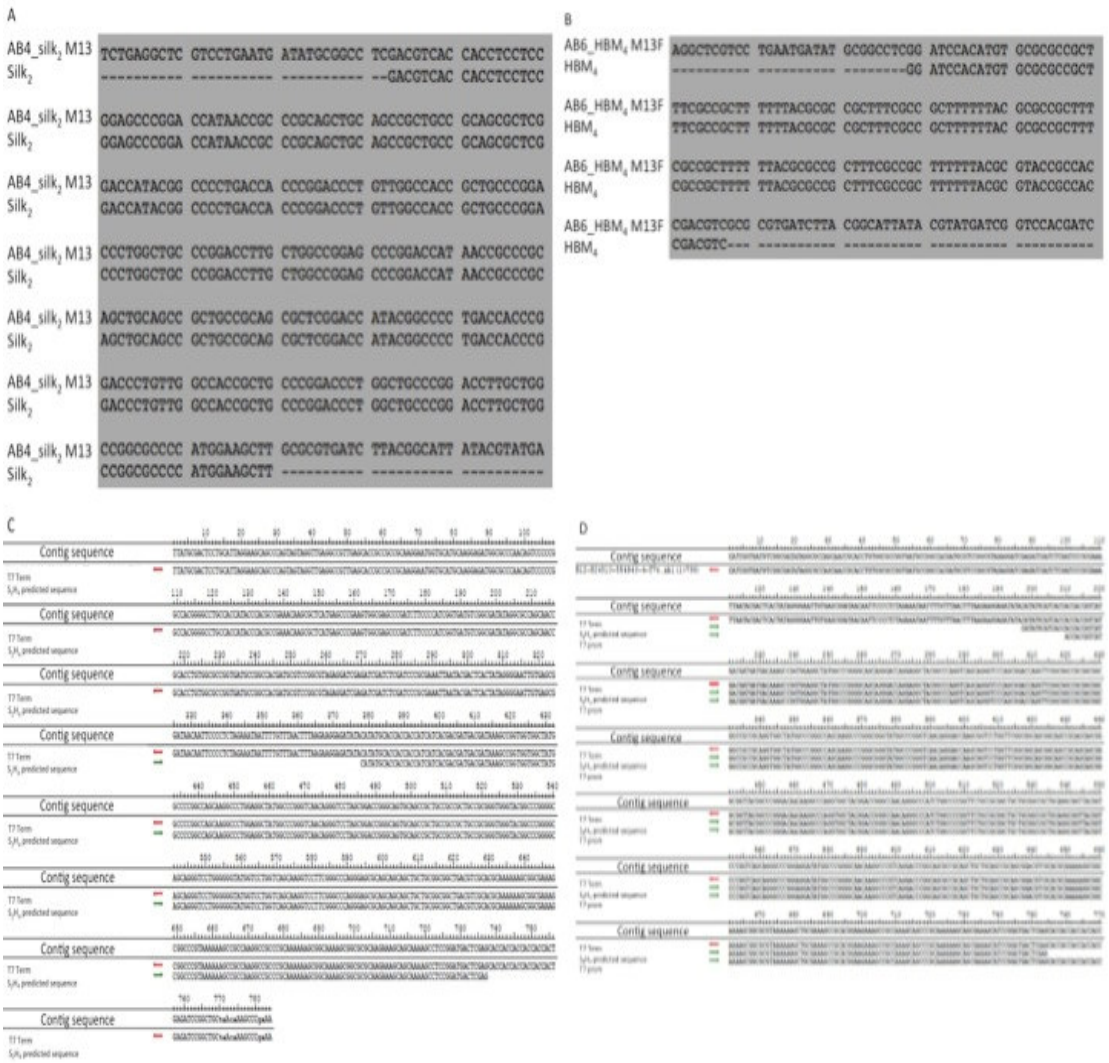

Figure A.3 Sequencing results from all constructs reported here. (A) $Silk_2$, (B) HBM_4, (C) S_2H_4, (D) S_4H_4

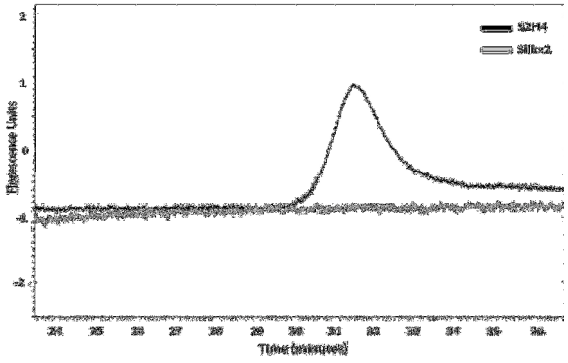

Figure A.4 HPLC analysis of both the recombinant MaSp2 silk protein (flat grey line) and the s2H4 chimera protein (black peak). Each protein was derivatized with OPA to detect an increase in the number of primary amines present in the proteins. Notice the distinct peak at 32 min for the chimera that is absent in the silk protein, indicating an increase in primary amines as a result of the lysine residues in the HBM portion of the protein.

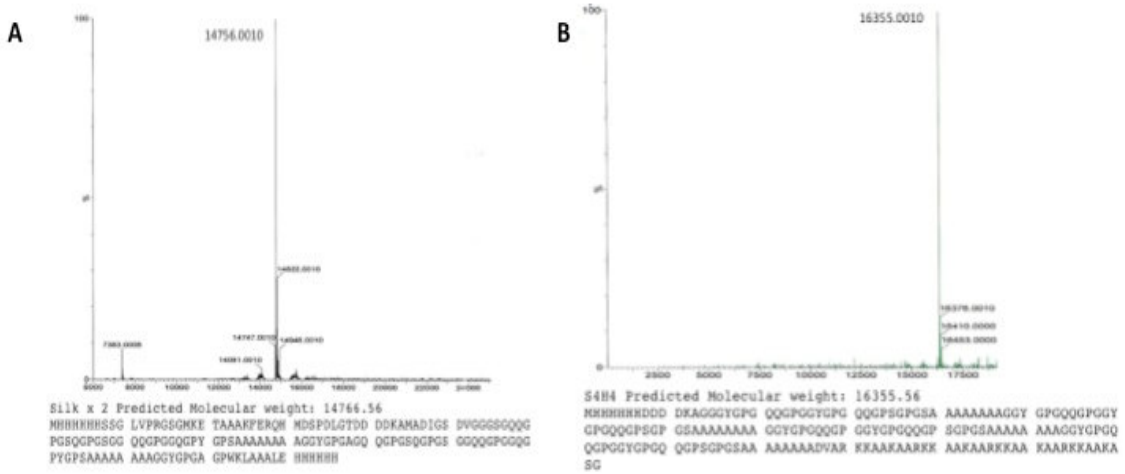

Figure A.5 Liquid chromatography electrospray ionization mass spectrometric validation of the desired recombinant modified silk fusion protein sequences. (A) Based on the amino acid sequence shown for silk$_2$, predicted to be 14766.56, the silk$_2$ protein was confirmed. (B) Based on the amino acid sequence shown for S_4H_4, predicted to be 16355.56, the S_4H_4 protein was

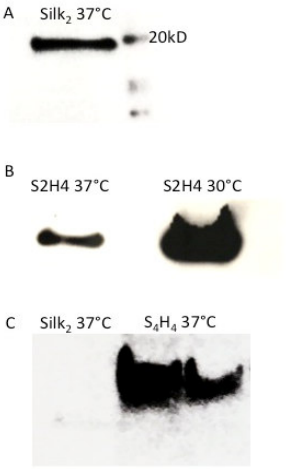

Figure A.6 Western blot of (A) Silk$_2$ protein, (B) S_2H_4, and (C) S_4H_4 (2 clones) using a HRP conjugated anti-His antibody. To improve yield two different induction temperatures were assessed for S_2H_4. Only in the Silk$_2$ blot can the molecular weight marker be seen. Note that all of the gels were nonreducing.

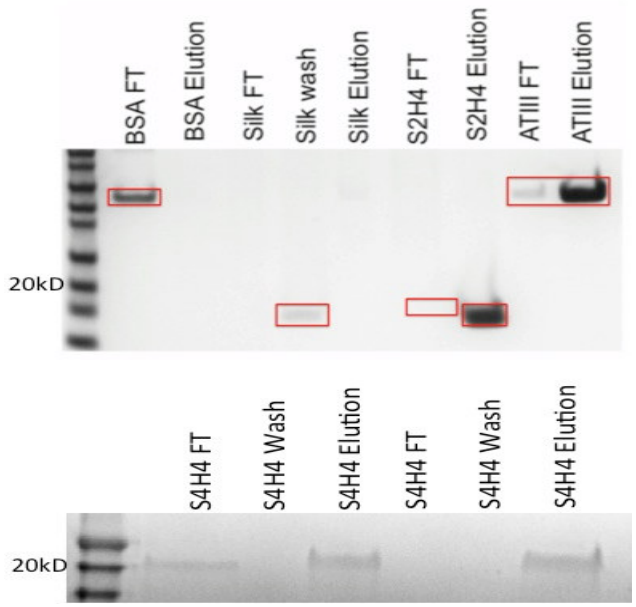

Figure A.7 SDS PAGE showing a solid phase functional assay using heparin affinity chromatography. Notice the increased ability of the recombinant S_2H_4 and S_4H_4 protein to bind heparin as indication by its elution in the finial high salt buffer. Two clones of S_4H_4 are shown. The binding capacity of the column was likely exceeded in the first clone, thereby giving rise to a band in the flow through fraction (FT). Bands of interest are highlighted by the boxes.

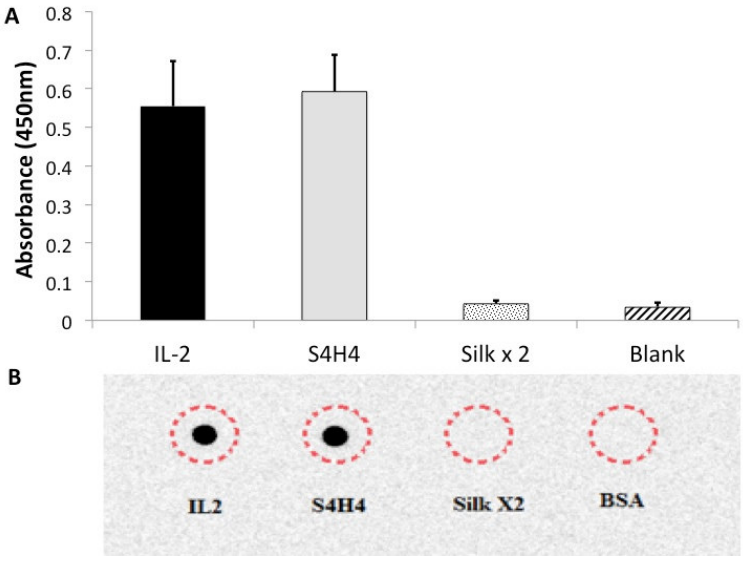

Figure A.8 (A) ELISA to detect the interaction of IL-2 (positive control), S_4H_4, $silk_2$, and BSA (negative control) with heparin. Notice that there is no statistical significance between the binding of heparin with S_4H_4 and the positive control and there is only a small amount of binding to silk. (B) S_4H_4 spotted on nitrocellulose binds heparin similar to the positive control IL-2. Notice that $silk_2$ was unable to bind heparin, similar to the BSA negative control. Areas were each test protein was spotted are indicated by a dashed circle.

REFERENCES

[1] D. Huh, G.A. Hamilton, D.E. Ingber, From 3D cell culture to organs-on-chips, Trends Cell Biol. 21 (2011) 745-754.

[2] G.D. Prestwich, Simplifying the extracellular matrix for 3-D cell culture and tissue engineering: a pragmatic approach, J. Cell. Biochem. 101 (2007) 1370-1383.

[3] R.K. Chhetri, Z.F. Phillips, M.A. Troester, A.L. Oldenburg, Longitudinal study of mammary epithelial and fibroblast co-cultures using optical coherence tomography reveals morphological hallmarks of pre-malignancy, PloS One 7 (2012) e49148.

[4] O.J. Trask Jr, A. Davies, S. Haney, F.M. Robertson, M.A. Ogasawara, Z. Ye, et al., Imaging and analysis of 3D tumor spheroids enriched for a cancer stem cell phenotype, J. Biomol. Screen. 15 (2010) 820-829.

[5] C.C. Park, W. Georgescu, A. Polyzos, C. Pham, K.M. Ahmed, H. Zhang, et al., Rapid and automated multidimensional fluorescence microscopy profiling of 3D human breast cultures, Integr. Biol. 5 (2013) 681-691.

[6] M.-O. Baradez, D. Marshall, The use of multidimensional image-based analysis to accurately monitor cell growth in 3D bioreactor culture, PloS One 6 (2011) e26104.

[7] S.R. Horman, J. To, A.P. Orth, An HTS-compatible 3D colony formation assay to identify tumor-specific chemotherapeutics, J. Biomol. Screen. (2013) 1087057113499405.

[8] P.A. Kenny, G.Y. Lee, C.A. Myers, R.M. Neve, J.R. Semeiks, P.T. Spellman, et al., The morphologies of breast cancer cell lines in three-dimensional assays correlate with their profiles of gene expression, Mol. Oncol. 1 (2007) 84-96.

[9] C. Albrecht, M. Helmreich, B. Tichy, S. Marlovits, R. Plasenzotti, M. Egerbacher, et al., Impact of 3D-culture on the expression of differentiation markers and hormone receptors in growth plate chondrocytes as compared to articular chondrocytes, Int. J. Mol. Med. 23 (2009) 347.

[10] J.B. Kim, Three-dimensional tissue culture models in cancer biology, Semin. Cancer Biol., Elsevier, 2005, p. 365-377.

[11] O. Trédan, C.M. Galmarini, K. Patel, I.F. Tannock, Drug resistance and the solid tumor microenvironment, J. Natl. Cancer Inst. 99 (2007) 1441-1454.

[12] D. Diekjürgen, D.W. Grainger, Drug transporter expression profiling in a three-dimensional kidney proximal tubule in vitro nephrotoxicity model, Pflugers Arch. submitted 2016 (2016).

[13] D. Diekjürgen, D.W. Grainger, An ex vivo 3D kidney proximal tubule model improves predictions of clinical drug-induced nephrotoxicity, Toxicol. Sci. submitted 2017 (2017).

[14] R. Edmondson, J.J. Broglie, A.F. Adcock, L. Yang, Three-dimensional cell culture systems and

their applications in drug discovery and cell-based biosensors, Assay Drug Dev. Technol. 12 (2014) 207-218.

[15] S. Breslin, L. O'Driscoll, Three-dimensional cell culture: the missing link in drug discovery, Drug Discov. Today 18 (2013) 240-249.

[16] M.W. Tibbitt, K.S. Anseth, Hydrogels as extracellular matrix mimics for 3D cell culture, Biotechnol. Bioeng. 103 (2009) 655-663.

[17] D.K. Mishra, J.H. Sakamoto, M.J. Thrall, B.N. Baird, S.H. Blackmon, M. Ferrari, et al., Human lung cancer cells grown in an ex vivo 3D lung model produce matrix metalloproteinases not produced in 2D culture, PloS one 7 (2012) e45308.

[18] K.M. Yamada, E. Cukierman, Modeling tissue morphogenesis and cancer in 3D, Cell 130 (2007) 601-610.

[19] A. Astashkina, D.W. Grainger, Critical analysis of 3-D organoid in vitro cell culture models for high-throughput drug candidate toxicity assessments, Adv. Drug Deliv. Rev. (2014).

[20] H. Huang, Y. Ding, X.S. Sun, T.A. Nguyen, Peptide hydrogelation and cell encapsulation for 3D culture of MCF-7 breast cancer cells, PloS one 8 (2013) e59482.

[21] B.M. Baker, C.S. Chen, Deconstructing the third dimension: how 3D culture microenvironments alter cellular cues, J. Cell Sci. 125 (2012) 3015-3024.

[22] J.B. Tarloff, L.H. Lash, Toxicology of the Kidney, CRC Press, 2004.

[23] J.B. Sullivan, G.R. Krieger, Clinical environmental health and toxic exposures, Lippincott Williams & Wilkins, 2001.

[24] O. Liangos, M.C. Perianayagam, V.S. Vaidya, W.K. Han, R. Wald, H. Tighiouart, et al., Urinary N-acetyl-β-(D)-glucosaminidase activity and kidney injury molecule-1 level are associated with adverse outcomes in acute renal failure, J. Am. Soc. Nephrol. 18 (2007) 904-912.

[25] L.A. Gurski, N.J. Petrelli, X. Jia, M.C. Farach-Carson, 3D matrices for anti-cancer drug testing and development, Oncology Issues 25 (2010) 20-25.

[26] X. Xu, L.A. Gurski, C. Zhang, D.A. Harrington, M.C. Farach-Carson, X. Jia, Recreating the tumor microenvironment in a bilayer, hyaluronic acid hydrogel construct for the growth of prostate cancer spheroids, Biomaterials 33 (2012) 9049-9060.

[27] R.Z. Lin, H.Y. Chang, Recent advances in three-dimensional multicellular spheroid culture for biomedical research, Biotechnol. J. 3 (2008) 1172-1184.

[28] A. Ivascu, M. Kubbies, Rapid generation of single-tumor spheroids for high-throughput cell function and toxicity analysis, J. Biomol. Screen. 11 (2006) 922-932.

[29] Y. Oda, Y. Yoshimura, H. Ohnishi, M. Tadokoro, Y. Katsube, M. Sasao, et al., Induction of pluripotent stem cells from human third molar mesenchymal stromal cells, J. Biol. Chem. 285 (2010) 29270-29278.

[30] A. Morizane, T. Kikuchi, K. Nishimura, J. Takahashi, Small-molecule inhibitors of bone morphogenic protein and activin/nodal signals promote highly efficient neural induction from human pluripotent stem cells, J. Neurosci. Res. 89 (2011) 117-126.

[31] M. Kijanska, J. Kelm, In vitro 3D Spheroids and microtissues: ATP-based cell viability and toxicity assays, In: G. Sittampalam, N. Coussens, K. Brimacombe (Eds), Assay Guidance Manual [Internet], Eli Lilly & Company and the National Center for Advancing Translational Sciences, Bethesda, 2016.

[32] Y.-C. Tung, A.Y. Hsiao, S.G. Allen, Y.-s. Torisawa, M. Ho, S. Takayama, High-throughput 3D spheroid culture and drug testing using a 384 hanging drop array, The Analyst 136 (2011) 473-478.

[33] T. Goodwin, T. Prewett, D.A. Wolf, G. Spaulding, Reduced shear stress: A major component in the ability of mammalian tissues to form three-dimensional assemblies in simulated microgravity, J. Cell. Biochem. 51 (1993) 301-311.

[34] Thermo Fisher Scientific Inc., Thermo Fisher Scientific. www.thermofisher.com, 2015, (accessed 2015).

[35] T. Bollenbach, P. Pantazis, A. Kicheva, C. Bökel, M. González-Gaitán, F. Jülicher, Precision of the Dpp gradient, Development 135 (2008) 1137-1146.

[36] R.R. Kay, P. Langridge, D. Traynor, O. Hoeller, Changing directions in the study of chemotaxis, Nature reviews. Molecular cell biology 9 (2008) 455-463.

[37] H.K. Kleinman, G.R. Martin, Matrigel: basement membrane matrix with biological activity, Semin. Cancer Biol., Elsevier, 2005, p. 378-386.

[38] G.Y. Lee, P.A. Kenny, E.H. Lee, M.J. Bissell, Three-dimensional culture models of normal and malignant breast epithelial cells, Nat. Methods 4 (2007) 359-365.

[39] B.A. Justice, N.A. Badr, R.A. Felder, 3D cell culture opens new dimensions in cell-based assays, Drug Discov. Today 14 (2009) 102-107.

[40] C. Ji, A. Khademhosseini, F. Dehghani, Enhancing cell penetration and proliferation in chitosan hydrogels for tissue engineering applications, Biomaterials 32 (2011) 9719-9729.

[41] D.T. Ward, S.J. McLarnon, D. Riccardi, Aminoglycosides increase intracellular calcium levels and ERK activity in proximal tubular OK cells expressing the extracellular calcium-sensing receptor, J. Am. Soc. Nephrol. 13 (2002) 1481-1489.

[42] I.A. Janson, A.J. Putnam, Extracellular matrix elasticity and topography: material-based cues that affect cell function via conserved mechanisms, J. Biomed. Mater. Res. A 103 (2015) 1246-1258.

[43] J.M. Aamodt, D.W. Grainger, Extracellular matrix-based biomaterial scaffolds and the host response, Biomaterials 86 (2016) 68-82.

[44] P. Gunness, K. Aleksa, K. Kosuge, S. Ito, G. Koren, Comparison of the novel HK-2 human renal proximal tubular cell line with the standard LLC-PK1 cell line in studying drug-induced nephrotoxicity, Can. J. Physiol. Pharmacol. 88 (2010) 448-455.

[45] M. Okuda, K. Tsuda, K. Masaki, Y. Hashimoto, K. Inui, Cisplatin-induced toxicity in LLC-PK1 kidney epithelial cells: role of basolateral membrane transport, Toxicol. Lett. 106 (1999) 229-235.

[46] E. Crivellato, L. Candussio, A.M. Rosati, G. Decorti, F.B. Klugmann, F. Mallardi, Kinetics of doxorubicin handling in the LLC-PK1 kidney epithelial cell line is mediated by both vesicle formation and P-glycoprotein drug transport, Histochem. J. 31 (1999) 635-643.

[47] A.I. Astashkina, B.K. Mann, G.D. Prestwich, D.W. Grainger, Comparing predictive drug nephrotoxicity biomarkers in kidney 3-D primary organoid culture and immortalized cell lines, Biomaterials 33 (2012) 4712-4721.

[48] P.J. Lee, N. Ghorashian, T.A. Gaige, P.J. Hung, Microfluidic system for automated cell-based assays, J. Assoc. Lab. Autom. 12 (2007) 363-367.

[49] W. Tan, R. Krishnaraj, T.A. Desai, Evaluation of nanostructured composite collagen–chitosan matrices for tissue engineering, Tissue Eng. 7 (2001) 203-210.

[50] I.K. Zervantonakis, S.K. Hughes-Alford, J.L. Charest, J.S. Condeelis, F.B. Gertler, R.D. Kamm, Three-dimensional microfluidic model for tumor cell intravasation and endothelial barrier function, Proc. Natl. Acad. Sci. 109 (2012) 13515-13520.

[51] Y. Gao, D. Majumdar, B. Jovanovic, C. Shaifer, P.C. Lin, A. Zijlstra, et al., A versatile valve-enabled microfluidic cell co-culture platform and demonstration of its applications to neurobiology and cancer biology, Biomed. Microdevices 13 (2011) 539-548.

[52] W.K. Han, V. Bailly, R. Abichandani, R. Thadhani, J.V. Bonventre, Kidney Injury Molecule-1 (KIM-1): a novel biomarker for human renal proximal tubule injury, Kidney Int. 62 (2002) 237-244.

[53] W. Han, S. Waikar, A. Johnson, R. Betensky, C. Dent, P. Devarajan, et al., Urinary biomarkers in the early diagnosis of acute kidney injury, Kidney Int. 73 (2008) 863-869.

[54] M. Blank, A. De Felice, F. Goodsaid, P. Harlow, E. Hausner, D. Jacobson-Kram, et al., Review of Qualification Data for Biomarkers of Nephrotoxicity Submitted by the Predictive Safety Testing Consortium, In: Center for Drug Evaluation and Research US Food and Drug Administration, 2009, pp. 4-74.

[55] P. Devarajan, Biomarkers for the early detection of acute kidney injury, Curr. Opin. Pediatr. 23 (2011) 194-200.

[56] S. Yokoo, A. Yonezawa, S. Masuda, A. Fukatsu, T. Katsura, K.-I. Inui, Differential contribution of organic cation transporters, OCT2 and MATE1, in platinum agent-induced nephrotoxicity, Biochem. Pharmacol. 74 (2007) 477-487.

[57] C. Van der Hauwaert, G. Savary, V. Gnemmi, F. Glowacki, N. Pottier, A. Bouillez, et al., Isolation and characterization of a primary proximal tubular epithelial cell model from human kidney by CD10/CD13 double labeling, PloS one 8 (2013) e66750.

[58] S.E. Jenkinson, G.W. Chung, E. van Loon, N.S. Bakar, A.M. Dalzell, C.D. Brown, The limitations of renal epithelial cell line HK-2 as a model of drug transporter expression and function in the proximal tubule, Pflugers Arch. 464 (2012) 601-611.

[59] C. Hilgendorf, G. Ahlin, A. Seithel, P. Artursson, A.L. Ungell, J. Karlsson, Expression of thirty-six drug transporter genes in human intestine, liver, kidney, and organotypic cell lines, Drug Metab. Dispos. 35 (2007) 1333-1340.

[60] A.I. Astashkina, B.K. Mann, G.D. Prestwich, D.W. Grainger, A 3-D organoid kidney culture model engineered for high-throughput nephrotoxicity assays, Biomaterials 33 (2012) 4700-4711.

[61] K.J. Jang, A.P. Mehr, G.A. Hamilton, L.A. McPartlin, S. Chung, K.Y. Suh, et al., Human kidney proximal tubule-on-a-chip for drug transport and nephrotoxicity assessment, Integr. Biol. (Camb) 5 (2013) 1119-1129.

[62] Y. Li, Z.Y. Oo, S.Y. Chang, P. Huang, K.G. Eng, J.L. Zeng, et al., An in vitro method for the prediction of renal proximal tubular toxicity in humans, Toxicol. Res. 2 (2013) 352.

[63] A.D. Doyle, R.J. Petrie, M.L. Kutys, K.M. Yamada, Dimensions in cell migration, Curr. Opin. Cell Biol. 25 (2013) 642-649.

[64] L.G. Griffith, M.A. Swartz, Capturing complex 3D tissue physiology in vitro, Nat. Rev. Mol. Cell Biol. 7 (2006) 211-224.

[65] T.M. DesRochers, L. Suter, A. Roth, D.L. Kaplan, Bioengineered 3D human kidney tissue, a platform for the determination of nephrotoxicity, PloS one 8 (2013) e59219.

[66] D. Yip, C.H. Cho, A multicellular 3D heterospheroid model of liver tumor and stromal cells in collagen gel for anti-cancer drug testing, Biochem Bioph Res Co 433 (2013) 327-332.

[67] L. Gasperini, J.F. Mano, R.L. Reis, Natural polymers for the microencapsulation of cells, J. R. Soc. Interface 11 (2014) 20140817.

[68] W.K. Han, J.V. Bonventre, Biologic markers for the early detection of acute kidney injury, Curr. Opin. Crit. Care 10 (2004) 476-482.

[69] J.L. Koyner, M.R. Bennett, E.M. Worcester, Q. Ma, J. Raman, V. Jeevanandam, et al., Urinary cystatin C as an early biomarker of acute kidney injury following adult cardiothoracic surgery, Kidney Int. 74 (2008) 1059-1069.

[70] M. Wieser, G. Stadler, P. Jennings, B. Streubel, W. Pfaller, P. Ambros, et al., hTERT alone immortalizes epithelial cells of renal proximal tubules without changing their functional characteristics, Am. J. Physiol. Renal Physiol. 295 (2008) F1365-F1375.

[71] L. Aschauer, A. Wilmes, A. Limonciel, M.O. Leonard, W. Pfaller, P. Jennings, Application of a human renal proximal tubule cell line, RPTEC/TERT1, for chemical safety assessment, Toxicol. Lett. 229 (2014) S242-S243.

[72] L. Aschauer, G. Carta, N. Vogelsang, E. Schlatter, P. Jennings, Expression of xenobiotic transporters in the human renal proximal tubule cell line RPTEC/TERT1, Toxicol. In Vitro 30 (2015) 95-105.

[73] L.C. Snouber, F. Letourneur, P. Chafey, C. Broussard, M. Monge, C. Legallais, et al., Analysis of transcriptomic and proteomic profiles demonstrates improved Madin-Darby canine kidney cell function in a renal microfluidic biochip, Biotechnol. Prog. 28 (2012) 474-484.

[74] L.S. Yu, Q. Shen, Q. Zhou, H.D. Jiang, H.C. Bi, M. Huang, et al., In vitro characterization of ABC transporters involved in the absorption and distribution of liensinine and its analogs, J. Ethnopharmacol. 150 (2013) 485-491.

[75] J. Mishra, C. Dent, R. Tarabishi, M.M. Mitsnefes, Q. Ma, C. Kelly, et al., Neutrophil gelatinase-associated lipocalin (NGAL) as a biomarker for acute renal injury after cardiac surgery, Lancet 365 (2005) 1231-1238.

[76] O. Liangos, H. Tighiouart, M.C. Perianayagam, A. Kolyada, W.K. Han, R. Wald, et al., Comparative analysis of urinary biomarkers for early detection of acute kidney injury following cardiopulmonary bypass, Biomarkers : biochemical indicators of exposure, response, and susceptibility to chemicals 14 (2009) 423-431.

[77] K.J. Price, A. Tsykin, K.M. Giles, R.T. Sladic, M.R. Epis, R. Ganss, et al., Matrigel Basement

Membrane Matrix influences expression of microRNAs in cancer cell lines, Biochem Bioph Res Co 427 (2012) 343-348.

[78] C.S. Szot, C.F. Buchanan, J.W. Freeman, M.N. Rylander, 3D in vitro bioengineered tumors based on collagen I hydrogels, Biomaterials 32 (2011) 7905-7912.

[79] V. Hongisto, S. Jernstrom, V. Fey, J.P. Mpindi, K. Kleivi Sahlberg, O. Kallioniemi, et al., High-throughput 3D screening reveals differences in drug sensitivities between culture models of JIMT1 breast cancer cells, PloS one 8 (2013) e77232.

[80] A.A. Tarhini, H. Edington, L.H. Butterfield, Y. Lin, Y. Shuai, H. Tawbi, et al., Immune monitoring of the circulation and the tumor microenvironment in patients with regionally advanced melanoma receiving neoadjuvant ipilimumab, PloS one 9 (2014) e87705.

[81] S.Y. Kim, A. Moon, Drug-induced nephrotoxicity and its biomarkers, Biomol. Ther. 20 (2012) 268.

[82] G.H. Tesch, A. Schwarting, K. Kinoshita, H.Y. Lan, B.J. Rollins, V.R. Kelley, Monocyte chemoattractant protein-1 promotes macrophage-mediated tubular injury, but not glomerular injury, in nephrotoxic serum nephritis, J. Clin. Invest. 103 (1999) 73.

[83] S.L. Deshmane, S. Kremlev, S. Amini, B.E. Sawaya, Monocyte chemoattractant protein-1 (MCP-1): an overview, J. Interferon Cytokine Res. 29 (2009) 313-326.

[84] F. Biomedical, NIH Definition of Biomarker, Clin. Pharmacol. Ther. 69 (2001) 89-95.

[85] L.E. Nee, T. McMorrow, E. Campbell, C. Slattery, M.P. Ryan, TNF-α and IL-1β–mediated regulation of MMP-9 and TIMP-1 in renal proximal tubular cells, Kidney Int. 66 (2004) 1376-1386.

[86] K.K. Washburn, M. Zappitelli, A.A. Arikan, L. Loftis, R. Yalavarthy, C.R. Parikh, et al., Urinary interleukin-18 is an acute kidney injury biomarker in critically ill children, Nephrol. Dial. Transplant. 23 (2008) 566-572.

[87] X. Zhao, J. Imig, Kidney CYP450 enzymes: biological actions beyond drug metabolism, Curr. Drug Metab. 4 (2003) 73-84.

[88] E. Hrycay, S. Bandiera, Expression, function and regulation of mouse cytochrome P450 enzymes: comparison with human cytochrome P450 enzymes, Curr. Drug Metab. 10 (2009) 1151-1183.

[89] X. Cheng, C.D. Klaassen, Perfluorocarboxylic acids induce cytochrome P450 enzymes in mouse liver through activation of PPAR-α and CAR transcription factors, Toxicol. Sci. 106 (2008) 29-36.

[90] C. Fang, M. Behr, F. Xie, S. Lu, M. Doret, H. Luo, et al., Mechanism of chloroform-induced renal toxicity: non-involvement of hepatic cytochrome P450-dependent metabolism, Toxicol. Appl. Pharmacol. 227 (2008) 48-55.

[91] R.L. Woosley, J. Cossman, Drug development and the FDA's Critical Path Initiative, Clin. Pharmacol. Ther. 81 (2007) 129-133.

[92] US Department of Health Human Services Food Drug Administration, Innovation or Stagnation: Challenge and Opportunity on the Critical Path to New Medical Products; 2004. http://www.fda.gov/downloads/ScienceResearch/SpecialTopics/CriticalPathInitiative/CriticalPathOpportunitiesReports/ucm113411.pdf, 2006, (accessed 2016).

[93] T.M. DesRochers, E. Palma, D.L. Kaplan, Tissue-engineered kidney disease models, Adv. Drug Deliv. Rev. 69 (2014) 67-80.

[94] T.C. Fuchs, P. Hewitt, Biomarkers for drug-induced renal damage and nephrotoxicity-an overview for applied toxicology, AAPS J. 13 (2011) 615-631.

[95] N. Pannu, M.K. Nadim, An overview of drug-induced acute kidney injury, Crit. Care Med. 36 (2008) S216-S223.

[96] G. Zbinden, Predictive value of animal studies in toxicology, Regul. Toxicol. Pharmacol. 14 (1991) 167-177.

[97] A. Knight, Systematic reviews of animal experiments demonstrate poor human clinical and toxicological utility, ATLA Altern. Lab. Anim. 35 (2007) 641.

[98] Y. Motoyoshi, T. Matsusaka, A. Saito, I. Pastan, T.E. Willnow, S. Mizutani, et al., Megalin contributes to the early injury of proximal tubule cells during nonselective proteinuria, Kidney Int. 74 (2008) 1262-1269.

[99] R. Giffin, S. Robinson, S. Olson, Accelerating the Development of Biomarkers for Drug Safety: Workshop Summary, National Academies Press, Washington, 2009.

[100] R.G. Schnellmann, Toxic responses of the kidney, In: Casarett and Doull's toxicology, 2001, pp. 491-514.

[101] T.R. Van Vleet, R.G. Schnellmann, Toxic nephropathy: environmental chemicals, Semin. Nephrol., Elsevier, 2003, p. 500-508.

[102] G. Ciarimboli, T. Ludwig, D. Lang, H. Pavenstädt, H. Koepsell, H.-J. Piechota, et al., Cisplatin nephrotoxicity is critically mediated via the human organic cation transporter 2, Am. J. Pathol. 167 (2005) 1477-1484.

[103] A. Astashkina, B. Mann, D.W. Grainger, A critical evaluation of in vitro cell culture models for high-throughput drug screening and toxicity, Pharmacol. Ther. 134 (2012) 82-106.

[104] F. Pampaloni, E.G. Reynaud, E.H. Stelzer, The third dimension bridges the gap between cell culture and live tissue, Nat. Rev. Mol. Cell Biol. 8 (2007) 839-845.

[105] G.D. Prestwich, Evaluating drug efficacy and toxicology in three dimensions: using synthetic extracellular matrices in drug discovery, Acc. Chem. Res. 41 (2008) 139-148.

[106] J.K. Chuah, D. Zink, Stem cell-derived kidney cells and organoids: Recent breakthroughs and emerging applications, Biotechnol. Adv. (2016).

[107] Y. Li, K. Kandasamy, J.K. Chuah, Y.N. Lam, W.S. Toh, Z.Y. Oo, et al., Identification of nephrotoxic compounds with embryonic stem-cell-derived human renal proximal tubular-like cells, Mol. Pharm. 11 (2014) 1982-1990.

[108] R. Morizane, A.Q. Lam, B.S. Freedman, S. Kishi, M.T. Valerius, J.V. Bonventre, Nephron organoids derived from human pluripotent stem cells model kidney development and injury, Nat. Biotechnol. 33 (2015) 1193-1200.

[109] S. Yamaguchi, R. Morizane, K. Homma, T. Monkawa, S. Suzuki, S. Fujii, et al., Generation of kidney tubular organoids from human pluripotent stem cells, Sci. Rep. 6 (2016) 38353.

[110] H. Izzedine, V. Launay-Vacher, G. Deray, Antiviral drug-induced nephrotoxicity, Am. J. Kidney Dis. 45 (2005) 804-817.

[111] H.Y. Tiong, P. Huang, S. Xiong, Y. Li, A. Vathsala, D. Zink, Drug-induced nephrotoxicity: clinical impact and preclinical in vitro models, Mol. Pharm. 11 (2014) 1933-1948.

[112] A.J. Olyaei, A.M. De Mattos, W.M. Bennett, Immunosuppressant-induced nephropathy, Drug Saf. 21 (1999) 471-488.

[113] A.C. Schoolwerth, D.A. Sica, B.J. Ballermann, C.S. Wilcox, Renal considerations in angiotensin converting enzyme inhibitor therapy, Circulation 104 (2001) 1985-1991.

[114] B.F. Palmer, Renal dysfunction complicating the treatment of hypertension, N. Engl. J. Med. 347 (2002) 1256-1261.

[115] C.A. Naughton, Drug-induced nephrotoxicity, Am. Fam. Physician 78 (2008).

[116] M. Schetz, J. Dasta, S. Goldstein, T. Golper, Drug-induced acute kidney injury, Curr. Opin. Crit. Care 11 (2005) 555-565.

[117] G.S. Markowitz, M.A. Perazella, Drug-induced renal failure: a focus on tubulointerstitial disease, Clin. Chim. Acta 351 (2005) 31-47.

[118] M.A. Perazella, Drug-Induced Renal Failure: Update on New Medications and Unique Mechanisms of Nephrotoxicity, Am. J. Med. Sci. 325 (2003) 349-362.

[119] M.A. Perazella, Drug-induced nephropathy: an update, Expert Opin. Drug Saf. 4 (2005) 689-706.

[120] J. Rossert, Drug-induced acute interstitial nephritis, Kidney Int. 60 (2001) 804-817.

[121] C.M. Fored, E. Ejerblad, P. Lindblad, J.P. Fryzek, P.W. Dickman, L.B. Signorello, et al., Acetaminophen, aspirin, and chronic renal failure, N. Engl. J. Med. 345 (2001) 1801-1808.

[122] G. Appel, Tubulointerstitial diseases: drug-induced chronic interstitial nephritis, ACP Medicine Online, New York, NY, WebMD, 2002.

[123] X. Guo, C. Nzerue, How to prevent, recognize, and treat drug-induced nephrotoxicity, Cleve Clin. J. Med. 69 (2002) 289-290, 293-284, 296-287 passim.

[124] M. Leblanc, J.A. Kellum, R.T.N. Gibney, W. Lieberthal, J. Tumlin, R. Mehta, Risk factors for acute renal failure: inherent and modifiable risks, Curr. Opin. Crit. Care 11 (2005) 533-536.

[125] R.W. Schrier, W. Wang, Acute renal failure and sepsis, N. Engl. J. Med. 351 (2004) 159-169.

[126] M.A. Perazella, Crystal-induced acute renal failure, Am. J. Med. 106 (1999) 459-465.

[127] D. Choudhury, Z. Ahmed, Drug-associated renal dysfunction and injury, Nat. Clin. Pract. Nephrol. 2 (2006) 80-91.

[128] A. Fry, K. Farrington, Management of acute renal failure, Postgrad. Med. J. 82 (2006) 106-116.

[129] R.L. Mehta, J.A. Kellum, S.V. Shah, B.A. Molitoris, C. Ronco, D.G. Warnock, et al., Acute Kidney Injury Network: report of an initiative to improve outcomes in acute kidney injury, Crit. Care

11 (2007) R31.

[130] R. Bellomo, C. Ronco, J.A. Kellum, R.L. Mehta, P. Palevsky, Acute renal failure–definition, outcome measures, animal models, fluid therapy and information technology needs: the Second International Consensus Conference of the Acute Dialysis Quality Initiative (ADQI) Group, Crit. Care Med. 8 (2004) R204.

[131] A. Khwaja, KDIGO clinical practice guidelines for acute kidney injury, Nephron. Clin. Pract. 120 (2012) c179-c184.

[132] S.G. Coca, R. Yalavarthy, J. Concato, C.R. Parikh, Biomarkers for the diagnosis and risk stratification of acute kidney injury: a systematic review, Kidney Int. 73 (2008) 1008-1016.

[133] M.J. Wilmer, C.P. Ng, H.L. Lanz, P. Vulto, L. Suter-Dick, R. Masereeuw, Kidney-on-a-Chip Technology for Drug-Induced Nephrotoxicity Screening, Trends Biotechnol. 34 (2016) 156-170.

[134] C.M. Sakolish, M.B. Esch, J.J. Hickman, M.L. Shuler, G.J. Mahler, Modeling Barrier Tissues In Vitro: Methods, Achievements, and Challenges, EBioMedicine 5 (2016) 30-39.

[135] H.H.T. Middelkamp, A.D. van der Meer, J.M. Hummel, D.F. Stamatialis, C.L. Mummery, R. Passier, et al., Organs-on-Chips in Drug Development: The Importance of Involving Stakeholders in Early Health Technology Assessment, Appl. In Vitro Toxicol. (2016).

[136] K.A. Homan, D.B. Kolesky, M.A. Skylar-Scott, J. Herrmann, H. Obuobi, A. Moisan, et al., Bioprinting of 3D Convoluted Renal Proximal Tubules on Perfusable Chips, Sci. Rep. 6 (2016) 34845.

[137] N. Gjorevski, N. Sachs, A. Manfrin, S. Giger, M.E. Bragina, P. Ordonez-Moran, et al., Designer matrices for intestinal stem cell and organoid culture, Nature 539 (2016) 560-564.

[138] K. Hariharan, A. Kurtz, K.M. Schmidt-Ott, Assembling Kidney Tissues from Cells: The Long Road from Organoids to Organs, Front Cell Dev. Biol. 3 (2015) 70.

[139] F. Liu, J. Huang, B. Ning, Z. Liu, S. Chen, W. Zhao, Drug Discovery via Human-Derived Stem Cell Organoids, Front Pharmacol. 7 (2016) 334.

[140] T. Mseka, J.R. Bamburg, L.P. Cramer, ADF/cofilin family proteins control formation of oriented actin-filament bundles in the cell body to trigger fibroblast polarization, J. Cell Sci. 120 (2007) 4332-4344.

[141] R. McBeath, D.M. Pirone, C.M. Nelson, K. Bhadriraju, C.S. Chen, Cell shape, cytoskeletal tension, and RhoA regulate stem cell lineage commitment, Dev. Cell 6 (2004) 483-495.

[142] S. Shaheen, M. Ahmed, F. Lorenzi, A.S. Nateri, Spheroid-Formation (Colonosphere) Assay for in Vitro Assessment and Expansion of Stem Cells in Colon Cancer, Stem Cell Rev. Rep. 12 (2016) 492-499.

[143] J. Alcaraz, R. Xu, H. Mori, C.M. Nelson, R. Mroue, V.A. Spencer, et al., Laminin and biomimetic extracellular elasticity enhance functional differentiation in mammary epithelia, EMBO J. 27 (2008) 2829-2838.

[144] D. Antoni, H. Burckel, E. Josset, G. Noel, Three-dimensional cell culture: a breakthrough in vivo, Int. J. Mol. Sci. 16 (2015) 5517-5527.

[145] M.A. Serban, G.D. Prestwich, Modular extracellular matrices: solutions for the puzzle,

Methods 45 (2008) 93-98.

[146] K.A. Kyburz, K.S. Anseth, Synthetic mimics of the extracellular matrix: how simple is complex enough?, Ann. Biomed. Eng. 43 (2015) 489-500.

[147] R.C. Dutta, A.K. Dutta, Cell-interactive 3D-scaffold; advances and applications, Biotechnol. Adv. 27 (2009) 334-339.

[148] G.D. Nicodemus, S.J. Bryant, Cell encapsulation in biodegradable hydrogels for tissue engineering applications, Tissue Eng. Part B Rev. 14 (2008) 149-165.

[149] N.A. Peppas, J.Z. Hilt, A. Khademhosseini, R. Langer, Hydrogels in biology and medicine: from molecular principles to bionanotechnology, Adv. Mater. 18 (2006) 1345-1360.

[150] A.W. Smith, J.D. Hoyne, P.K. Nguyen, D.A. McCreedy, H. Aly, I.R. Efimov, et al., Direct reprogramming of mouse fibroblasts to cardiomyocyte-like cells using Yamanaka factors on engineered poly(ethylene glycol) (PEG) hydrogels, Biomaterials 34 (2013) 6559-6571.

[151] S.L. Schor, A.M. Schor, B. Winn, G. Rushton, The use of three-dimensional collagen gels for the study of tumour cell invasion in vitro: Experimental parameters influencing cell migration into the gel matrix, Int. J. Cancer 29 (1982) 57-62.

[152] E. Bell, B. Ivarsson, C. Merrill, Production of a tissue-like structure by contraction of collagen lattices by human fibroblasts of different proliferative potential in vitro, Proc. Natl. Acad. Sci. 76 (1979) 1274-1278.

[153] S. Nehrer, H.A. Breinan, A. Ramappa, G. Young, S. Shortkroff, L.K. Louie, et al., Matrix collagen type and pore size influence behaviour of seeded canine chondrocytes, Biomaterials 18 (1997) 769-776.

[154] W. Friess, Collagen–biomaterial for drug delivery, Eur. J. Pharm. Biopharm. 45 (1998) 113-136.

[155] R. Parenteau-Bareil, R. Gauvin, F. Berthod, Collagen-based biomaterials for tissue engineering applications, Materials 3 (2010) 1863-1887.

[156] H. Uludag, P. De Vos, P.A. Tresco, Technology of mammalian cell encapsulation, Adv. Drug Deliv. Rev. 42 (2000) 29-64.

[157] K.Y. Lee, D.J. Mooney, Alginate: properties and biomedical applications, Prog. Polym. Sci. 37 (2012) 106-126.

[158] L. Wang, J. Shansky, C. Borselli, D. Mooney, H. Vandenburgh, Design and fabrication of a biodegradable, covalently crosslinked shape-memory alginate scaffold for cell and growth factor delivery, Tissue Eng. Part A 18 (2012) 2000-2007.

[159] T. Andersen, P. Auk-Emblem, M. Dornish, 3D Cell Culture in Alginate Hydrogels, Microarrays 4 (2015) 133-161.

[160] F. Gelain, A. Horii, S. Zhang, Designer self-assembling peptide scaffolds for 3-d tissue cell cultures and regenerative medicine, Macromol. Biosci. 7 (2007) 544-551.

[161] S. Kyle, A. Aggeli, E. Ingham, M.J. McPherson, Recombinant self-assembling peptides as biomaterials for tissue engineering, Biomaterials 31 (2010) 9395-9405.

[162] A.C. Mendes, E.T. Baran, P. Lisboa, R.L. Reis, H.S. Azevedo, Microfluidic fabrication of self-assembled peptide-polysaccharide microcapsules as 3D environments for cell culture, Biomacromolecules 13 (2012) 4039-4048.

[163] N.J. Boudreau, P.L. Jones, Extracellular matrix and integrin signalling: the shape of things to come, Biochem. J. 339 (1999) 481-488.

[164] K. Burridge, K. Fath, T. Kelly, G. Nuckolls, C. Turner, Focal adhesions: transmembrane junctions between the extracellular matrix and the cytoskeleton, Annu. Rev. Cell Biol. 4 (1988) 487-525.

[165] A. Aplin, A. Howe, S. Alahari, R. Juliano, Signal transduction and signal modulation by cell adhesion receptors: the role of integrins, cadherins, immunoglobulin-cell adhesion molecules, and selectins, Pharmacol. Rev. 50 (1998) 197-264.

[166] F.G. Giancotti, E. Ruoslahti, Integrin signaling, Science 285 (1999) 1028-1033.

[167] K. Ghosh, D.E. Ingber, Micromechanical control of cell and tissue development: implications for tissue engineering, Adv. Drug Deliv. Rev. 59 (2007) 1306-1318.

[168] D.E. Ingber, Tensegrity: the architectural basis of cellular mechanotransduction, Annu. Rev. Physiol. 59 (1997) 575-599.

[169] J.A. Rowley, G. Madlambayan, D.J. Mooney, Alginate hydrogels as synthetic extracellular matrix materials, Biomaterials 20 (1999) 45-53.

[170] S. Tang, W. Yang, X. Mao, Agarose/collagen composite scaffold as an anti-adhesive sheet, Biomed. Mater. 2 (2007) S129.

[171] G.O. Aspinall, The polysaccharides, Academic Press, New York, 2014.

[172] B.O. Fraser-Reid, K. Tatsuta, J. Thiem, Glycoscience-Chemistry and Chemical Biology I-III, Springer Science & Business Media, 2001.

[173] J. BeMiller, Classification, structure, and chemistry of polysaccharides of foods, Food Sci. Technol. (2001) 603-612.

[174] J.N. Bemiller, Structure property correlations of non starch food polysaccharides, Macromol. Symp., Wiley Online Library, 1999, p. 1-15.

[175] W. Lennarz, The biochemistry of glycoproteins and proteoglycans, Springer Science & Business Media, 2012.

[176] T. Hardingham, A. Fosang, Proteoglycans: many forms and many functions, FASEB J. 6 (1992) 861-870.

[177] M. Izydorczyk, S.W. Cui, Q. Wang, Polysaccharide gums: structures. Functional properties, and applications, In: Food carbohydrates: chemistry, physical properties, and applications, CRC Press, Boca Raton, 2005, pp. 263-307.

[178] A.D. Augst, H.J. Kong, D.J. Mooney, Alginate hydrogels as biomaterials, Macromol. Biosci. 6 (2006) 623-633.

[179] K.H. Bouhadir, K.Y. Lee, E. Alsberg, K.L. Damm, K.W. Anderson, D.J. Mooney, Degradation of partially oxidized alginate and its potential application for tissue engineering, Biotechnol. Prog.

17 (2001) 945-950.

[180] L. IRO Alginate Industry Co., IRO Alginate Industry. www.iroalginate.com, 2014, (accessed 2014).

[181] O. Smidsrød, G. Skja, Alginate as immobilization matrix for cells, Trends Biotechnol. 8 (1990) 71-78.

[182] C.K. Kuo, P.X. Ma, Ionically crosslinked alginate hydrogels as scaffolds for tissue engineering: part 1. Structure, gelation rate and mechanical properties, Biomaterials 22 (2001) 511-521.

[183] H. Grasdalen, O. Smidsrød, Gelation of gellan gum, Carbohydr. Polym. 7 (1987) 371-393.

[184] F.X. Quinn, T. Hatakeyama, H. Yoshida, M. Takahashi, H. Hatakeyama, The conformational properties of gellan gum hydrogels, Polym. Gels Netw. 1 (1993) 93-114.

[185] V. Crescenzi, M. Dentini, T. Coviello, R. Rizzo, Comparative analysis of the behavior of gellan gum (S-60) and welan gum (S-130) in dilute aqueous solution, Carbohydr. Res. 149 (1986) 425-432.

[186] P. Deasy, K.J. Quigley, Rheological evaluation of deacetylated gellan gum (Gelrite) for pharmaceutical use, Int. J. Pharm. 73 (1991) 117-123.

[187] M. Milas, X. Shi, M. Rinaudo, On the physicochemical properties of gellan gum, Biopolymers 30 (1990) 451-464.

[188] E. Miyoshi, T. Takaya, K. Nishinari, Rheological and thermal studies of gel-sol transition in gellan gum aqueous solutions, Carbohydr. Polym. 30 (1996) 109-119.

[189] K. Nakajima, T. Ikehara, T. Nishi, Observation of gellan gum by scanning tunneling microscopy, Carbohydr. Polym. 30 (1996) 77-81.

[190] E. Ogawa, R. Takahashi, H. Yajima, K. Nishinari, Effects of molar mass on the coil to helix transition of sodium-type gellan gums in aqueous solutions, Food Hydrocoll. 20 (2006) 378-385.

[191] K. Smetana, Cell biology of hydrogels, Biomaterials 14 (1993) 1046-1050.

[192] E. Alsberg, H. Kong, Y. Hirano, M. Smith, A. Albeiruti, D. Mooney, Regulating bone formation via controlled scaffold degradation, J. Dent. Res. 82 (2003) 903-908.

[193] B. Balakrishnan, A. Jayakrishnan, Self-cross-linking biopolymers as injectable in situ forming biodegradable scaffolds, Biomaterials 26 (2005) 3941-3951.

[194] J.A. Rowley, D.J. Mooney, Alginate type and RGD density control myoblast phenotype, J. Biomed. Mater. Res. 60 (2002) 217-223.

[195] E. Westhaus, P.B. Messersmith, Triggered release of calcium from lipid vesicles: a bioinspired strategy for rapid gelation of polysaccharide and protein hydrogels, Biomaterials 22 (2001) 453-462.

[196] A.M. Smith, J.J. Harris, R.M. Shelton, Y. Perrie, 3D culture of bone-derived cells immobilised in alginate following light-triggered gelation, J. Control. Release 119 (2007) 94-101.

[197] A. Atala, W. Kim, K. Paige, C. Vacanti, A. Retik, Endoscopic treatment of vesicoureteral reflux

with a chondrocyte-alginate suspension, J. Urol. 152 (1994) 641-643; discussion 644.

[198] F. Lim, A.M. Sun, Microencapsulated islets as bioartificial endocrine pancreas, Science 210 (1980) 908-910.

[199] K.E. Gregory, M.E. Marsden, J. Anderson-MacKenzie, J.B. Bard, P. Bruckner, J. Farjanel, et al., Abnormal collagen assembly, though normal phenotype, in alginate bead cultures of chick embryo chondrocytes, Exp. Cell Res. 246 (1999) 98-107.

[200] A.E. Bent, R.T. Tutrone, M.T. McLennan, K. Lloyd, M.J. Kennelly, G. Badlani, Treatment of intrinsic sphincter deficiency using autologous ear chondrocytes as a bulking agent, Neurourol. Urodyn. 20 (2001) 157-165.

[201] A. Joly, J.-F. Desjardins, B. Fremond, M. Desille, J.-P. Campion, Y. Malledant, et al., Survival, proliferation, and functions of porcine hepatocytes encapsulated in coated alginate beads: a step towards a reliable biartificial liver, Transplantation 63 (1997) 795-803.

[202] K.T. Paige, L.G. Cima, M.J. Yaremchuk, J.P. Vacanti, C.A. Vacanti, Injectable cartilage, Plast. Reconstr. Surg. 96 (1995) 1390-1398.

[203] S.C. Chang, J.A. Rowley, G. Tobias, N.G. Genes, A.K. Roy, D.J. Mooney, et al., Injection molding of chondrocyte/alginate constructs in the shape of facial implants, J. Biomed. Mater. Res. 55 (2001) 503-511.

[204] S.A. Pangas, H. Saudye, L.D. Shea, T.K. Woodruff, Novel approach for the three-dimensional culture of granulosa cell-oocyte complexes, Tissue Eng. 9 (2003) 1013-1021.

[205] Ø. Arlov, E. Öztürk, M. Steinwachs, G. Skjåk-Bræk, M. Zenobi-Wong, Biomimetic sulphated alginate hydrogels suppress IL-1β-induced inflammatory responses in human chondrocytes, Eur. Cell Mater. 33 (2017) 76.

[206] Ø. Arlov, G. Skjåk-Bræk, A.M. Rokstad, Sulfated alginate microspheres associate with factor H and dampen the inflammatory cytokine response, Acta Biomater. 42 (2016) 180-188.

[207] L. Shapiro, S. Cohen, Novel alginate sponges for cell culture and transplantation, Biomaterials 18 (1997) 583-590.

[208] M. Szekalska, Puci, #x142, A. owska, Szyma, #x144, et al., Alginate: Current Use and Future Perspectives in Pharmaceutical and Biomedical Applications, Int. J. Polym. Sci. 2016 (2016) 17.

[209] C. Godugu, A.R. Patel, U. Desai, T. Andey, A. Sams, M. Singh, AlgiMatrix™ based 3D cell culture system as an in-vitro tumor model for anticancer studies, PloS one 8 (2013) e53708.

[210] L.F. Mellor, T.L. Baker, R.J. Brown, L.W. Catlin, J.T. Oxford, Optimal 3D culture of primary articular chondrocytes for use in the rotating wall vessel bioreactor, Aviat. Space Env. Med. 85 (2014) 798-804.

[211] M. Otterlei, K. Østgaard, G. Skjåk-Bræk, O. Smidsrød, P. Soon-Shiong, T. Espevik, Induction of cytokine production from human monocytes stimulated with alginate, J. Immunother. 10 (1991) 286-291.

[212] U. Zimmermann, G. Klöck, K. Federlin, K. Hannig, M. Kowalski, R.G. Bretzel, et al., Production of mitogen-contamination free alginates with variable ratios of mannuronic acid to guluronic acid by free flow electrophoresis, Electrophoresis 13 (1992) 269-274.

[213] G. Orive, R.M. Hernández, A.R. Gascón, R. Calafiore, T.M. Chang, P. De Vos, et al., Cell encapsulation: promise and progress, Nat. Med. 9 (2003) 104-107.

[214] P. de Vos, M. Bucko, P. Gemeiner, M. Navratil, J. Svitel, M. Faas, et al., Multiscale requirements for bioencapsulation in medicine and biotechnology, Biomaterials 30 (2009) 2559-2570.

[215] P.D. Vos, B.D. Haan, G. Wolters, J. Strubbe, R.V. Schilfgaarde, Improved biocompatibility but limited graft survival after purification of alginate for microencapsulation of pancreatic islets, Diabetologia 40 (1997) 262-270.

[216] A. Brasileiro, AgarGel. http://www.agargel.com.br, 2003, (accessed 2015).

[217] E.G. Popa, M.E. Gomes, R.L. Reis, Cell delivery systems using alginate--carrageenan hydrogel beads and fibers for regenerative medicine applications, Biomacromolecules 12 (2011) 3952-3961.

[218] E. Popa, R. Reis, M. Gomes, Chondrogenic phenotype of different cells encapsulated in κ-carrageenan hydrogels for cartilage regeneration strategies, Biotechnol. Appl. Biochem. 59 (2012) 132-141.

[219] E.G. Popa, M.T. Rodrigues, D.F. Coutinho, M.B. Oliveira, J.F. Mano, R.L. Reis, et al., Cryopreservation of cell laden natural origin hydrogels for cartilage regeneration strategies, Soft matter 9 (2013) 875-885.

[220] V.E. Santo, A.M. Frias, M. Carida, R. Cancedda, M.E. Gomes, J.F. Mano, et al., Carrageenan-based hydrogels for the controlled delivery of PDGF-BB in bone tissue engineering applications, Biomacromolecules 10 (2009) 1392-1401.

[221] A.M. Salgueiro, A.L. Daniel-da-Silva, S. Fateixa, T. Trindade, κ-Carrageenan hydrogel nanocomposites with release behavior mediated by morphological distinct Au nanofillers, Carbohydr. Polym. 91 (2013) 100-109.

[222] H. Hezaveh, I.I. Muhamad, I. Noshadi, L. Shu Fen, N. Ngadi, Swelling behaviour and controlled drug release from cross-linked κ-carrageenan/NaCMC hydrogel by diffusion mechanism, J. Microencapsul. 29 (2012) 368-379.

[223] E. Shumilina, Y.A. Shchipunov, Chitosan–carrageenan gels, Colloid J. 64 (2002) 372-378.

[224] T. Sakiyama, C.-H. Chu, T. Fujii, T. Yano, Preparation of a polyelectrolyte complex gel from chitosan and κ-carrageenan and its pH-sensitive swelling, J. Appl. Polym. Sci. 50 (1993) 2021-2025.

[225] S.M. Mihaila, A.K. Gaharwar, R.L. Reis, A.P. Marques, M.E. Gomes, A. Khademhosseini, Photocrosslinkable Kappa-Carrageenan Hydrogels for Tissue Engineering Applications, Adv. Healthcare Mater. 2 (2013) 895-907.

[226] A.J. Granero, J.M. Razal, G.G. Wallace, Conducting gel-fibres based on carrageenan, chitosan and carbon nanotubes, J. Mat. Chem. 20 (2010) 7953-7956.

[227] M.M. Daly, D. Knorr, Chitosan-Alginate Complex Coacervate Capsules: Effects of Calcium Chloride, Plasticizers, and Polyelectrolytes on Mechanical Stability, Biotechnol. Prog. 4 (1988) 76-81.

[228] J.L. Dofeliz, N.R.L. Rojas, Heparin-Functionalized chitosan/κ-carrageenan complexes as

potential scaffolds for tissue engineering, 30th Philippine Chemistry Congress, Philippines, 2015.

[229] S. Ahmed, S. Ikram, Chitosan Based Scaffolds and Their Applications in Wound Healing, Achiev. Life Sci. 10 (2016) 27-37.

[230] S.M. Mihaila, E.G. Popa, R.L. Reis, A.P. Marques, M.E. Gomes, Fabrication of endothelial cell-laden carrageenan microfibers for microvascularized bone tissue engineering applications, Biomacromolecules 15 (2014) 2849-2860.

[231] P.M. Rocha, V.E. Santo, M.E. Gomes, R.L. Reis, J.F. Mano, Encapsulation of adipose-derived stem cells and transforming growth factor- 1 in carrageenan-based hydrogels for cartilage tissue engineering, J. Bioact. Compat. Polym. 26 (2011) 493-507.

[232] G.P. Dillon, X. Yu, A. Sridharan, J.P. Ranieri, R.V. Bellamkonda, The influence of physical structure and charge on neurite extension in a 3D hydrogel scaffold, J. Biomater. Sci. Polym. Ed. 9 (1998) 1049-1069.

[233] A.J. Putnam, D.J. Mooney, Tissue engineering using synthetic extracellular matrices, Nat. Med. 2 (1996) 824-826.

[234] M. Borkenhagen, J.F. Clémence, H. Sigrist, P. Aebischer, Three-dimensional extracellular matrix engineering in the nervous system, J. Biomed. Mater. Res. 40 (1998) 392-400.

[235] M. Meddens, J. Thompson, P. Leijh, R. Van Furth, Role of granulocytes in the induction of an experimental endocarditis with a dextran-producing Streptococcus sanguis and its dextran-negative mutant, Br. J. Exp. Pathol. 65 (1984) 257.

[236] J. Banas, M. Vickerman, Glucan-binding proteins of the oral streptococci, Crit. Rev. Oral Biol. Med. 14 (2003) 89-99.

[237] N.W. Cheetham, E. Fiala-Beer, G.J. Walker, Dextran structural details from high-field proton NMR spectroscopy, Carbohydr. Polym. 14 (1990) 149-158.

[238] G.L. Coˆte, T.D. Leathers, A method for surveying and classifying Leuconostoc spp. glucansucrases according to strain-dependent acceptor product patterns, J. Ind. Microbiol. Biotechnol. 32 (2005) 53-60.

[239] D. Kim, J.F. Robyt, S.-Y. Lee, J.-H. Lee, Y.-M. Kim, Dextran molecular size and degree of branching as a function of sucrose concentration, pH, and temperature of reaction of Leuconostoc mesenteroides B-512FMCM dextransucrase, Carbohydr. Res. 338 (2003) 1183-1189.

[240] M. Naessens, A. Cerdobbel, W. Soetaert, E.J. Vandamme, Leuconostoc dextransucrase and dextran: production, properties and applications, J. Chem. Technol. Biot. 80 (2005) 845-860.

[241] J. Robyt, Dextran, 1986.

[242] P.E. Marszalek, A.F. Oberhauser, Y.-P. Pang, J.M. Fernandez, Polysaccharide elasticity governed by chair–boat transitions of the glucopyranose ring, Nature 396 (1998) 661-664.

[243] R. Terg, C.D. Miguez, L. Castro, H. Araldi, S. Dominguez, M. Rubio, Pharmacokinetics of Dextran-70 in patients with cirrhosis and ascites undergoing therapeutic paracentesis, J. Hepatol. 25 (1996) 329-333.

[244] S.R. Van Tomme, M.J. van Steenbergen, S.C. De Smedt, C.F. van Nostrum, W.E. Hennink, Self-gelling hydrogels based on oppositely charged dextran microspheres, Biomaterials 26 (2005)

2129-2135.

[245] Y. Liu, M.B. Chan-Park, A biomimetic hydrogel based on methacrylated dextran-graft-lysine and gelatin for 3D smooth muscle cell culture, Biomaterials 31 (2010) 1158-1170.

[246] B. Katzbauer, Properties and applications of xanthan gum, Polym. Degrad. Stab. 59 (1998) 81-84.

[247] F. Garcıa-Ochoa, V. Santos, J. Casas, E. Gomez, Xanthan gum: production, recovery, and properties, Biotechnol. Adv. 18 (2000) 549-579.

[248] C. Garnier, C. Schorsch, J.-L. Doublier, Phase separation in dextran/locust bean gum mixtures, Carbohydr. Polym. 28 (1995) 313-317.

[249] M. Hamcerencu, J. Desbrieres, M. Popa, A. Khoukh, G. Riess, New unsaturated derivatives of Xanthan gum: Synthesis and characterization, Polymer 48 (2007) 1921-1929.

[250] I. Capron, G. Brigand, G. Muller, About the native and renatured conformation of xanthan exopolysaccharide, Polymer 38 (1997) 5289-5295.

[251] A. Rodd, D. Dunstan, D. Boger, Characterisation of xanthan gum solutions using dynamic light scattering and rheology, Carbohydr. Polym. 42 (2000) 159-174.

[252] A.C. Mendes, E.T. Baran, R.C. Pereira, H.S. Azevedo, R.L. Reis, Encapsulation and survival of a chondrocyte cell line within xanthan gum derivative, Macromol. Biosci. 12 (2012) 350-359.

[253] P.-E. Jansson, B. Lindberg, P.A. Sandford, Structural studies of gellan gum, an extracellular polysaccharide elaborated by Pseudomonas elodea, Carbohydr. Res. 124 (1983) 135-139.

[254] B. Nisbet, I. Sutherland, I. Bradshaw, M. Kerr, E. Morris, W. Shepperson, XM-6: a new gel-forming bacterial polysaccharide, Carbohydr. Polym. 4 (1984) 377-394.

[255] K.S. Kang, G.T. Colegrove, G.T. Veeder, Deacetylated polysaccharide S-60, Google Patents, 1982.

[256] A.M. Smith, R.M. Shelton, Y. Perrie, J.J. Harris, An initial evaluation of gellan gum as a material for tissue engineering applications, J. Biomater. Appl. 22 (2007) 241-254.

[257] J.T. Oliveira, L. Martins, R. Picciochi, P.B. Malafaya, R.A. Sousa, N.M. Neves, et al., Gellan gum: a new biomaterial for cartilage tissue engineering applications, J. Biomed. Mater. Res. A 93 (2010) 852-863.

[258] T. Coviello, P. Matricardi, C. Marianecci, F. Alhaique, Polysaccharide hydrogels for modified release formulations, J. Control. Release 119 (2007) 5-24.

[259] D. Bruneel, E. Schacht, End group modification of pullulan, Polymer 36 (1995) 169-172.

[260] T.D. Leathers, Biotechnological production and applications of pullulan, Appl. Microbiol. Biotechnol. 62 (2003) 468-473.

[261] T. Kimoto, T. Shibuya, S. Shiobara, Safety studies of a novel starch, pullulan: chronic toxicity in rats and bacterial mutagenicity, Food Chem. Toxicol. 35 (1997) 323-329.

[262] D.H. Ball, B.J. Wiley, E.T. Reese, Effect of substitution at C-6 on the susceptibility of pullulan to pullulanases. Enzymatic degradation of modified pullulans, Can. J. Microbiol. 38 (1992) 324-

327.

[263] H. Bae, A.F. Ahari, H. Shin, J.W. Nichol, C.B. Hutson, M. Masaeli, et al., Cell-laden microengineered pullulan methacrylate hydrogels promote cell proliferation and 3D cluster formation, Soft matter 7 (2011) 1903-1911.

[264] A. Autissier, D. Letourneur, C. Le Visage, Pullulan-based hydrogel for smooth muscle cell culture, J. Biomed. Mater. Res. A 82 (2007) 336-342.

[265] J.C. Fricain, S. Schlaubitz, C. Le Visage, I. Arnault, S.M. Derkaoui, R. Siadous, et al., A nano-hydroxyapatite--pullulan/dextran polysaccharide composite macroporous material for bone tissue engineering, Biomaterials 34 (2013) 2947-2959.

[266] S.E. Bulman, C.M. Coleman, J.M. Murphy, N. Medcalf, A.E. Ryan, F. Barry, Pullulan: a new cytoadhesive for cell-mediated cartilage repair, Stem Cell Res. Ther. 6 (2015) 34.

[267] R. Atalla, Celluloses, In: Comprehensive natural products chemistry, 1999, pp. 529-598.

[268] R.M. Brown, Cellulose and other natural polymer systems: biogenesis, structure, and degradation, Plenum Press, New York, 1982.

[269] D. Klemm, B. Heublein, H.P. Fink, A. Bohn, Cellulose: fascinating biopolymer and sustainable raw material, Angewandte Chemie 44 (2005) 3358-3393.

[270] I. Tarchevsky, G.N. Marchenko, Cellulose: biosynthesis and structure, Springer-Verlag, 1991.

[271] P. Albersheim, A. Darvill, M. O'Neill, H. Schols, A. Voragen, An hypothesis: the same six polysaccharides are components of the primary cell walls of all higher plants, Pectins and pectinases 14 (1996) 47-53.

[272] G.O. Aspinall, Chemistry of cell wall polysaccharides, In: The Biochemistry of plants: a comprehensive treatise (USA), 1980.

[273] M. McNeil, A.G. Darvill, S.C. Fry, P. Albersheim, Structure and function of the primary cell walls of plants, Annu. Rev. Biochem. 53 (1984) 625-663.

[274] D. Mohnen, Biosynthesis of pectins and galactomannans, In: Comprehensive natural products chemistry, 1999, pp. 497-527.

[275] K. Shimizu, Chemistry of hemicelluloses, Wood Cell. Chem. (1991) 177-214.

[276] R.L. Whistler, E. Richards, Hemicelluloses, The carbohydrates 2 (1970) 447-469.

[277] R. Kita, T. Kaku, K. Kubota, T. Dobashi, Pinning of phase separation of aqueous solution of hydroxypropylmethylcellulose by gelation, Physics Lett. A 259 (1999) 302-307.

[278] T. Delair, In situ forming polysaccharide-based 3D-hydrogels for cell delivery in regenerative medicine, Carbohydr. Polym. 87 (2012) 1013-1019.

[279] M. Bhattacharya, M.M. Malinen, P. Lauren, Y.R. Lou, S.W. Kuisma, L. Kanninen, et al., Nanofibrillar cellulose hydrogel promotes three-dimensional liver cell culture, J. Control. Release 164 (2012) 291-298.

[280] M.M. Malinen, L.K. Kanninen, A. Corlu, H.M. Isoniemi, Y.R. Lou, M.L. Yliperttula, et al., Differentiation of liver progenitor cell line to functional organotypic cultures in 3D nanofibrillar

cellulose and hyaluronan-gelatin hydrogels, Biomaterials 35 (2014) 5110-5121.

[281] Y.R. Lou, L. Kanninen, T. Kuisma, J. Niklander, L.A. Noon, D. Burks, et al., The use of nanofibrillar cellulose hydrogel as a flexible three-dimensional model to culture human pluripotent stem cells, Stem Cells Dev. 23 (2014) 380-392.

[282] R. Derda, A. Laromaine, A. Mammoto, S.K. Tang, T. Mammoto, D.E. Ingber, et al., Paper-supported 3D cell culture for tissue-based bioassays, Proc. Natl. Acad. Sci. 106 (2009) 18457-18462.

[283] D.J. Modulevsky, C. Lefebvre, K. Haase, Z. Al-Rekabi, A.E. Pelling, Apple derived cellulose scaffolds for 3D mammalian cell culture, PloS one 9 (2014) e97835.

[284] H. Lotzkar, T. Schultz, H. Owens, W. Maclay, Effect of salts on the viscosity of pectinic acid solutions, J. Phys. Chem. 50 (1946) 200-210.

[285] F. Munarin, S.G. Guerreiro, M.A. Grellier, M.C. Tanzi, M.A. Barbosa, P. Petrini, et al., Pectin-based injectable biomaterials for bone tissue engineering, Biomacromolecules 12 (2011) 568-577.

[286] S.C. Neves, D.B. Gomes, A. Sousa, S.J. Bidarra, P. Petrini, L. Moroni, et al., Biofunctionalized pectin hydrogels as 3D cellular microenvironments, J. Mat. Chem. B 3 (2015) 2096-2108.

[287] D. French, R. Whistler, J. BeMiller, E. Paschall, Starch: Chemistry and technology, Academic Press, New York, 1984.

[288] J. Hawker, C. Jenner, C. Niemietz, Sugar metabolism and compartmentation, Funct. Plant Biol. 18 (1991) 227-237.

[289] D.J. Manners, Recent developments in our understanding of amylopectin structure, Carbohydr. Polym. 11 (1989) 87-112.

[290] W. Brown, T. Poon, Introduction to organic chemistry, Wiley, 2005.

[291] M.E. Gomes, V.I. Sikavitsas, E. Behravesh, R.L. Reis, A.G. Mikos, Effect of flow perfusion on the osteogenic differentiation of bone marrow stromal cells cultured on starch-based three-dimensional scaffolds, J. Biomed. Mater. Res. A 67 (2003) 87-95.

[292] M.I. Santos, I. Pashkuleva, C.M. Alves, M.E. Gomes, S. Fuchs, R.E. Unger, et al., Surface-modified 3D starch-based scaffold for improved endothelialization for bone tissue engineering, J. Mat. Chem. 19 (2009) 4091.

[293] W.C. Hsieh, J.J. Liau, Cell culture and characterization of cross-linked poly(vinyl alcohol)-g-starch 3D scaffold for tissue engineering, Carbohydr. Polym. 98 (2013) 574-580.

[294] R.A. Muzzarelli, Biochemical significance of exogenous chitins and chitosans in animals and patients, Carbohydr. Polym. 20 (1993) 7-16.

[295] A. Chenite, C. Chaput, D. Wang, C. Combes, M. Buschmann, C. Hoemann, et al., Novel injectable neutral solutions of chitosan form biodegradable gels in situ, Biomaterials 21 (2000) 2155-2161.

[296] J.L. Drury, D.J. Mooney, Hydrogels for tissue engineering: scaffold design variables and applications, Biomaterials 24 (2003) 4337-4351.

[297] D.K. SINGH, A.R. RAY, Biomedical applications of chitin, chitosan, and their derivatives, J.

Macromol. Sci. Polym. Rev. 40 (2000) 69-83.

[298] J. Li, Y. Du, H. Liang, Influence of molecular parameters on the degradation of chitosan by a commercial enzyme, Polym. Degrad. Stab. 92 (2007) 515-524.

[299] J.S. Mao, Y.L. Cui, X.H. Wang, Y. Sun, Y.J. Yin, H.M. Zhao, et al., A preliminary study on chitosan and gelatin polyelectrolyte complex cytocompatibility by cell cycle and apoptosis analysis, Biomaterials 25 (2004) 3973-3981.

[300] C.L. Bueter, C.K. Lee, V.A. Rathinam, G.J. Healy, C.H. Taron, C.A. Specht, et al., Chitosan but not chitin activates the inflammasome by a mechanism dependent upon phagocytosis, J. Biol. Chem. 286 (2011) 35447-35455.

[301] C.L. Bueter, C.A. Specht, S.M. Levitz, Innate sensing of chitin and chitosan, PLoS Pathog. 9 (2013) e1003080.

[302] A. Schlosser, T. Thomsen, J.B. Moeller, O. Nielsen, I. Tornøe, J. Mollenhauer, et al., Characterization of FIBCD1 as an acetyl group-binding receptor that binds chitin, J. Immunol. 183 (2009) 3800-3809.

[303] T. Semeňuk, P. Krist, J. Pavlíček, K. Bezouška, M. Kuzma, P. Novák, et al., Synthesis of chitooligomer-based glycoconjugates and their binding to the rat natural killer cell activation receptor NKR-P1, Glycoconj. J. 18 (2001) 817-826.

[304] H.L. Cash, C.V. Whitham, C.L. Behrendt, L.V. Hooper, Symbiotic bacteria direct expression of an intestinal bactericidal lectin, Science 313 (2006) 1126-1130.

[305] J. Seetharaman, A. Kanigsberg, R. Slaaby, H. Leffler, S.H. Barondes, J.M. Rini, X-ray crystal structure of the human galectin-3 carbohydrate recognition domain at 2.1-Å resolution, J. Biol. Chem. 273 (1998) 13047-13052.

[306] Y. Yeo, J.A. Burdick, C.B. Highley, R. Marini, R. Langer, D.S. Kohane, Peritoneal application of chitosan and UV-cross-linkable chitosan, J. Biomed. Mater. Res. A 78 (2006) 668-675.

[307] Y. Yeo, W. Geng, T. Ito, D.S. Kohane, J.A. Burdick, M. Radisic, Photocrosslinkable hydrogel for myocyte cell culture and injection, J. Biomed. Mater. Res. B Appl. Biomater. 81 (2007) 312-322.

[308] K. Crompton, J. Goud, R. Bellamkonda, T. Gengenbach, D. Finkelstein, M. Horne, et al., Polylysine-functionalised thermoresponsive chitosan hydrogel for neural tissue engineering, Biomaterials 28 (2007) 441-449.

[309] K. Yagi, N. Michibayashi, N. Kurikawa, Y. Nakashima, T. Mizoguchi, A. Harada, et al., Effectiveness of fructose-modified chitosan as a scaffold for hepatocyte attachment, Biol. Pharm. Bull. 20 (1997) 1290-1294.

[310] H. Yura, M. Goto, H. Okazaki, K. Kobayashi, T. Akaike, Structural effect of galactose residue in synthetic glycoconjugates on interaction with rat hepatocytes, J. Biomed. Mater. Res. 29 (1995) 1557-1565.

[311] E.A. Eser, Y.M. Elcin, G.D. Pappas, Neural tissue engineering: adrenal chromaffin cell attachment and viability on chitosan scaffolds, Neurol. Res. 20 (1998) 648-654.

[312] R. Muzzarelli, C. Zucchini, P. Ilari, A. Pugnaloni, M.M. Belmonte, G. Biagini, et al., Osteoconductive properties of methylpyrrolidinone chitosan in an animal model, Biomaterials 14 (1993) 925-929.

[313] K. Tuzlakoglu, C.M. Alves, J.F. Mano, R.L. Reis, Production and characterization of chitosan fibers and 3-D fiber mesh scaffolds for tissue engineering applications, Macromol. Biosci. 4 (2004) 811-819.

[314] R. Jayakumar, M. Prabaharan, S.V. Nair, H. Tamura, Novel chitin and chitosan nanofibers in biomedical applications, Biotechnol. Adv. 28 (2010) 142-150.

[315] J. Fukuda, A. Khademhosseini, Y. Yeo, X. Yang, J. Yeh, G. Eng, et al., Micromolding of photocrosslinkable chitosan hydrogel for spheroid microarray and co-cultures, Biomaterials 27 (2006) 5259-5267.

[316] H.K. Dhiman, A.R. Ray, A.K. Panda, Three-dimensional chitosan scaffold-based MCF-7 cell culture for the determination of the cytotoxicity of tamoxifen, Biomaterials 26 (2005) 979-986.

[317] Y.L. Chen, H.P. Lee, H.Y. Chan, L.Y. Sung, H.C. Chen, Y.C. Hu, Composite chondroitin-6-sulfate/dermatan sulfate/chitosan scaffolds for cartilage tissue engineering, Biomaterials 28 (2007) 2294-2305.

[318] C.B. Machado, J.M. Ventura, A.F. Lemos, J.M. Ferreira, M.F. Leite, A.M. Goes, 3D chitosan-gelatin-chondroitin porous scaffold improves osteogenic differentiation of mesenchymal stem cells, Biomed. Mater. 2 (2007) 124-131.

[319] A. Mahmoudzadeh, H. Mohammadpour, Tumor cell culture on collagen–chitosan scaffolds as three-dimensional tumor model: A suitable model for tumor studies, J. Food Drug Anal. 24 (2016) 620-626.

[320] M.O. Cho, Z. Li, H.-E. Shim, I.-S. Cho, M. Nurunnabi, H. Park, et al., Bioinspired tuning of glycol chitosan for 3D cell culture, NPG Asia Materials 8 (2016) e309.

[321] J.E. Silbert, M. Bernfield, R. Kokenyesi, Proteoglycans: a special class of glycoproteins, In: New Comprehensive Biochemistry, 1997, pp. 1-31.

[322] H. Kresse, Proteoglycans–structure and functions, In: Glycosciences: Status and Perspectives, Chapman & Hall GmbH, Weinheim, 1997, pp. 201-222.

[323] K.R. Taylor, R.L. Gallo, Glycosaminoglycans and their proteoglycans: host-associated molecular patterns for initiation and modulation of inflammation, FASEB J. 20 (2006) 9-22.

[324] H.E. Bülow, O. Hobert, The molecular diversity of glycosaminoglycans shapes animal development, Annu. Rev. Cell Dev. Biol. 22 (2006) 375-407.

[325] L.-Å. Fransson, Mammalian glycosaminoglycans, Polysaccharides 3 (1985) 337-415.

[326] D.A. Rees, E.R. Morris, D. Thom, J.K. Madden, Shapes and interactions of carbohydrate chains, Polysaccharides 1 (1982) 195-290.

[327] R.V. Iozzo, Proteoglycans and neoplasia, Cancer Metastasis Rev. 7 (1988) 39-50.

[328] A.D. Snow, T.N. Wight, Proteoglycans in the pathogenesis of Alzheimer's disease and other amyloidoses, Neurobiol. Aging 10 (1989) 481-497.

[329] J.A. Vazquez, I. Rodriguez-Amado, M.I. Montemayor, J. Fraguas, P. Gonzalez Mdel, M.A. Murado, Chondroitin sulfate, hyaluronic acid and chitin/chitosan production using marine waste sources: characteristics, applications and eco-friendly processes: a review, Mar. Drugs 11 (2013) 747-774.

[330] Q. Li, C.G. Williams, D.D. Sun, J. Wang, K. Leong, J.H. Elisseeff, Photocrosslinkable polysaccharides based on chondroitin sulfate, J. Biomed. Mater. Res. A 68 (2004) 28-33.

[331] S.J. Bryant, K.A. Davis-Arehart, N. Luo, R.K. Shoemaker, J.A. Arthur, K.S. Anseth, Synthesis and characterization of photopolymerized multifunctional hydrogels: water-soluble poly (vinyl alcohol) and chondroitin sulfate macromers for chondrocyte encapsulation, Macromolecules 37 (2004) 6726-6733.

[332] S.J. Bryant, J.A. Arthur, K.S. Anseth, Incorporation of tissue-specific molecules alters chondrocyte metabolism and gene expression in photocrosslinked hydrogels, Acta Biomater. 1 (2005) 243-252.

[333] D.-A. Wang, S. Varghese, B. Sharma, I. Strehin, S. Fermanian, J. Gorham, et al., Multifunctional chondroitin sulphate for cartilage tissue–biomaterial integration, Nat. Mater. 6 (2007) 385-392.

[334] S. Varghese, N.S. Hwang, A.C. Canver, P. Theprungsirikul, D.W. Lin, J. Elisseeff, Chondroitin sulfate based niches for chondrogenic differentiation of mesenchymal stem cells, Matrix Biol. 27 (2008) 12-21.

[335] C.-T. Lee, P.-H. Kung, Y.-D. Lee, Preparation of poly(vinyl alcohol)-chondroitin sulfate hydrogel as matrices in tissue engineering, Carbohydr. Polym. 61 (2005) 348-354.

[336] A. Conovaloff, A. Panitch, Characterization of a chondroitin sulfate hydrogel for nerve root regeneration, J. Neural Eng. 8 (2011) 056003.

[337] J.M. Trowbridge, R.L. Gallo, Dermatan sulfate: new functions from an old glycosaminoglycan, Glycobiology 12 (2002) 117R-125R.

[338] S. Mizumoto, D. Fongmoon, K. Sugahara, Interaction of chondroitin sulfate and dermatan sulfate from various biological sources with heparin-binding growth factors and cytokines, Glycoconj. J. 30 (2013) 619-632.

[339] G. Westergren-Thorsson, P.O. Önnervik, L.Å. Fransson, A. Malmström, Proliferation of cultured fibroblasts is inhibited by L-Iduronate—containing glycosaminoglycans, J. Cell. Physiol. 147 (1991) 523-530.

[340] R. Lever, C.P. Page, Novel drug development opportunities for heparin, Nat. Rev. Drug Discov. 1 (2002) 140-148.

[341] S. Ashikari-Hada, H. Habuchi, Y. Kariya, N. Itoh, A.H. Reddi, K. Kimata, Characterization of growth factor-binding structures in heparin/heparan sulfate using an octasaccharide library, J. Biol. Chem. 279 (2004) 12346-12354.

[342] Z.H. Shriver, I. Capila, G. Venkataraman, R. Sasisekharan, Heparin and Heparan Sulfate: Analyzing Structure and Microheterogeneity [chapter], In: Heparin-A Century of Progress, Springer, Berlin Heidelberg, 2012, pp. 159-176.

[343] R. Jin, L.S. Moreira Teixeira, P.J. Dijkstra, C.A. van Blitterswijk, M. Karperien, J. Feijen, Chondrogenesis in injectable enzymatically crosslinked heparin/dextran hydrogels, J. Control. Release 152 (2011) 186-195.

[344] G. Tae, Y.-J. Kim, W.-I. Choi, M. Kim, P.S. Stayton, A.S. Hoffman, Formation of a novel heparin-based hydrogel in the presence of heparin-binding biomolecules, Biomacromolecules 8 (2007) 1979-1986.

[345] M. Kim, J.Y. Lee, C.N. Jones, A. Revzin, G. Tae, Heparin-based hydrogel as a matrix for encapsulation and cultivation of primary hepatocytes, Biomaterials 31 (2010) 3596-3603.

[346] J. Zhong, A. Chan, L. Morad, H.I. Kornblum, G. Fan, S.T. Carmichael, Hydrogel matrix to support stem cell survival after brain transplantation in stroke, Neurorehabil. Neural Repair 24 (2010) 636-644.

[347] D.S. Benoit, A.R. Durney, K.S. Anseth, The effect of heparin-functionalized PEG hydrogels on three-dimensional human mesenchymal stem cell osteogenic differentiation, Biomaterials 28 (2007) 66-77.

[348] R. Mammadov, B. Mammadov, M.O. Guler, A.B. Tekinay, Growth factor binding on heparin mimetic peptide nanofibers, Biomacromolecules 13 (2012) 3311-3319.

[349] J.J. Roberts, B.L. Farrugia, R.A. Green, J. Rnjak-Kovacina, P.J. Martens, In situ formation of poly (vinyl alcohol)–heparin hydrogels for mild encapsulation and prolonged release of basic fibroblast growth factor and vascular endothelial growth factor, J. Tissue Eng. 7 (2016) 2041731416677132.

[350] T.C. Laurent, J. Fraser, Hyaluronan, FASEB J. 6 (1992) 2397-2404.

[351] V.C. Hascall, A.K. Majors, C.A. de la Motte, S.P. Evanko, A. Wang, J.A. Drazba, et al., Intracellular hyaluronan: a new frontier for inflammation?, Biochim. Biophys. Acta 1673 (2004) 3-12.

[352] A. Shiedlin, R. Bigelow, W. Christopher, S. Arbabi, L. Yang, R.V. Maier, et al., Evaluation of Hyaluronan from Different Sources: Streptococcus z ooepidemicus, Rooster Comb, Bovine Vitreous, and Human Umbilical Cord, Biomacromolecules 5 (2004) 2122-2127.

[353] L. Liu, Y. Liu, J. Li, G. Du, J. Chen, Microbial production of hyaluronic acid: current state, challenges, and perspectives, Microb. Cell Fact 10 (2011) 99.

[354] S.-J. Kim, S.-Y. Park, C.-W. Kim, A novel approach to the production of hyaluronic acid by Streptococcus zooepidemicus, J. Microbiol. Biotechnol. 16 (2006) 1849-1855.

[355] V. Rangaswamy, D. Jain, An efficient process for production and purification of hyaluronic acid from Streptococcus equi subsp. zooepidemicus, Biotechnol. Lett. 30 (2008) 493-496.

[356] L.-S. Liu, A.Y. Thompson, M.A. Heidaran, J.W. Poser, R.C. Spiro, An osteoconductive collagen/hyaluronate matrix for bone regeneration, Biomaterials 20 (1999) 1097-1108.

[357] K.Y. Lee, D.J. Mooney, Hydrogels for tissue engineering, Chem. Rev. 101 (2001) 1869-1879.

[358] S. Misra, V.C. Hascall, R.R. Markwald, S. Ghatak, Interactions between hyaluronan and its receptors (CD44, RHAMM) regulate the activities of inflammation and cancer, Front Immunol. 6 (2015) 201.

[359] B.P. Toole, S.I. Munaim, S. Welles, C.B. Knudson, Hyaluronate Cell Interactions and Growth Factor Regulation of Hyaluronate Synthesis During Limb Development, Ciba Foundation Symp. 143-The Biology of Hyaluronan, Wiley Online Library, 1989, p. 138-149.

[360] Q. Yu, S.D. Banerjee, B.P. Toole, The role of hyaluronan-binding protein in assembly of pericellular matrices, Developmental dynamics 193 (1992) 145-151.

[361] C.B. Underhill, B.P. Toole, Binding of hyaluronate to the surface of cultured cells, J. Cell Biol.

82 (1979) 475-484.

[362] C.B. Underhill, The interaction of hyaluronate with the cell surface: the hyaluronate receptor and the core protein, In: The biology of hyaluronan, John Wiley&Sons Ltd, Chichester, 1989, pp. 87-106.

[363] R.E. Nemec, B.P. Toole, W. Knudson, The cell surface hyaluronate binding sites of invasive human bladder carcinoma cells, Biochem Bioph Res Co 149 (1987) 249-257.

[364] B.P. Toole, Proteoglycans and hyaluronan in morphogenesis and differentiation, In: Cell biology of extracellular matrix, Springer, 1991, pp. 305-341.

[365] V.C. Hascall, D. Heinegård, Aggregation of cartilage proteoglycans I. The role of hyaluronic acid, J. Biol. Chem. 249 (1974) 4232-4241.

[366] V.C. Hascall, D. Heinegård, Aggregation of cartilage proteoglycans II. Oligosaccharide competitors of the proteoglycan-hyaluronic acid interaction, J. Biol. Chem. 249 (1974) 4242-4249.

[367] J.E. Christner, M.L. Brown, D.D. Dziewiatkowski, Interaction of cartilage proteoglycans with hyaluronic acid. The role of the hyaluronic acid carboxyl groups, Biochem. J. 167 (1977) 711-716.

[368] A. Aruffo, I. Stamenkovic, M. Melnick, C.B. Underhill, B. Seed, CD44 is the principal cell surface receptor for hyaluronate, Cell 61 (1990) 1303-1313.

[369] M. Culty, K. Miyake, P.W. Kincade, E. Sikorski, E.C. Butcher, C. Underhill, et al., The hyaluronate receptor is a member of the CD44 (H-CAM) family of cell surface glycoproteins, J. Cell. Biol. 111 (1990) 2765-2774.

[370] E.A. Turley, P.W. Noble, L.Y. Bourguignon, Signaling properties of hyaluronan receptors, J. Biol. Chem. 277 (2002) 4589-4592.

[371] A. Masellis-Smith, A. Belch, M. Mant, E. Turley, L. Pilarski, Hyaluronan-dependent motility of B cells and leukemic plasma cells in blood, but not of bone marrow plasma cells, in multiple myeloma: alternate use of receptor for hyaluronan-mediated motility (RHAMM) and CD44, Blood 87 (1996) 1891-1899.

[372] R.C. Savani, G. Cao, P.M. Pooler, A. Zaman, Z. Zhou, H.M. DeLisser, Differential involvement of the hyaluronan (HA) receptors CD44 and receptor for HA-mediated motility in endothelial cell function and angiogenesis, J. Biol. Chem. 276 (2001) 36770-36778.

[373] V. Hascall, J.D. Esko, Hyaluronan, In: A. Varki, R.D. Cummings, J.D. Esko, H.H. Freeze, P. Stanley, C.R. Bertozzi, et al. (Eds),Essentials of Glycobiology, The Consortium of Glycobiology Editors, La Jolla, California., Cold Spring Harbor NY, 2009.

[374] B. Beck-Schimmer, B. Oertli, T. Pasch, R. Wüthrich, Hyaluronan induces monocyte chemoattractant protein-1 expression in renal tubular epithelial cells, JASN 9 (1998) 2283-2290.

[375] M.R. Horton, S. Shapiro, C. Bao, C.J. Lowenstein, P.W. Noble, Induction and regulation of macrophage metalloelastase by hyaluronan fragments in mouse macrophages, J. Immunol. 162 (1999) 4171-4176.

[376] C. Chung, J.A. Burdick, Influence of three-dimensional hyaluronic acid microenvironments on mesenchymal stem cell chondrogenesis, Tissue Eng. Part A 15 (2008) 243-254.

[377] S. Goodison, V. Urquidi, D. Tarin, CD44 cell adhesion molecules, Mol. Pathol. 52 (1999) 189.

[378] K. Vorvolakos, I.S. Isayeva, H.-M.D. Luu, D.V. Patwardhan, S.K. Pollack, Ionically cross-linked hyaluronic acid: wetting, lubrication, and viscoelasticity of a modified adhesion barrier gel, Med. Devices (Auckland, N.Z.) 4 (2011) 1-10.

[379] A. Kayitmazer, A. Koksal, E.K. Iyilik, Complex coacervation of hyaluronic acid and chitosan: effects of pH, ionic strength, charge density, chain length and the charge ratio, Soft matter 11 (2015) 8605-8612.

[380] K.A. Smeds, M.W. Grinstaff, Photocrosslinkable polysaccharides for in situ hydrogel formation, J. Biomed. Mater. Res. 54 (2001) 115-121.

[381] K.S. Masters, D.N. Shah, L.A. Leinwand, K.S. Anseth, Crosslinked hyaluronan scaffolds as a biologically active carrier for valvular interstitial cells, Biomaterials 26 (2005) 2517-2525.

[382] C. Chung, J. Mesa, M.A. Randolph, M. Yaremchuk, J.A. Burdick, Influence of gel properties on neocartilage formation by auricular chondrocytes photoencapsulated in hyaluronic acid networks, J. Biomed. Mater. Res. A 77 (2006) 518-525.

[383] X.Z. Shu, S. Ahmad, Y. Liu, G.D. Prestwich, Synthesis and evaluation of injectable, in situ crosslinkable synthetic extracellular matrices for tissue engineering, J. Biomed. Mater. Res. A 79 (2006) 902-912.

[384] X.Z. Shu, Y. Liu, F.S. Palumbo, Y. Luo, G.D. Prestwich, In situ crosslinkable hyaluronan hydrogels for tissue engineering, Biomaterials 25 (2004) 1339-1348.

[385] J.B. Leach, K.A. Bivens, C.N. Collins, C.E. Schmidt, Development of photocrosslinkable hyaluronic acid-polyethylene glycol-peptide composite hydrogels for soft tissue engineering, J. Biomed. Mater. Res. A 70 (2004) 74-82.

[386] J. Baier Leach, K.A. Bivens, C.W. Patrick Jr, C.E. Schmidt, Photocrosslinked hyaluronic acid hydrogels: natural, biodegradable tissue engineering scaffolds, Biotechnol. Bioeng. 82 (2003) 578-589.

[387] J. Kim, I.S. Kim, T.H. Cho, K.B. Lee, S.J. Hwang, G. Tae, et al., Bone regeneration using hyaluronic acid-based hydrogel with bone morphogenic protein-2 and human mesenchymal stem cells, Biomaterials 28 (2007) 1830-1837.

[388] L. Flynn, G.D. Prestwich, J.L. Semple, K.A. Woodhouse, Adipose tissue engineering with naturally derived scaffolds and adipose-derived stem cells, Biomaterials 28 (2007) 3834-3842.

[389] E.M. Horn, M. Beaumont, X.Z. Shu, A. Harvey, G.D. Prestwich, K.M. Horn, et al., Influence of cross-linked hyaluronic acid hydrogels on neurite outgrowth and recovery from spinal cord injury, J. Neurosurg. 6 (2007) 133-140.

[390] V. Crescenzi, L. Cornelio, C. Di Meo, S. Nardecchia, R. Lamanna, Novel hydrogels via click chemistry: synthesis and potential biomedical applications, Biomacromolecules 8 (2007) 1844-1850.

[391] H. Nandivada, X. Jiang, J. Lahann, Click chemistry: versatility and control in the hands of materials scientists, Adv. Mater. 19 (2007) 2197-2208.

[392] C.A. DeForest, B.D. Polizzotti, K.S. Anseth, Sequential click reactions for synthesizing and patterning three-dimensional cell microenvironments, Nat. Mater. 8 (2009) 659-664.

[393] Y. Liu, X.Z. Shu, G.D. Prestwich, Osteochondral defect repair with autologous bone marrow-

derived mesenchymal stem cells in an injectable, in situ, cross-linked synthetic extracellular matrix, Tissue Eng. 12 (2006) 3405-3416.

[394] E.S. Sokol, D.H. Miller, A. Breggia, K.C. Spencer, L.M. Arendt, P.B. Gupta, Growth of human breast tissues from patient cells in 3D hydrogel scaffolds, Breast Cancer Res. 18 (2016) 19.

[395] T.D. Mehra, K. Ghosh, X.Z. Shu, G.D. Prestwich, R.A. Clark, Molecular stenting with a crosslinked hyaluronan derivative inhibits collagen gel contraction, J. Invest. Dermatol. 126 (2006) 2202-2209.

[396] M.D. Brigham, A. Bick, E. Lo, A. Bendali, J.A. Burdick, A. Khademhosseini, Mechanically robust and bioadhesive collagen and photocrosslinkable hyaluronic acid semi-interpenetrating networks, Tissue Eng. Part A 15 (2008) 1645-1653.

[397] X. Xin, A. Borzacchiello, P. Netti, L. Ambrosio, L. Nicolais, Hyaluronic-acid-based semi-interpenetrating materials, J. Biomater. Sci. Polym. Ed. 15 (2004) 1223-1236.

[398] S. Suri, C.E. Schmidt, Cell-laden hydrogel constructs of hyaluronic acid, collagen, and laminin for neural tissue engineering, Tissue Eng. Part A 16 (2010) 1703-1716.

[399] A. Borzacchiello, L. Russo, B.M. Malle, K. Schwach-Abdellaoui, L. Ambrosio, Hyaluronic acid based hydrogels for regenerative medicine applications, Biomed. Res. Int. 2015 (2015).

[400] P.H. Seeberger, Automated oligosaccharide synthesis, Chem. Soc. Rev. 37 (2008) 19-28.

[401] L. Krasnova, C.-H. Wong, Understanding the chemistry and biology of glycosylation with glycan synthesis, Annu. Rev. Biochem. 85 (2016) 599-630.

[402] S. Kobayashi, Challenge of synthetic cellulose, J. Polym. Sci. A: Polym. Chem. 43 (2005) 693-710.

[403] S. Kobayashi, J. Sakamoto, S. Kimura, In vitro synthesis of cellulose and related polysaccharides, Prog. Polym. Sci. 26 (2001) 1525-1560.

[404] S. Kobayashi, S.-i. Shoda, H. Uyama, Enzymatic polymerization and oligomerization, In: Polymer Synthesis/Polymer Engineering, Springer, 1995, pp. 1-30.

[405] S. Kobayashi, H. Uyama, S. Kimura, Enzymatic polymerization, Chem. Rev. 101 (2001) 3793-3818.

[406] S. Kobayashi, H. Uyama, M. Ohmae, Enzymatic polymerization for precision polymer synthesis, Bull. Chem. Soc. Jpn. 74 (2001) 613-635.

[407] S. Kobayashi, New developments of polysaccharide synthesis via enzymatic polymerization, Proc. Jpn. Acad. Ser. B 83 (2007) 215-247.

[408] K. Kobayashi, Biological functions of synthetic polysaccharides, Macromol. Symp., Wiley Online Library, 1995, p. 157-167.

[409] H. Liu, L. Wang, A. Brock, C.-H. Wong, P.G. Schultz, A method for the generation of glycoprotein mimetics, J. Am. Chem. Soc. 125 (2003) 1702-1703.

[410] S. Eller, M. Collot, J. Yin, H.S. Hahm, P.H. Seeberger, Automated Solid-Phase Synthesis of Chondroitin Sulfate Glycosaminoglycans, Angew. Chem. Int. Ed. 52 (2013) 5858-5861.

[411] H.A. Orgueira, A. Bartolozzi, P. Schell, R.E. Litjens, E.R. Palmacci, P.H. Seeberger, Modular synthesis of heparin oligosaccharides, Chem. Eur. J. 9 (2003) 140-169.

[412] A. Varma, J. Kennedy, P. Galgali, Synthetic polymers functionalized by carbohydrates: a review, Carbohydr. Polym. 56 (2004) 429-445.

[413] R. Bahulekar, T. Tokiwa, J. Kano, T. Matsumura, I. Kojima, M. Kodama, Polyacrylamide containing sugar residues: synthesis, characterization and cell compatibility studies, Carbohydr. Polym. 37 (1998) 71-78.

[414] K. Ohno, Y. Izu, S. Yamamoto, T. Miyamoto, T. Fukuda, Nitroxide-controlled free radical polymerization of a sugar-carrying acryloyl monomer, Macromol. Chem. Phys. 200 (1999) 1619-1625.

[415] L. Mogas-Soldevila, J. Duro-Royo, N. Oxman, Water-Based Robotic Fabrication: Large-Scale Additive Manufacturing of Functionally Graded Hydrogel Composites via Multichamber Extrusion, 3D Printing and Additive Manufacturing 1 (2014) 141-151.

[416] J. Radhakrishnan, A. Subramanian, U.M. Krishnan, S. Sethuraman, Injectable and 3D Bioprinted Polysaccharide Hydrogels: From Cartilage to Osteochondral Tissue Engineering, Biomacromolecules 18 (2017) 1-26.

[417] T.J. Hinton, Q. Jallerat, R.N. Palchesko, J.H. Park, M.S. Grodzicki, H.-J. Shue, et al., Three-dimensional printing of complex biological structures by freeform reversible embedding of suspended hydrogels, Sci. Adv. 1 (2015).

[418] Y. He, F. Yang, H. Zhao, Q. Gao, B. Xia, J. Fu, Research on the printability of hydrogels in 3D bioprinting, Sci. Rep. 6 (2016) 29977.

[419] E. Axpe, M.L. Oyen, Applications of alginate-based bioinks in 3D bioprinting, Int. J. Mol. Sci. 17 (2016) 1976.

[420] V. Gorboulev, J.C. Ulzheimer, A. Akhoundova, I. Ulzheimer-Teuber, U. Karbach, S. Quester, et al., Cloning and characterization of two human polyspecific organic cation transporters, DNA Cell Biol. 16 (1997) 871-881.

[421] M. Hosoyamada, T. Sekine, Y. Kanai, H. Endou, Molecular cloning and functional expression of a multispecific organic anion transporter from human kidney, Am. J. Physiol. Renal Physiol. 276 (1999) F122-F128.

[422] J.E. Race, S.M. Grassl, W.J. Williams, E.J. Holtzman, Molecular cloning and characterization of two novel human renal organic anion transporters (hOAT1 and hOAT3), Biochem Bioph Res Co 255 (1999) 508-514.

[423] A.S. Ray, T. Cihlar, K.L. Robinson, L. Tong, J.E. Vela, M.D. Fuller, et al., Mechanism of active renal tubular efflux of tenofovir, Antimicrob. Agents Chemother. 50 (2006) 3297-3304.

[424] B. Rennick, Renal tubule transport of organic cations, Am. J. Physiol. Renal Physiol. 240 (1981) F83-F89.

[425] F. Thiebaut, T. Tsuruo, H. Hamada, M.M. Gottesman, I. Pastan, M.C. Willingham, Cellular localization of the multidrug-resistance gene product P-glycoprotein in normal human tissues, Proc. Natl. Acad. Sci. 84 (1987) 7735-7738.

[426] K. Nooter, A.M. Westerman, M.J. Flens, G. Zaman, R.J. Scheper, K. Van Wingerden, et al.,

Expression of the multidrug resistance-associated protein (MRP) gene in human cancers, Clin. Cancer Res. 1 (1995) 1301-1310.

[427] M. Huls, C. Brown, A. Windass, R. Sayer, J. Van Den Heuvel, S. Heemskerk, et al., The breast cancer resistance protein transporter ABCG2 is expressed in the human kidney proximal tubule apical membrane, Kidney Int. 73 (2008) 220-225.

[428] N. Anzai, H. Endou, Renal drug transporters and nephrotoxicity, AATEX 14 (2007) 447-452.

[429] K. Inui, S. Masuda, H. Saito, Cellular and molecular aspects of drug transport in the kidney, Kidney Int. 58 (2000) 944-958.

[430] D.M. Moss, M. Neary, A. Owen, The role of drug transporters in the kidney: lessons from tenofovir, Front Pharmacol. 5 (2014) 248.

[431] S.K. Nigam, W. Wu, K.T. Bush, M.P. Hoenig, R.C. Blantz, V. Bhatnagar, Handling of Drugs, Metabolites, and Uremic Toxins by Kidney Proximal Tubule Drug Transporters, Clin. J. Am. Soc. Nephrol. 10 (2015) 2039-2049.

[432] H. Baharvand, S.M. Hashemi, S.K. Ashtian, A. Farrokhi, Differentiation of human embryonic stem cells into hepatocytes in 2D and 3D culture systems in vitro, Int. J. Dev. Biol. 50 (2006) 645-652.

[433] C.M. Nelson, M.J. Bissell, Modeling dynamic reciprocity: Engineering three-dimensional culture models of breast architecture, function, and neoplastic transformation, Semin. Cancer Biol. 15 (2005) 342-352.

[434] J. Lee, M.J. Cuddihy, N.A. Kotov, Three-dimensional cell culture matrices: state of the art, Tissue Eng. Part B Rev. 14 (2008) 61-86.

[435] M. Zietarska, C.M. Maugard, A. Filali-Mouhim, M. Alam-Fahmy, P.N. Tonin, D.M. Provencher, et al., Molecular description of a 3D in vitro model for the study of epithelial ovarian cancer (EOC), Mol Carcinogen 46 (2007) 872-885.

[436] G. Gstraunthaler, W. Pfaller, P. Kotanko, Biochemical characterization of renal epithelial cell cultures (LLC-PK1 and MDCK), Am. J. Physiol. Renal Physiol. 248 (1985) F536-F544.

[437] H. Koyama, C. Goodpasture, M. Miller, R. Teplitz, A.D. Riggs, Establishment and characterization of a cell line from the American opossum (Didelphys virginiana), In vitro 14 (1978) 239-246.

[438] M.J. Ryan, G. Johnson, J. Kirk, S.M. Fuerstenberg, R.A. Zager, B. Torok-Storb, HK-2: an immortalized proximal tubule epithelial cell line from normal adult human kidney, Kidney Int. 45 (1994) 48-57.

[439] M.J. Wilmer, M.A. Saleem, R. Masereeuw, L. Ni, T.J. van der Velden, F.G. Russel, et al., Novel conditionally immortalized human proximal tubule cell line expressing functional influx and efflux transporters, Cell Tissue Res. 339 (2010) 449-457.

[440] L.E. O'Brien, M.M. Zegers, K.E. Mostov, Building epithelial architecture: insights from three-dimensional culture models, Nat. Rev. Mol. Cell Biol. 3 (2002) 531-537.

[441] D. Khaitan, S. Chandna, M.B. Arya, B.S. Dwarakanath, Establishment and characterization of multicellular spheroids from a human glioma cell line; Implications for tumor therapy, J. Transl. Med. 4 (2006).

[442] G. Mehta, A.Y. Hsiao, M. Ingram, G.D. Luker, S. Takayama, Opportunities and challenges for use of tumor spheroids as models to test drug delivery and efficacy, J. Control. Release 164 (2012) 192-204.

[443] S. Terryn, F. Jouret, F. Vandenabeele, I. Smolders, M. Moreels, O. Devuyst, et al., A primary culture of mouse proximal tubular cells, established on collagen-coated membranes, Am. J. Physiol. Renal Physiol. 293 (2007) F476-485.

[444] R.L. Miller, P. Zhang, T. Chen, A. Rohrwasser, R.D. Nelson, Automated method for the isolation of collecting ducts, Am. J. Physiol. Renal Physiol. 291 (2006) F236-F245.

[445] G.D. Prestwich, J.W. Kuo, Chemically-modified HA for therapy and regenerative medicine, Curr. Pharm. Biotechnol. 9 (2008) 242-245.

[446] G.D. Prestwich, Hyaluronic acid-based clinical biomaterials derived for cell and molecule delivery in regenerative medicine, J. Control. Release 155 (2011) 193-199.

[447] K.J. Livak, T.D. Schmittgen, Analysis of relative gene expression data using real-time quantitative PCR and the 2(-Delta Delta C(T)) Method, Methods 25 (2001) 402-408.

[448] M.W. Pfaffl, A. Tichopad, C. Prgomet, T.P. Neuvians, Determination of stable housekeeping genes, differentially regulated target genes and sample integrity: BestKeeper--Excel-based tool using pair-wise correlations, Biotechnol. Lett. 26 (2004) 509-515.

[449] C.L. Andersen, J.L. Jensen, T.F. Orntoft, Normalization of real-time quantitative reverse transcription-PCR data: a model-based variance estimation approach to identify genes suited for normalization, applied to bladder and colon cancer data sets, Cancer Res. 64 (2004) 5245-5250.

[450] J. Vandesompele, K. De Preter, F. Pattyn, B. Poppe, N. Van Roy, A. De Paepe, et al., Accurate normalization of real-time quantitative RT-PCR data by geometric averaging of multiple internal control genes, Genome Biol. 3 (2002) RESEARCH0034.

[451] N. Silver, S. Best, J. Jiang, S.L. Thein, Selection of housekeeping genes for gene expression studies in human reticulocytes using real-time PCR, BMC Mol. Biol. 7 (2006) 33.

[452] H. Koepsell, H. Endou, The SLC22 drug transporter family, Pflugers Arch. 447 (2004) 666-676.

[453] K. Inui, T. Terada, S. Masuda, H. Saito, Physiological and pharmacological implications of peptide transporters, PEPT1 and PEPT2, Nephrol. Dial. Transplant. 15 (2000) 11-13.

[454] Y. Shitara, T. Horie, Y. Sugiyama, Transporters as a determinant of drug clearance and tissue distribution, Eur. J. Pharm. Sci. 27 (2006) 425-446.

[455] Y. Shitara, H. Sato, Y. Sugiyama, Evaluation of drug-drug interaction in the hepatobiliary and renal transport of drugs, Annu. Rev. Pharmacol. Toxicol. 45 (2005) 689-723.

[456] V.M. Weaver, O.W. Petersen, F. Wang, C. Larabell, P. Briand, C. Damsky, et al., Reversion of the malignant phenotype of human breast cells in three-dimensional culture and in vivo by integrin blocking antibodies, J. Cell. Biol. 137 (1997) 231-245.

[457] K. Bhadriraju, C.S. Chen, Engineering cellular microenvironments to cell-based drug testing improve, Drug Discov. Today 7 (2002) 612-620.

[458] A. Birgersdotter, R. Sandberg, I. Ernberg, Gene expression perturbation in vitro - A growing

case for three-dimensional (3D) culture systems, Semin. Cancer Biol. 15 (2005) 405-412.

[459] I. Behrens, W. Kamm, A.H. Dantzig, T. Kissel, Variation of peptide transporter (PepT1 and HPT1) expression in Caco-2 cells as a function of cell origin, J. Pharm. Sci. 93 (2004) 1743-1754.

[460] J. Taipalensuu, S. Tavelin, L. Lazorova, A.-C. Svensson, P. Artursson, Exploring the quantitative relationship between the level of MDR1 transcript, protein and function using digoxin as a marker of MDR1-dependent drug efflux activity, Eur. J. Pharm. Sci. 21 (2004) 69-75.

[461] A. Yonezawa, K.-i. Inui, Organic cation transporter OCT/SLC22A and H+/organic cation antiporter MATE/SLC47A are key molecules for nephrotoxicity of platinum agents, Biochem. Pharmacol. 81 (2011) 563-568.

[462] B. Fernandez-Fernandez, A. Montoya-Ferrer, A.B. Sanz, Sanchez-Ni, M.D., et al., Tenofovir Nephrotoxicity: 2011 Update, AIDS Res. Treat 2011 (2011) 11.

[463] H.A. Mutsaers, M.J. Wilmer, L.P. van den Heuvel, J.G. Hoenderop, R. Masereeuw, Basolateral transport of the uraemic toxin p-cresyl sulfate: role for organic anion transporters?, Nephrol. Dial. Transplant. 26 (2011) 4149.

[464] J.M. McKim, Building a Tiered Approach to In Vitro Predictive Toxicity Screening: A Focus on Assays with In Vivo Relevance, Comb. Chem. High Throughput Screen. 13 (2010) 188-206.

[465] Z. Yang, H.-R. Xiong, In vitro, Tissue-Based Models as a Replacement for Animal Models in Testing of Drugs at the Preclinical Stages, In: L. Ceccherini-Nelli (Ed), Biomed. Tiss. Culture, InTech, 2012.

[466] G. Greenburg, E.D. Hay, Epithelia suspended in collagen gels can lose polarity and express characteristics of migrating mesenchymal cells, J. Cell. Biol. 95 (1982) 333-339.

[467] P.P. Provenzano, K.W. Eliceiri, D.R. Inman, P.J. Keely, Engineering Three-Dimensional Collagen Matrices to Provide Contact Guidance during 3D Cell Migration, Curr. Protoc. Cell Biol. (2010) 10.17. 11-10.17. 11.

[468] L. Rebelo, M. Carmo-Fonseca, T.F. Moura, Redistribution of microvilli and membrane enzymes in isolated rat proximal tubule cells, Biol. Cell 74 (1992) 203-209.

[469] W. Li, M. Lam, D. Choy, A. Birkeland, M.E. Sullivan, J.M. Post, Human primary renal cells as a model for toxicity assessment of chemo-therapeutic drugs, Toxicol. In Vitro 20 (2006) 669-676.

[470] Z. Lin, Y. Will, Evaluation of drugs with specific organ toxicities in organ-specific cell lines, Toxicol. Sci. 126 (2012) 114-127.

[471] J.H. Zhang, T.D. Chung, K.R. Oldenburg, A Simple Statistical Parameter for Use in Evaluation and Validation of High Throughput Screening Assays, J. Biomol. Screen. 4 (1999) 67-73.

[472] T.A. Lasko, J.G. Bhagwat, K.H. Zou, L. Ohno-Machado, The use of receiver operating characteristic curves in biomedical informatics, J. Biomed. Inform. 38 (2005) 404-415.

[473] W.J. Youden, Index for rating diagnostic tests, Cancer 3 (1950) 32-35.

[474] R. Parikh, A. Mathai, S. Parikh, G.C. Sekhar, R. Thomas, Understanding and using sensitivity, specificity and predictive values, Indian J. Ophthalmol. 56 (2008) 45.

[475] P.J. O'Brien, W. Irwin, D. Diaz, E. Howard-Cofield, C.M. Krejsa, M.R. Slaughter, et al., High

concordance of drug-induced human hepatotoxicity with in vitro cytotoxicity measured in a novel cell-based model using high content screening, Arch. Toxicol. 80 (2006) 580-604.

[476] J.H.J. Xu, P.V. Henstock, M.C. Dunn, A.R. Smith, J.R. Chabot, D. de Graaf, Cellular imaging predictions of clinical drug-induced liver injury, Toxicol. Sci. 105 (2008) 97-105.

[477] M. Persson, A.F. Loye, T. Mow, J.J. Hornberg, A high content screening assay to predict human drug-induced liver injury during drug discovery, J. Pharmacol. Toxicol. Methods 68 (2013) 302-313.

[478] N.D. Keirstead, M.P. Wagoner, P. Bentley, M. Blais, C. Brown, L. Cheatham, et al., Early prediction of polymyxin-induced nephrotoxicity with next-generation urinary kidney injury biomarkers, Toxicol. Sci. 137 (2014) 278-291.

[479] M.D. Brand, D.G. Nicholls, Assessing mitochondrial dysfunction in cells, Biochem. J. 435 (2011) 297-312.

[480] M. Fallahi-Sichani, S. Honarnejad, L.M. Heiser, J.W. Gray, P.K. Sorger, Metrics other than potency reveal systematic variation in responses to cancer drugs, Nat. Chem. Biol. 9 (2013) 708-714.

[481] S. Goutelle, M. Maurin, F. Rougier, X. Barbaut, L. Bourguignon, M. Ducher, et al., The Hill equation: a review of its capabilities in pharmacological modelling, Fundam. Clin. Pharmacol. 22 (2008) 633-648.

[482] A. Pointon, N. Abi-Gerges, M.J. Cross, J.E. Sidaway, Phenotypic profiling of structural cardiotoxins in vitro reveals dependency on multiple mechanisms of toxicity, Toxicol. Sci. 132 (2013) 317-326.

[483] P.J. O'Brien, High-content analysis in toxicology: screening substances for human toxicity potential, elucidating subcellular mechanisms and in vivo use as translational safety biomarkers, Basic Clin. Pharmacol. Toxicol. 115 (2014) 4-17.

[484] P.Y. Muller, M.N. Milton, The determination and interpretation of the therapeutic index in drug development, Nat. Rev. Drug Discov. 11 (2012) 751-761.

[485] M. Adler, S. Ramm, M. Hafner, J.L. Muhlich, E.M. Gottwald, E. Weber, et al., A Quantitative Approach to Screen for Nephrotoxic Compounds In Vitro, J. Am. Soc. Nephrol. 27 (2016) 1015-1028.

[486] Y. Wu, D. Connors, L. Barber, S. Jayachandra, U.M. Hanumegowda, S.P. Adams, Multiplexed assay panel of cytotoxicity in HK-2 cells for detection of renal proximal tubule injury potential of compounds, Toxicol. In Vitro 23 (2009) 1170-1178.

[487] V. Pinzani, F. Bressolle, I.J. Haug, M. Galtier, J.P. Blayac, P. Balmes, Cisplatin-induced renal toxicity and toxicity-modulating strategies: a review, Cancer Chemother. Pharmacol. 35 (1994) 1-9.

[488] D.W. Schwertz, J.I. Kreisberg, M.A. Venkatachalam, Gentamicin-induced alterations in pig kidney epithelial (LLC-PK1) cells in culture, J. Pharmacol. Exp. Ther. 236 (1986) 254-262.

[489] T.H. Mathew, Drug-induced renal disease, Med. J. Aust. 156 (1992) 724-728.

[490] T.S. Lahoti, D. Patel, V. Thekkemadom, R. Beckett, S.D. Ray, Doxorubicin-induced in vivo nephrotoxicity involves oxidative stress-mediated multiple pro- and anti-apoptotic signaling

pathways, Curr. Neurovasc. Res. 9 (2012) 282-295.

[491] Gilead Sciences, Vistide (cidofovir). 2010, (accessed 2016).

[492] P.J. Bergen, C.B. Landersdorfer, J. Zhang, M. Zhao, H.J. Lee, R.L. Nation, et al., Pharmacokinetics and pharmacodynamics of 'old' polymyxins: what is new?, Diagn. Microbiol. Infect. Dis. 74 (2012) 213-223.

[493] M.E. Falagas, S.K. Kasiakou, Toxicity of polymyxins: a systematic review of the evidence from old and recent studies, Crit. Care 10 (2006) R27.

[494] H. Tsubery, I. Ofek, S. Cohen, M. Fridkin, N-terminal modifications of Polymyxin B nonapeptide and their effect on antibacterial activity, Peptides 22 (2001) 1675-1681.

[495] K. Abdelraouf, K.H. Braggs, T. Yin, L.D. Truong, M. Hu, V.H. Tam, Characterization of polymyxin B-induced nephrotoxicity: implications for dosing regimen design, Antimicrob. Agents Chemother. 56 (2012) 4625-4629.

[496] M. Larsson, G. Hjälm, A.M. Sakwe, Å. Engström, A.-S. Höglund, E. Larsson, et al., Selective interaction of megalin with postsynaptic density-95 (PSD-95)-like membrane-associated guanylate kinase (MAGUK) proteins, Biochem. J. 373 (2003) 381-391.

[497] A. Benesic, G. Schwerdt, S. Mildenberger, R. Freudinger, N. Gordjani, M. Gekle, Disturbed Ca 2+-signaling by chloroacetaldehyde: a possible cause for chronic ifosfamide nephrotoxicity, Kidney Int. 68 (2005) 2029-2041.

[498] B. Gowda, M. Sar, X. Mu, J. Cidlowski, T. Welbourne, Coordinate modulation of glucocorticoid receptor and glutaminase gene expression in LLC-PK1-F+ cells, Am. J. Physiol. Cell Physiol. 270 (1996) C825-C831.

[499] V.S. Vaidya, J.S. Ozer, F. Dieterle, F.B. Collings, V. Ramirez, S. Troth, et al., Kidney injury molecule-1 outperforms traditional biomarkers of kidney injury in preclinical biomarker qualification studies, Nat. Biotechnol. 28 (2010) 478-485.

[500] H. Olson, G. Betton, D. Robinson, K. Thomas, A. Monro, G. Kolaja, et al., Concordance of the toxicity of pharmaceuticals in humans and in animals, Regul. Toxicol. Pharmacol. 32 (2000) 56-67.

[501] P. McGonigle, B. Ruggeri, Animal models of human disease: challenges in enabling translation, Biochem. Pharmacol. 87 (2014) 162-171.

[502] C.M. Sakolish, G.J. Mahler, A novel microfluidic device to model the human proximal tubule and glomerulus, RSC Adv. 7 (2017) 4216-4225.

[503] A.E. Brooks, S.R. Nelson, J.A. Jones, C. Koenig, M. Hinman, S. Stricker, et al., Distinct contributions of model MaSp1 and MaSp2 like peptides to the mechanical properties of synthetic major ampullate silk fibers as revealed in silico, Nanotechnol. Sci. Appl. 1 (2008) 9-16.

[504] M.B. Hinman, J.A. Jones, R.V. Lewis, Synthetic spider silk: a modular fiber, Trends Biotechnol. 18 (2000) 374-379.

[505] C.Y. Hayashi, N.H. Shipley, R.V. Lewis, Hypotheses that correlate the sequence, structure, and mechanical properties of spider silk proteins, Int. J. Biol. Macromol. 24 (1999) 271-275.

[506] K. Ohgo, F. Bagusat, T. Asakura, U. Scheler, Investigation of structural transition of

regenerated silk fibroin aqueous solution by Rheo-NMR spectroscopy, J. Am. Chem. Soc. 130 (2008) 4182-4186.

[507] K. Yazawa, E. Yamaguchi, D. Knight, T. Asakura, 13 C solid-state NMR study of the 13 C-labeled peptide, (E)8 GGLGGQGAG(A)6 GGAGQGGYGG as a model for the local structure of Nephila clavipes dragline silk (MaSp1) before and after spinning, Biopolymers 97 (2012) 347-354.

[508] S.T. Krishnaji, D.L. Kaplan, Bioengineered chimeric spider silk-uranium binding proteins, Macromol. Biosci. 13 (2013) 256-264.

[509] S. Gomes, J. Gallego-Llamas, I.B. Leonor, J.F. Mano, R.L. Reis, D.L. Kaplan, Biological responses to spider silk-antibiotic fusion protein, J. Tissue Eng. Regen. Med. 6 (2012) 356-368.

[510] L.L. Canabady-Rochelle, D.J. Belton, O. Deschaume, H.A. Currie, D.L. Kaplan, C.C. Perry, Bioinspired silicification of silica-binding peptide-silk protein chimeras: comparison of chemically and genetically produced proteins, Biomacromolecules 13 (2012) 683-690.

[511] E. Bini, C.W.P. Foo, J. Huang, V. Karageorgiou, B. Kitchel, D.L. Kaplan, RGD-functionalized bioengineered spider dragline silk biomaterial, Biomacromolecules 7 (2006) 3139-3145.

[512] S. Gomes, K. Numata, I.B. Leonor, J.F. Mano, R.L. Reis, D.L. Kaplan, AFM study of morphology and mechanical properties of a chimeric spider silk and bone sialoprotein protein for bone regeneration, Biomacromolecules 12 (2011) 1675-1685.

[513] J. Scheller, D. Henggeler, A. Viviani, U. Conrad, Purification of spider silk-elastin from transgenic plants and application for human chondrocyte proliferation, Transgenic Res. 13 (2004) 51-57.

[514] J. Wang, W. Hu, Q. Liu, S. Zhang, Dual-functional composite with anticoagulant and antibacterial properties based on heparinized silk fibroin and chitosan, Colloids Surf. B Biointerfaces 85 (2011) 241-247.

[515] I.K. Jang, M.J. Hursting, When heparins promote thrombosis: review of heparin-induced thrombocytopenia, Circulation 111 (2005) 2671-2683.

[516] H.E. Conrad, Heparinoid/Protein Interactions, In: H.E. Conrad (Ed),Heparin-Binding Proteins, Academic Press, San Diego, 1998, pp. 183-202.

[517] H. Edward Conrad, Chapter 1 - Heparin vs Heparan Sulfate, In: H.E. Conrad (Ed),Heparin-Binding Proteins, Academic Press, San Diego, 1998, pp. 1-5.

[518] H. Edward Conrad, Chapter 4 - Structural Modification of Heparinoids, In: H.E. Conrad (Ed),Heparin-Binding Proteins, Academic Press, San Diego, 1998, pp. 115-136.

[519] H. Edward Conrad, Chapter 8 - Heparin-Binding Proteins in Hemostasis, In: H.E. Conrad (Ed),Heparin-Binding Proteins, Academic Press, San Diego, 1998, pp. 239-300.

[520] A.D. Cardin, H.J. Weintraub, Molecular modeling of protein-glycosaminoglycan interactions, Arterioscler. Thromb. Vasc. Biol. 9 (1989) 21-32.

[521] M. Pasupuleti, A. Schmidtchen, M. Malmsten, Antimicrobial peptides: key components of the innate immune system, Crit. Rev. Biotechnol. 32 (2012) 143-171.

[522] S.C. Gomes, I.B. Leonor, J.F. Mano, R.L. Reis, D.L. Kaplan, Antimicrobial functionalized genetically engineered spider silk, Biomaterials 32 (2011) 4255-4266.

[523] C. Vepari, D. Matheson, L. Drummy, R. Naik, D.L. Kaplan, Surface modification of silk fibroin with poly(ethylene glycol) for antiadhesion and antithrombotic applications, J. Biomed. Mater. Res. A 93 (2010) 595-606.

[524] A. Verrecchio, M.W. Germann, B.P. Schick, B. Kung, T. Twardowski, J.D.S. Antonio, Design of Peptides with High Affinities for Heparin and Endothelial Cell Proteoglycans, J. Biol. Chem. 275 (2000) 7701-7707.

[525] M. Malmsten, G. Kasetty, M. Pasupuleti, J. Alenfall, A. Schmidtchen, Highly selective end-tagged antimicrobial peptides derived from PRELP, PloS one 6 (2011) e16400.

[526] J.Y. Lee, J.E. Choo, Y.S. Choi, K.Y. Lee, D.S. Min, S.H. Pi, et al., Characterization of the surface immobilized synthetic heparin binding domain derived from human fibroblast growth factor-2 and its effect on osteoblast differentiation, J. Biomed. Mater. Res. A 83 (2007) 970-979.

[527] M.C. Martins, S.A. Curtin, S.C. Freitas, P. Salgueiro, B.D. Ratner, M.A. Barbosa, Molecularly designed surfaces for blood deheparinization using an immobilized heparin-binding peptide, J. Biomed. Mater. Res. A 88 (2009) 162-173.

[528] B. Panilaitis, G.H. Altman, J. Chen, H.J. Jin, V. Karageorgiou, D.L. Kaplan, Macrophage responses to silk, Biomaterials 24 (2003) 3079-3085.

[529] X. Wang, X. Zhang, J. Castellot, I. Herman, M. Iafrati, D.L. Kaplan, Controlled release from multilayer silk biomaterial coatings to modulate vascular cell responses, Biomaterials 29 (2008) 894-903.

[530] Y. Wang, H.J. Kim, G. Vunjak-Novakovic, D.L. Kaplan, Stem cell-based tissue engineering with silk biomaterials, Biomaterials 27 (2006) 6064-6082.

[531] M. Nagaoka, H.L. Jiang, T. Hoshiba, T. Akaike, C.S. Cho, Application of recombinant fusion proteins for tissue engineering, Ann. Biomed. Eng. 38 (2010) 683-693.

[532] S. Gomes, I.B. Leonor, J.F. Mano, R.L. Reis, D.L. Kaplan, Natural and Genetically Engineered Proteins for Tissue Engineering, Prog. Polym. Sci. 37 (2012) 1-17.

[533] D.J. Belton, A.J. Mieszawska, H.A. Currie, D.L. Kaplan, C.C. Perry, Silk-silica composites from genetically engineered chimeric proteins: materials properties correlate with silica condensation rate and colloidal stability of the proteins in aqueous solution, Langmuir : the ACS journal of surfaces and colloids 28 (2012) 4373-4381.

[534] C. Wong Po Foo, S.V. Patwardhan, D.J. Belton, B. Kitchel, D. Anastasiades, J. Huang, et al., Novel nanocomposites from spider silk-silica fusion (chimeric) proteins, Proc. Natl. Acad. Sci. 103 (2006) 9428-9433.

[535] P. Appelgren, U. Ransjo, L. Bindslev, F. Espersen, O. Larm, Surface heparinization of central venous catheters reduces microbial colonization in vitro and in vivo: results from a prospective, randomized trial, Crit. Care Med. 24 (1996) 1482-1489.

[536] A.E. Brooks, S.M. Stricker, S.B. Joshi, T.J. Kamerzell, C.R. Middaugh, R.V. Lewis, Properties of synthetic spider silk fibers based on Argiope aurantia MaSp2, Biomacromolecules 9 (2008) 1506-1510.

[537] N. Betz, C. Cowan, S. Krueger, S. Fly, J. Stevens, M. Bjerke, Maxwell 16 Polyhistidine Protein Purification Kit, Promega Notes 95 (2007) 12-15.

[538] F. Teule, A.R. Cooper, W.A. Furin, D. Bittencourt, E.L. Rech, A. Brooks, et al., A protocol for the production of recombinant spider silk-like proteins for artificial fiber spinning, Nat. Protoc. 4 (2009) 341-355.

[539] R.K. Scopes, Protein Purification: Principles and Practice, Springer Science & Business Media, 2013.

[540] T. Hattori, K. Kimura, E. Seyrek, P.L. Dubin, Binding of bovine serum albumin to heparin determined by turbidimetric titration and frontal analysis continuous capillary electrophoresis, Anal. Biochem. 295 (2001) 158-167.

[541] S. Najjam, R.V. Gibbs, M.Y. Gordon, C.C. Rider, Characterization of human recombinant interleukin 2 binding to heparin and heparan sulfate using an ELISA approach, Cytokine 9 (1997) 1013-1022.

[542] S. Najjam, B. Mulloy, J. Theze, M. Gordon, R. Gibbs, C.C. Rider, Further characterization of the binding of human recombinant interleukin 2 to heparin and identification of putative binding sites, Glycobiology 8 (1998) 509-516.

[543] L. Wood, Research and Markets: The Market For Drug Eluting Coronary Stents Is Exhibiting Clear Evidence of Recovery with Average Annual PCI Volumes Rising by 5% in the US and 4% in Europe. http://www.businesswire.com, 2009, (accessed 2016).

[544] J. Gunn, D. Cumberland, Stent coatings and local drug delivery. State of the art, Eur. Heart J. 20 (1999) 1693-1700.

[545] K. Christensen, R. Larsson, H. Emanuelsson, G. Elgue, A. Larsson, Improved blood compatibility of a stent graft by combining heparin coating and abciximab, Thromb. Res. 115 (2005) 245-253.

[546] E.M. Hietala, P. Maasilta, T. Välimaa, A.L. Harjula, P. Törmälä, U.S. Salminen, et al., Platelet responses and coagulation activation on polylactide and heparin–polycaprolactone-L-lactide-coated polylactide stent struts, J. Biomed. Mater. Res. A 67 (2003) 785-791.

[547] P.L. Foley, C.H. Barthel, H.R. Brausa, Effect of covalently bound heparin coating on patency and biocompatibility of long-term indwelling catheters in the rat jugular vein, Comp. Med. 52 (2002) 243-248.

[548] X.M. Mueller, H.T. Tevaearai, D. Hayoz, L.K. von Segesser, Morphometric analysis of heparin coated versus standard intra-aortic balloons, ASAIO J. 44 (1998) M401-M404.

[549] G.M. Harbers, K. Emoto, C. Greef, S.W. Metzger, H.N. Woodward, J.J. Mascali, et al., A functionalized poly(ethylene glycol)-based bioassay surface chemistry that facilitates bio-immobilization and inhibits non-specific protein, bacterial, and mammalian cell adhesion, Chem. Mater. 19 (2007) 4405-4414.

[550] L.K. Kairaitis, T. Gottlieb, Outcome and complications of temporary haemodialysis catheters, Nephrol. Dial. Transplant. 14 (1999) 1710-1714.

[551] M. Stigter, J. Bezemer, K. De Groot, P. Layrolle, Incorporation of different antibiotics into carbonated hydroxyapatite coatings on titanium implants, release and antibiotic efficacy, J. Control. Release 99 (2004) 127-137.

[552] S.K. Hendricks, C. Kwok, M. Shen, T.A. Horbett, B.D. Ratner, J.D. Bryers, Plasma-deposited membranes for controlled release of antibiotic to prevent bacterial adhesion and biofilm formation,

J. Biomed. Mater. Res. 50 (2000) 160-170.

[553] I.A. Rojas, J.B. Slunt, D.W. Grainger, Polyurethane coatings release bioactive antibodies to reduce bacterial adhesion, J. Control. Release 63 (2000) 175-189.

[554] H. Ghandehari, Recombinant biomaterials for pharmaceutical and biomedical applications, Pharm. Res. 25 (2008) 672-673.

[555] M. Cestari, V. Muller, J.H.d.S. Rodrigues, C.V. Nakamura, A.F. Rubira, E.C. Muniz, Preparing silk fibroin nanofibers through electrospinning: further heparin immobilization toward hemocompatibility improvement, Biomacromolecules 15 (2014) 1762-1767.

[556] M.F. Elahi, G. Guan, L. Wang, X. Zhao, F. Wang, M.W. King, Surface modification of silk fibroin fabric using layer-by-layer polyelectrolyte deposition and heparin immobilization for small-diameter vascular prostheses, Langmuir : the ACS journal of surfaces and colloids 31 (2015) 2517-2526.

[557] F.P. Seib, M. Herklotz, K.A. Burke, M.F. Maitz, C. Werner, D.L. Kaplan, Multifunctional silk-heparin biomaterials for vascular tissue engineering applications, Biomaterials 35 (2014).

[558] S. Bailey, Coating of endovascular stents, In: Textbook of interventional cardiology, 1994, pp. 754-765.

[559] M. Hinman, Z. Dong, M. Xu, R.V. Lewis, Spider silk: a mystery starting to unravel, Results Probl. Cell Differ. 19 (1992) 227-254.

[560] H. Sletta, A. Tøndervik, S. Hakvåg, T.E.V. Aune, A. Nedal, R. Aune, et al., The Presence of N-Terminal Secretion Signal Sequences Leads to Strong Stimulation of the Total Expression Levels of Three Tested Medically Important Proteins during High-Cell-Density Cultivations of Escherichia coli, Appl. Environ. Microbiol. 73 (2007) 906-912.

[561] Y. Li, Recombinant production of antimicrobial peptides in Escherichia coli: A review, Protein Expr. Purif. 80 (2011) 260-267.

[562] C. Luan, Y.G. Xie, Y.T. Pu, H.W. Zhang, F.F. Han, J. Feng, et al., Recombinant expression of antimicrobial peptides using a novel self-cleaving aggregation tag in Escherichia coli, Can. J. Microbiol. 60 (2014) 113-120.

[563] M. Zorko, R. Jerala, Production of Recombinant Antimicrobial Peptides in Bacteria, In: A. Giuliani, A.C. Rinaldi (Eds),Antimicrobial Peptides, Humana Press, 2010, pp. 61-76.

[564] D.W. Lim, K. Trabbic-Carlson, J.A. MacKay, A. Chilkoti, Improved Non-chromatographic Purification of a Recombinant Protein by Cationic Elastin-like Polypeptides, Biomacromolecules 8 (2007) 1417-1424.

[565] Y. Shen, H.-X. Ai, R. Song, Z.-N. Liang, J.-F. Li, S.-Q. Zhang, Expression and purification of moricin CM4 and human β-defensins 4 in Escherichia coli using a new technology, Microbiol. Res. 165 (2010) 713-718.

[566] K. Yang, Y. Su, J. Li, J. Sun, Y. Yang, Expression and purification of the antimicrobial peptide cecropin AD by fusion with cationic elastin-like polypeptides, Protein Expr. Purif. 85 (2012) 200-203.

[567] S. Raghavan, M. Dikshit, Recent advances in the status and targets of antithrombotic agents, Drugs Future 27 (2002) 669-688.

[568] R.I.W. Osmond, W.C. Kett, S.E. Skett, D.R. Coombe, Protein-heparin interactions measured by BIAcore 2000 are affected by the method of heparin immobilization, Anal. Biochem. 310 (2002) 199-207.

[569] H. Yu, E.M. Muñoz, R.E. Edens, R.J. Linhardt, Kinetic studies on the interactions of heparin and complement proteins using surface plasmon resonance, Biochim. Biophys. Acta 1726 (2005) 168-176.

[570] E.M. Muñoz, R.J. Linhardt, Heparin-Binding Domains in Vascular Biology, Arterioscler. Thromb. Vasc. Biol. 24 (2004) 1549-1557.

[571] E. Stellwagen, J.D. Prantner, N.C. Stellwagen, Do zwitterions contribute to the ionic strength of a solution?, Anal. Biochem. 373 (2008) 407-409.

[572] J.-m. Zheng, A. Wexler, G.H. Pollack, Effect of buffers on aqueous solute-exclusion zones around ion-exchange resins, J. Colloid Interface Sci. 332 (2009) 511-514.

[573] J.O. Sevy, M.H. Slawson, D.W. Grainger, A.E. Brooks, Assay method for polymer-controlled antibiotic release from allograft bone to target orthopaedic infections - biomed 2010, Biomed. Sci. Instrum. 46 (2010) 136-141.